PREPARATIVE-SCALE ISOELECTRIC TRAPPING SEPARATIONS IN A MULTICOMPARTMENTAL ELECTROLYZER: IMPLEMENTATION AND MONITORING

A Dissertation

by

JOSEPH BRIAN MONTEJO SINAJON

Submitted to the Office of Graduate Studies of
Texas A&M University
in partial fulfillment of the requirements for the degree of

DOCTOR OF PHILOSOPHY

August 2007

Major Subject: Chemistry

PREPARATIVE-SCALE ISOELECTRIC TRAPPING SEPARATIONS IN A MULTICOMPARTMENTAL ELECTROLYZER: IMPLEMENTATION AND MONITORING

A Dissertation

by

JOSEPH BRIAN MONTEJO SINAJON

Submitted to the Office of Graduate Studies of
Texas A&M University
in partial fulfillment of the requirements for the degree of

DOCTOR OF PHILOSOPHY

Approved by:

Chair of Committee,	Gyula Vigh
Committee Members,	Emile A. Schweikert
	Manuel P. Soriaga
	Charles J. Glover
Head of Department,	David H. Russell

August 2007

Major Subject: Chemistry

ABSTRACT

Preparative-scale Isoelectric Trapping Separations in a Multicompartmental Electrolyzer: Implementation and Monitoring. (August 2007)

Joseph Brian Montejo Sinajon, B.S., University of San Carlos, Philippines

Chair of Advisory Committee: Dr. Gyula Vigh

Preparative-scale protein separations have always been critical to the advancement of the life sciences. Among preparative-scale separation techniques, isoelectric trapping (IET) promises efficient separations and high production rates. This dissertation focuses on the improvement of two aspects of preparative-scale IET protein separations: the instrumentation used and the monitoring of the separation.

The first aspect (preparative-scale) is the IET device: the improvement of a multicompartmental electrolyzer (MCE) to increase the efficiency and production rate of IET separations. The redesign focused on three major areas: (1) the sealing system, (2) the configuration of the liquid flow path, and (3) the cooling system.

The second aspect (analytical-scale) is the monitoring of the IET separation: the design and manufacture of durable surface-modified capillaries which provide controlled, variable anodic and cathodic electroosmotic flow (EOF) to help develop, plan, and monitor the IET separations.

DEDICATION

To my family for all the love, support, encouragement, and prayers

ACKNOWLEDGEMENTS

I would like to thank my advisor, Prof. Gyula Vigh for his patience and mentorship throughout my stay. His passion and dedication to teaching and research have taught me the ideals of Science.

I would also like to thank my colleagues in the Separation Science Group, both past and present for their friendship, mentorship, and support: Ivan Spanik, Brent Busby, Adriana Salinas, Omar Maldonado, Silvia Sanchez, Shulan Li, Evan Shave, Kingsley Nzeadibe, Ann Hwang, Peniel Lim, Sanjiv Lalwani, Roy Estrada III, Edward Tutu, Rob North, and Ming-Chien Li.

Lastly, and certainly not the least, I'd like to thank God for all His blessings and for always giving me the things that I truly needed.

TABLE OF CONTENTS

Page

Page

Page

Page

LIST OF FIGURES

FIGURE Page

FIGURE Page

FIGURE Page

FIGURE Page

FIGURE Page

FIGURE Page

FIGURE Page

LIST OF TABLES

TABLE Page

NOMENCLATURE

AA	Acrylamide
ALB	Ovalbumin
AFM	Atomic force microscopy
AMPS	2-acrylamido-2-methyl-1-propanesulfonate ion
APBA	4-aminophenyl butyric acid
APTA	(3-acrylamidopropyl)trimethylammonium ion
ARG	Arginine
ASP	Aspartic acid
AVI	Avidin
BDMASP	1,3-bis(*N,N*-dimethylamino)-2-*O*-sulfo-propane
BDPASP	1,3-bis(dipropylamino)-2-*O*-sulfo-propane
BGE	Background electrolyte
BMSP	1,3-bis(4-morpholino)-2-*O*-sulfo-propane
BPSP	3-bis(1-piperidino)-2-*O*-sulfo-propane
BS^-	Benzenesulfonate ion
BSH	Benzenesulfonic acid
$BTMA^+$	benzyltrimethylammonium ion
BTMAOH	Benzyltrimethylammonium hydroxide
CA	Carrier ampholyte
CAR	Carnosine

CD	Cyclodextrin
CE	Capillary electrophoresis
CE-ESI-MS	Capillary electrophoresis-Electrospray Ionization-Mass Spectrometry
cIEF	Capillary isoelectric focusing
CIP	*R,S*-Ciprofibrate
cITP	Capillary isotachophoresis
CTAB	Cetyltrimethylammonium bromide
cZE	Capillary zone electrophoresis
DDAB	Didodecyldimethylammonium bromide
DEBA	Bisphenol A diglycidyl ether
DLPC	1,2-dilauroyl-*sn*-phosphatidylcholine
DMF	Dimethylformamide
DMSO	Dimethylsulfoxide
EOF	Electroosmotic flow
EW	Egg white
GLOB	Ovoglobulin
GLU	Glutamic acid
HBMMB	4-hydroxy-3,5-bis(morpholinomethyl) benzoic acid
HDMS-β-CD	Heptakis-(2,3-dimethyl-6-sulfo)-β-cyclodextrin
HEC	Hydroxyethylcellulose
HIS	Histidine

HMMB	4-hydroxy-3-methylmorpholino benzoic acid
HPLC	High performance liquid chromatography
HPMC	Hydroxypropylmethylcellulose
ID	Internal diameter
IDA	Iminodiacetic acid
IEC	Ion exchange chromatography
IEF	Isoelectric focusing
IET	Isoelectric trapping
IN-R	Initiator-monomer radical or initiator-polymer radical
IPG	Immobilized pH gradient
IQ^2	IsoelectriQ^2
IS	Ionic strength
LAB	Labetalol
LYS	Lysine
LYZ	Lysozyme
MABA	Meta-amino benzoic acid
MBA	*N,N'*-methylenebis(acrylamide)
MeLYS	Methyl lysine
MCE	Multicompartmental electrolyzer
MUC	Ovomucoid
NAP	*R,S*-Naproxen
PAA	Polyacrylamide

PAEM	Poly(aminoethylmethacrylate)
PAGE	Polyacrylamide gel electrophoresis
PDADMAC	Poly(diallyldimethylammonium)
PDMA	Poly(*N,N*-dimethylacrylamide)
PEG	Poly(ethylene glycol)
PEI	Polyethyleneimine
PEMEDA-β-CD	Mono(6-deoxy-6-*N,N,N',N',N'*-penta-methylethylene-diammonio)cyclomaltoheptaose
PreMCE	Pressure mediated capillary electrophoresis
PVA	Poly(vinyl alcohol)
PVAC	Poly(vinyl acetate)
PVP	Poly(vinylpyrrolidone)
QDAA	*N,N*-bis(carboxymethyl)dimethylammonium hydroxide inner salt
QDBA	*N,N*-bis(carboxypropanyl)diethylammonium hydroxide
RSD	Relative standard deviation
SDS-PAGE	Sodium dodecylsulfate-polyacrylamide gel electrophoresis
TEMED	*N,N,N',N'*-tetramethyl-ethylenediamine
THAM	Tris-(hydroxymethyl) aminomethane
TRANS	Ovotransferrin
TYRA	Tyramine
UFSC	Untreated fused silica capillary

UV	Ultraviolet
2DE	2-dimensional electrophoresis

1 INTRODUCTION

1.1 Preparative-scale protein separations

The isolation, identification, and preparative-scale processing of amino acids, peptides and proteins are of major interest in the field of proteomics, clinical diagnostics, production of biopharmaceuticals, and life sciences research in general. Finding protein biomarkers that signal malfunction of cells or tissues might help the early detection and diagnosis of diseases, as well as the search for new targets in the development of new drugs [1].

The aim of analytical protein separations is only to identify and quantitate the protein of interest. Preparative protein separations, on the other hand, aim at isolating a certain amount of purified component and using it for a further goal. This goal may include further downstream analysis of the isolated compound, online or offline, or use as a product (*e.g.*, pure reagent or pharmaceutical). In both cases, the concern of the preparative separation is always to produce as concentrated a fraction as possible through the fastest, most cost-effective way that guarantees a contaminant-free material [2].

This dissertation follows the style of *Electrophoresis.*

Chromatography and electrophoresis are important methodologies in the preparative-scale separation of proteins. The most frequently used preparative-scale chromatographic protein separation techniques include gel permeation chromatography (which exploits size differences), ion exchange chromatography and chromatofocusing (which exploit charge and isoelectric point differences), reversed-phased liquid chromatography (which exploits hydrophobicity differences) and affinity chromatography (which exploits differences in the nature and topology of the binding groups) [2-4].

In ion exchange chromatography (IEC), the relative adsorption affinities for most pairs of proteins differ the most when the salt concentrations in the eluents are low [5]. In IEC, however, proteins are eluted with a salt gradient that can reach quite high salt concentration levels. According to Yamamoto [5], the resolution of proteins in IEC is highest when the pH of the liquid phase is near the p*I* of the proteins being separated. However, IEC performed with a salt gradient typically employs a fixed pH eluent, precluding the possibility to operate the process near the p*I* of each protein [6].

Chromatofocusing [6-10] helps mitigate some of the limitations of IEC. In chromatofocusing, a pH gradient that moves through the ion-exchange column is formed and allows for the elution of proteins at a low ionic strength (IS), at pH values that are near to their p*I* values. However, chromatofocusing separations are typically limited to the $4 < pH < 9$ range.

The differences in the charge-to-size ratios, acidities, basicities and isoelectric points of proteins can often be exploited in electrophoretic separations better than in chromatographic separations. Just like chromatographic separations, electrophoretic separations can also be implemented as analytical and preparative-scale separations. Separations that utilize a focusing mechanism, such as isoelectric focusing are more suitable for preparative purposes. Isoelectric focusing (IEF) separations can be achieved either in pH gradients created by carrier ampholytes (CAs) in gels or in capillaries, or in immobilized pH gradients (IPGs). Proteins differing only by 0.001 in their p*I* values have been separated by IEF [11, 12]. Unfortunately, Joule heat dissipation in gels and IPG strips is poor; this limits their preparative utility.

1.2 Preparative-scale IEF protein separations

Since Joule heat removal from free solution is more efficient than from gels, free solution IEF techniques are more suitable for preparative protein separations.

1.2.1 Free solution IEF in a convection-limiting device

In 1976, Bours introduced an IEF instrument [13] that contained specially shaped separation chambers designed to mitigate the effects of convective mixing and permit IEF without the use of anti-convective media. The instrument had a lid with corrugations spaced 10 mm apart and 10 mm deep, and a corresponding base with similar corrugations. The sample (containing up to 1 g of protein), mixed in a solution of carrier ampholytes, was poured into the corrugations on the bottom plate. The lid was placed on

top, such that the corrugations formed inter-digitating projections and created a zig-zag shaped separation channel. The bottom plate was cooled. A vertical density gradient developed as the proteins focused into a given region: the denser protein solution concentrated at the bottom of the channel. It took more than two days to separate a 1-g protein load, and it was very difficult to monitor the separation because when the lid was lifted off to extract a sample, remixing occurred.

1.2.2 Free-zone IEF stabilized by rotation

In 1967, Hjerten found that the undesirable effects of convection could be mitigated by rotating a horizontal electrophoresis tube about its longitudinal axis [14], as shown in Figure 1.

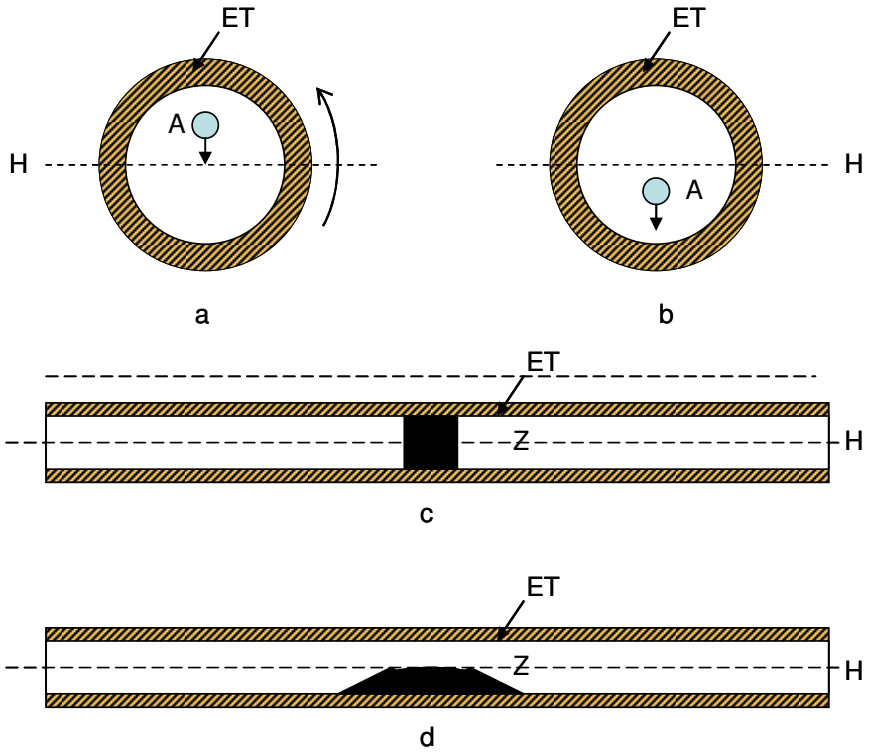

Figure 1. Stabilizing effect of rotation. ET: electrophoresis tube; H: horizontal plane; A: liquid element with a higher density than the background electrolyte; Z: sample zone. If only gravity and friction act upon A, A always goes downward. Thus, A moves away from the ET wall when it is in the upper half of the cross-section (a) and toward the ET wall when in the lower half (b). A is forced by the rotation of the tube to move to-and-fro *vis-à-vis* the tube wall, which results in zone stabilization. Once rotation is stopped, the sharp zone Z in (c) broadens rapidly as shown in (d). Figure redrawn from [14].

This idea was extended to IEF [15]: the ends of the separation tube were packed with polyacrylamide beads to prevent mixing of the carrier ampholytes with the solutions in the electrode compartments. This small instrument could handle only sample loads of up to 100 µg.

This design was scaled-up successfully to accommodate much higher protein loads. Rilbe in 1980 [16] applied this technique to his preparative multicompartmental

electrolyzer (MCE) that contained 46 separation compartments, with a total volume of about 7.6 L. The compartments were closed; internal cooling and stirring were achieved by periodic rotation of the whole apparatus in a tank filled with cold water. The apparatus was run with a power load of up to 5000 W. It took 3 days to completely separate the main components in 14 g of whey protein: serum albumin (p*I* 4.60), α-lactalbumin (p*I* 5.01), and β-lactoglobulin (p*I* 5.13-5.23), whereas the latter component was partially separated into its subcomponents A and B.

Another rotating IEF device, called the Rotofor (Figure 2) was introduced in 1983: a horizontal annulus was formed between a Plexiglas outer surface and a ceramic tube inner surface that rotate together, at about 1 rpm, as a single body [17]. The 15 cm long annulus was divided into twenty, 50-ml compartments along its longitudinal axis by polyester screens that discourage convective mixing between the compartments during a run. Up to about 1 g of protein could be processed in the Rotofor, in 4 to 6 hours, using 12-15 W of power [18].

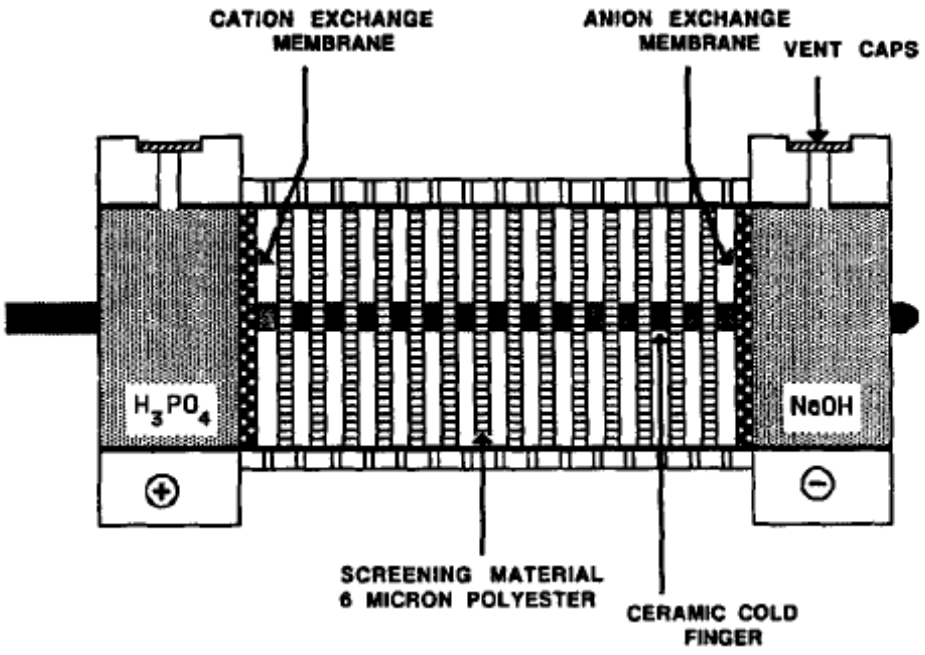

Figure 2. Schematic diagram of the Rotofor. Polyester screens act as anti-convective barriers for the focused zones [18].

Vertical rotational stabilization introduced in the late 1980s was further developed by Ivory in 2004 [17, 19] leading to a vortex stabilized IEF device (Figure 3). This device has a 30-cm long annular chamber created by a smaller diameter cylinder inside a larger diameter hollow cylinder. Counter-rotating fluid vortices created by rotating the smaller inner cylinder stabilize the aqueous medium in the annulus against natural convection and improve heat and mass transfer. The system can be operated at voltages of up to 20 kV, electric field strengths of up to 65 kV/m, and power densities of up to 10 MW/m^3.

The pH gradient is formed along the *z* axis of the annulus from carrier ampholytes or non-ampholytic buffers. The electrode compartments at the top and bottom of the annulus (separation column) are separated from the sample chamber by dialysis membranes to prevent bulk mixing. At the end of the separation, fractions can be withdrawn from the annulus, from the top down, into a 96-well tray *via* six electronically actuated microvalves. The current unit has an annular volume of about 25 mL and can be used to fractionate protein batches of up to 100 mg in about 5 hours.

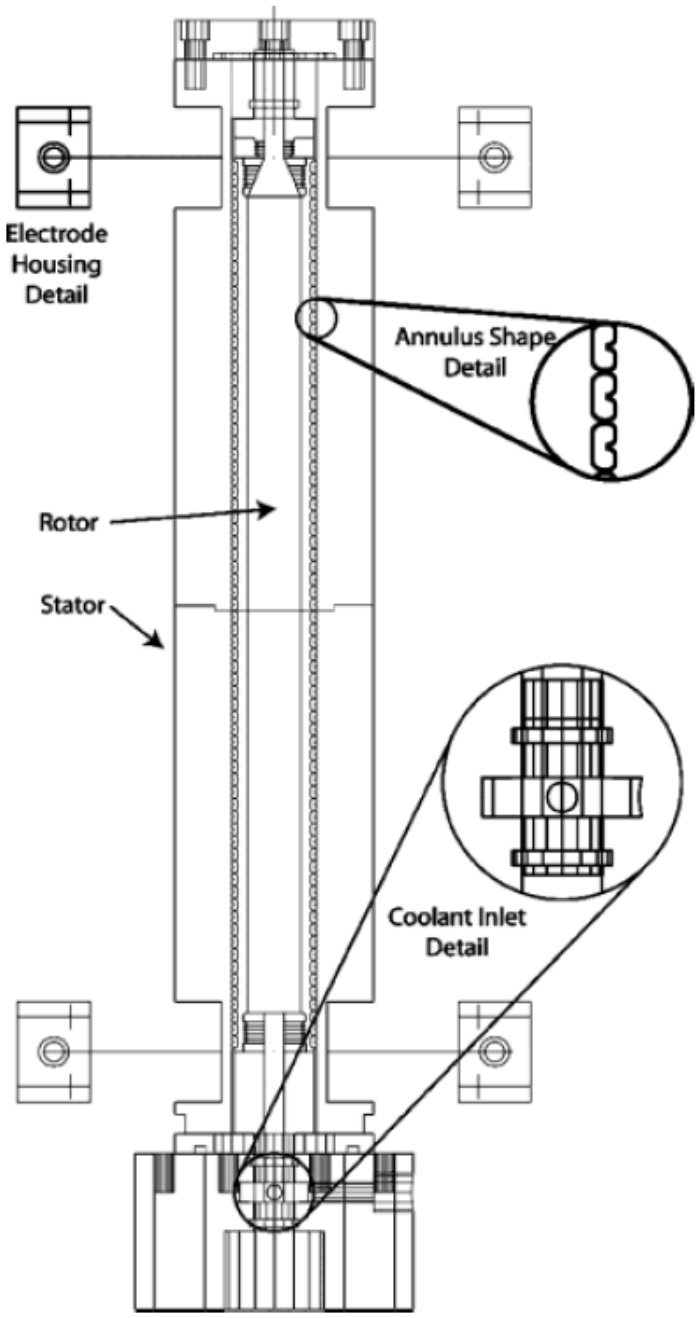

Figure 3. Schematic of the annular chamber rotor and stator. The coolant inlet assembly and one electrode housing are shown in detail. The annulus shape resembles a string of kidney beans connected by a short, narrow channel. The grooves were designed to have a tip-to-tip spacing roughly twice the rotor-to-stator spacing so that the vortex cells take the geometric form set by the shape of the rotor and the stator. Figure reproduced from [17].

1.2.3 Continuous free-flow IEF devices

The previously discussed devices can only be operated in batch mode, which limits the sample volumes that can be processed. In continuous free flow instruments the volume of the separation chamber does not limit the sample volume that can be processed, because the size of the external sample reservoirs can be varied as needed. A typical continuous, free-flow device, the Octopus [20-22] is shown schematically in Figure 4.

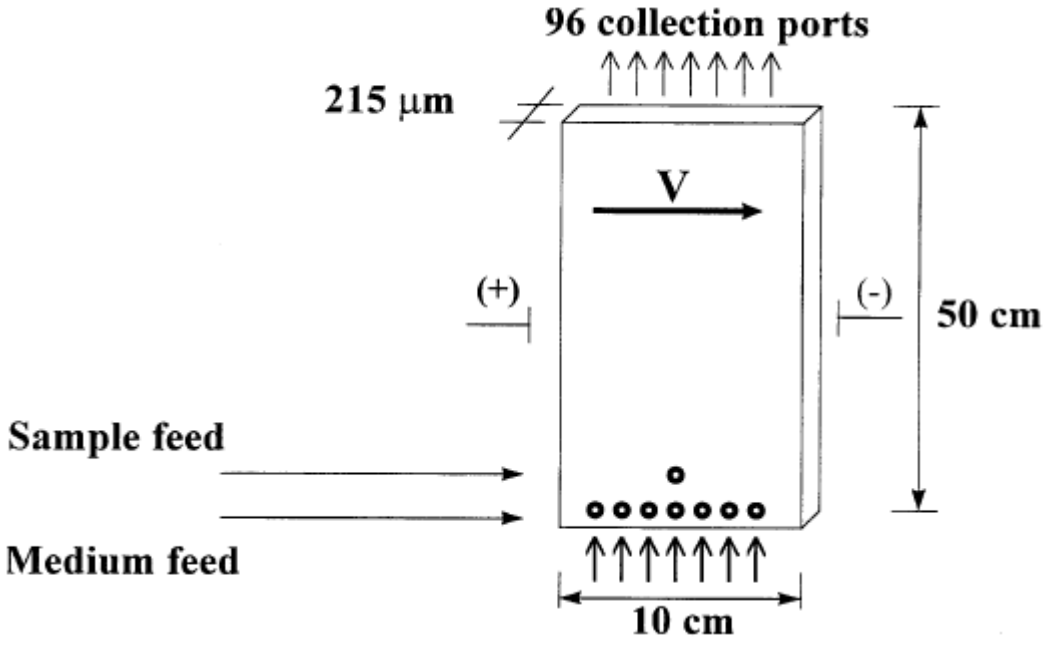

Figure 4. Schematic of the Octopus unit. Figure reproduced from [21].

The separation compartment in the Octopus unit is 55 cm long, 11 cm wide and 0.25 mm deep. The separation medium (carrier ampholyte solution) is introduced as a laminar stream at the bottom of the separation chamber; it leaves at the top end of the chamber through 96 outlet lines which drip into a 96 well plate, providing a 1 mm / channel lateral resolution. The flow direction is orthogonal to the direction of the electric field.

Though the long term stability and reproducibility of the separations achieved in the unit are satisfactory [23], production rates are low, because the rate of Joule heat dissipation is insufficient.

1.3 Limitations of the preparative-scale IEF separations

All IEF-based separations possess certain inherent limitations. Firstly, cathodic and anodic drift [24, 25] change the shape of the pH gradient over time: the pH gradient becomes flattened in the middle as the most acidic and basic ampholytes migrate out into the electrolyte compartments forcing the rest of the bands to become wider. This change in the shape of the pH gradient is particularly critical for longer separations. Secondly, the sample concentration has to be low, because protein solubility is low in isoelectric state. Thirdly, at the end of the IEF separation, the target proteins are still mixed with the carrier ampholytes and further separation is required to obtain a pure protein. The carrier ampholytes, which in fact act as contaminants also complicate downstream analysis (e.g., mass spectrometry) and often preclude the use of the isolated proteins in biological experiments. Finally, the high cost of carrier ampholytes hinders the large scale application of IEF.

1.4 Isoelectric trapping

Isoelectric trapping (IET) is an electrophoretic technique that has been introduced in the late 1970s to help solve some of the inherent problems of isoelectric focusing separations [26]. IET is normally carried in multicompartmental electrolyzers (MCEs)

[27], formed by a series of compartments separated by buffering membranes that permit passage of certain ions (both small and large), but prevent convective mixing of the contents of the adjacent compartments**.** The buffering membranes [26] form a stepwise pH gradient through the subsequent separation compartments: the lowest pH membrane is next to the anode, followed by membranes of increasing pH values and ending with the highest pH membrane next to the cathode. A schematic of a simple MCE is shown in Figure 5.

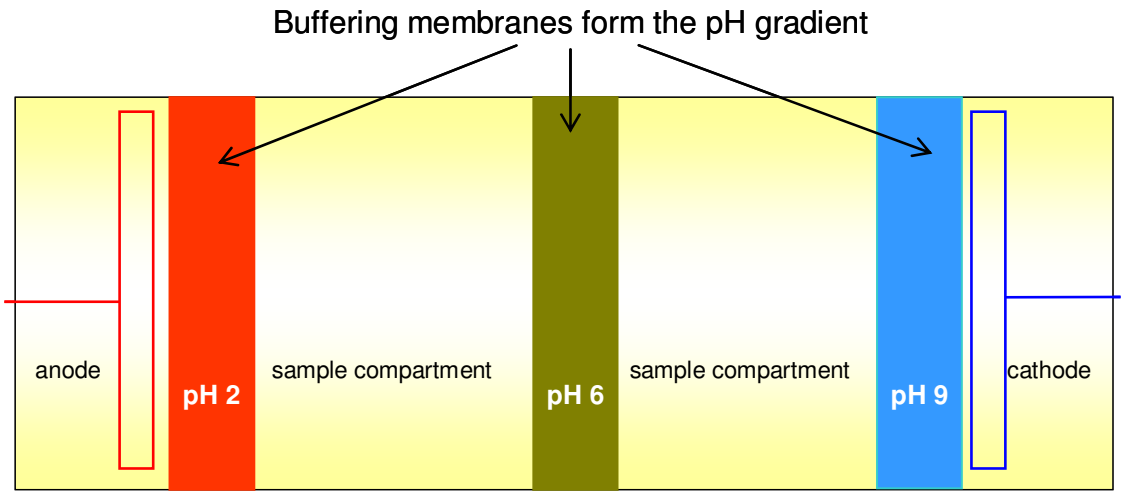

Figure 5. A schematic diagram of a simple MCE device.

Buffering membranes were first made by covalent attachment of –COOH groups (by binding chloroacetic acid) and different amounts of diethanolamine (*via* epichlorohydrin) to an agarose gel. Only 4.8 < pH < 5.5 membranes could be made with this technology [26]. Righetti copolymerized acrylamide, *N,N'*-

methylenebis(acrylamide) and acrylamido weak acids and acrylamido weak bases (Immobilines) to form hydrogels on glass fiber filters that could buffer over the $3 < pH < 10$ range [28-30]. The type, ratio and amount of weak acid and weak base incorporated into the hydrogel backbone dictate the pH and buffering capacity of the membranes [31, 32].

Polyacrylamide-based membranes, however, are not sufficiently stable either mechanically (usually, of single-use only) or hydrolytically (hydrolyze both in acidic and basic solutions). As alternatives, mechanically and hydrolytically more stable poly(vinyl alcohol)-based buffering membranes were recently developed [33-35]. Their pH can be regulated in the $1.7 < pH < 13$ range; they have been exposed to 1 M solutions of strong acids and 3 M solutions of strong bases. A schematic representation of the synthesis of PVA-based buffering membranes is shown in Figure 6.

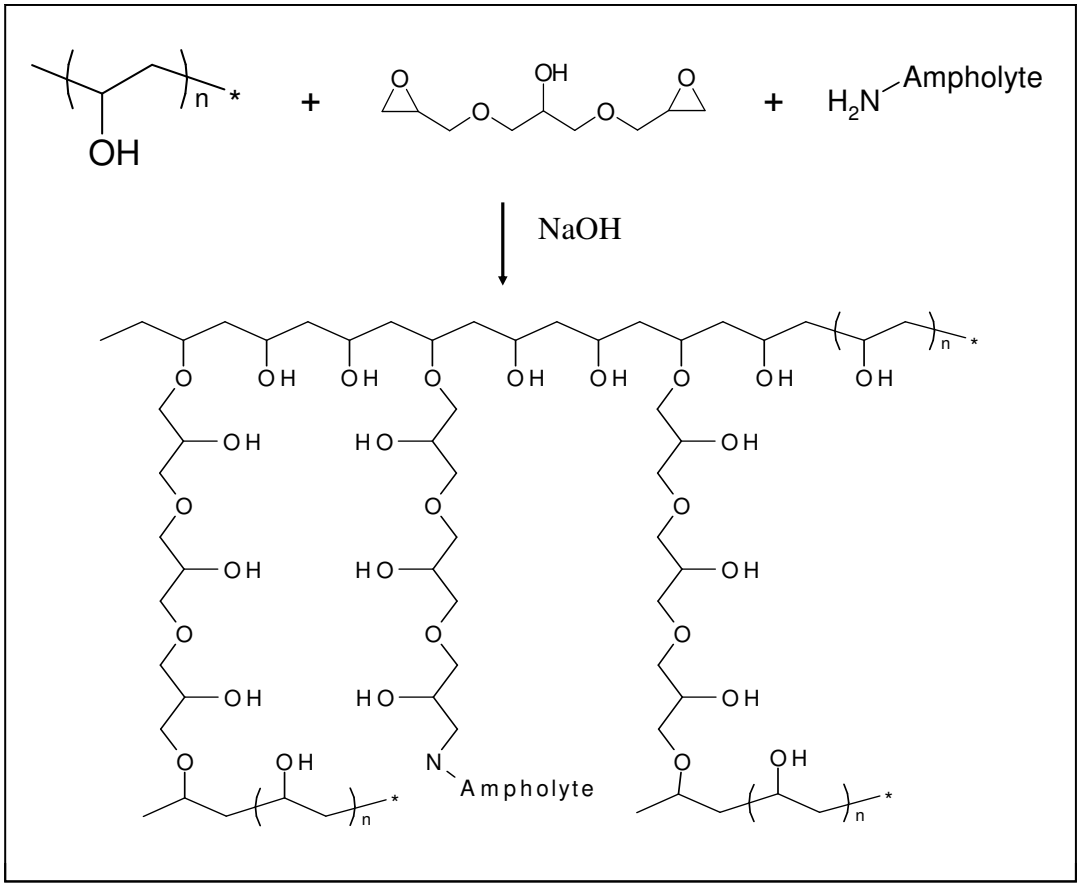

Figure 6. Schematic representation of the synthesis of a PVA-based buffering membrane.

Figure 7 is an example of a simple classical IET experiment in a serially arranged multi-compartmental electrolyzer. There are 4 compartments in the IET unit: 2 sample compartments in the middle, 2 electrode compartments at the ends. A stepwise pH-gradient is created (from anode to cathode) by the buffering membranes (pH 2, 6, and 9) that demarcate the compartments. In the diagram, the anolyte is a pH 1.5 solution; the catholyte is a pH 12 solution. The sample solution, containing p*I* 4 and p*I* 7 ampholytes is loaded into each sample compartment. Upon application of an electric field, the p*I* 7 ampholytes move toward the cathode, the p*I* 4 ampholytes move toward the anode. The p*I* 7 ampholyte from the anodic separation compartment can pass through the pH 6 membrane, because the ampholyte remains positively charged, but it cannot cross the pH 9 membrane, because it becomes negatively charged there. Similarly, the p*I* 4 ampholyte from the cathodic separation compartment can pass through the pH 6 membrane, because the ampholyte remains negatively charged, but it cannot cross the pH 2 membrane, because the ampholyte becomes positively charged there. Thus, the p*I* 4 component cannot leave the compartment that is bracketed by the pH 2 and pH 6 membranes, the p*I* 7 component cannot leave the compartment that is bracketed by the pH 6 and pH 9 membranes. In time, the separation is completed when all ampholytes of the same p*I* value are trapped in compartments bounded by buffering membranes with pH values that bracket the p*I* values of the said ampholytes [36].

A

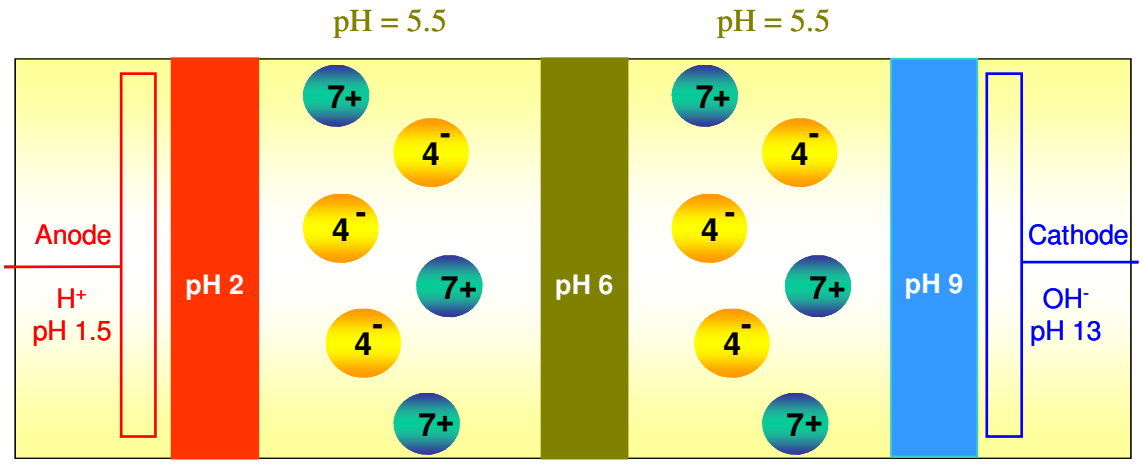

B

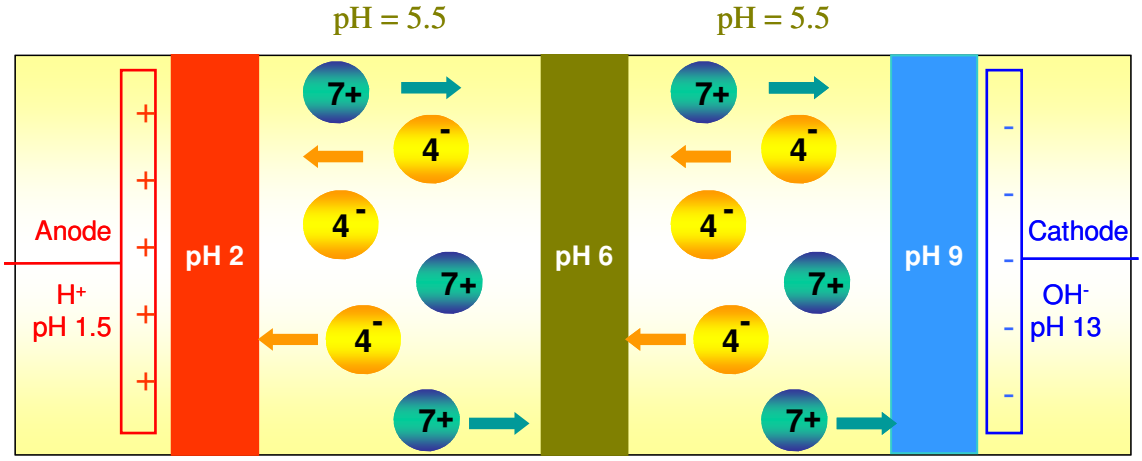

Figure 7. A schematic diagram showing a classical IET experiment: (A) initial set-up, solutions are loaded into the appropriate compartments; (B) electrical potential is applied and ampholytes start to migrate.

C

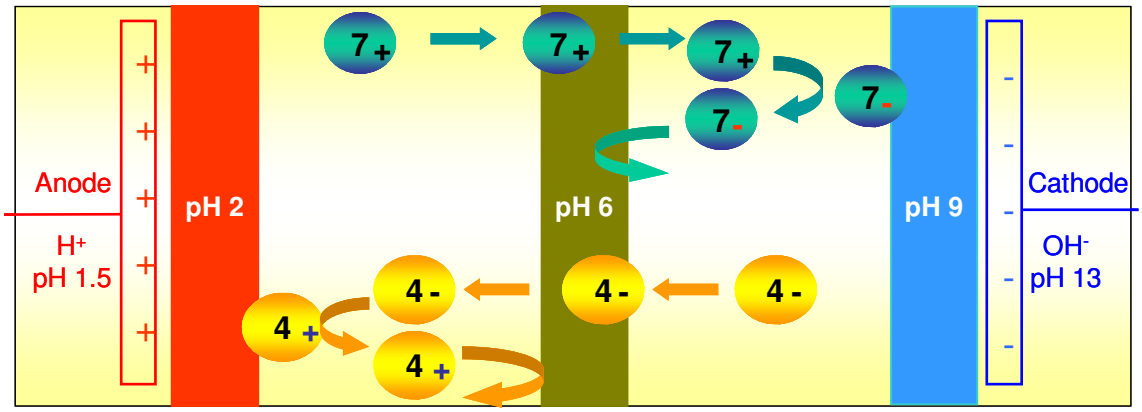

D

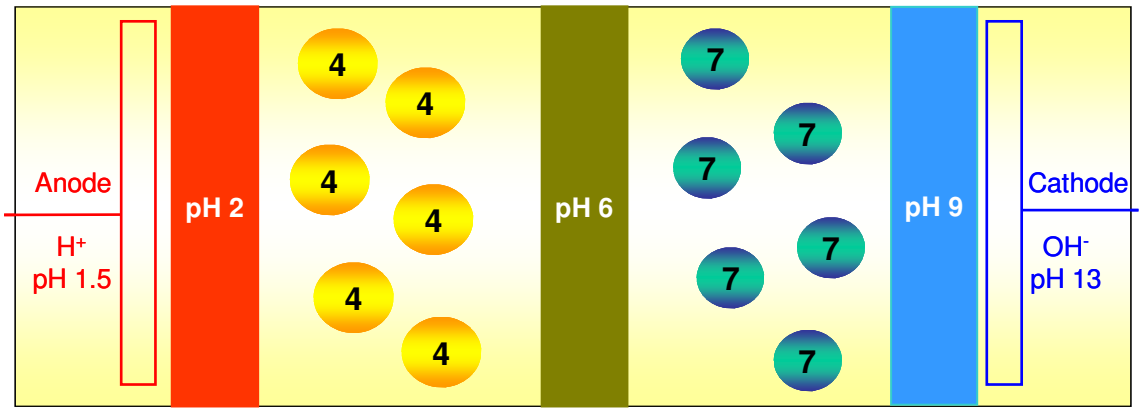

Figure 7. Continued. (C) separation continues as ampholytes traverse through the membranes and compartments by electrophoresis; (D) final conditions, where ampholytes are trapped in the compartments delimited by buffering membranes with pH values that bracket the p*I* value of the ampholytes. Figure reproduced from [37].

1.5 pH-biased isoelectric trapping

In classical IET, the closer the target ampholyte approaches its isoelectric state, the slower the mobility of the ampholyte becomes. This is particularly detrimental if the ampholyte has to travel through many compartments (long migration path) before reaching its final compartment. Moreover, the solubility of the ampholyte in its isoelectric state is low, which may result in aggregation and precipitation, especially for

proteins. Shave and Vigh realized that these inherent drawbacks of classical IET could be mitigated by maintaining the proteins in a charged state during the entire course of the separation; this notion led to the development of pH-biased isoelectric trapping [38]. In pH-biased IET, suitable auxiliary isoelectric agents, also referred to as "pH-biasers", are mixed with the protein solution. These auxiliary isoelectric agents are selected such that (i) they are trapped by the respective buffering membranes; (ii) their p*I* values are different from the p*I* values of the target proteins; (iii) the solubilities of the auxiliary agents are relatively high, even in their isoelectric state; and (iv) they have high buffering capacity, which occurs when $| pI - pKa | < 1.5$. The proteins are kept charged by the biasers throughout the entire course of the IET separation. This gives a two-fold advantage to pH-biased IET over classical IET: both the electrophoretic mobilities and the solubilities of the charged target proteins are higher than in their isoelectric states. Common amino acids that can be used as good auxiliary isoelectric agents include: iminodiacetic acid (approximate p*I* 2.2), aspartic acid (approximate p*I* 2.8), glutamic acid (approximate p*I* 3.2), histidine (approximate p*I* 7.6), methyl lysine (approximate p*I* 9.9), and arginine (approximate p*I* 10.6). Recently, two additional families of isoelectric buffers were synthesized: quaternary ammonium dicarboxylic acids [39] with p*I* values lower than 4.3 and diamino sulfates [40] with p*I* values greater than 5.7. Table 1 lists the currently available isoelectric buffers.

Table 1. Isoelectric buffers for use in pH-biased IET, and their approximate p*I* values [41].

Isoelectric buffer	p*I*
N,*N*-bis(carboxymethyl)dimethylammonium hydroxide, inner salt (QDAA)	~1.6
cysteic acid	1.8
iminodiacetic acid (IDA)	2.2
aspartic acid (ASP)	2.8
glutamic acid (GLU)	3.2
N,*N*-bis(carboxypropanyl)diethylammonium hydroxide (QDBA)	4.2
1,3-bis(4-morpholino)-2-*O*-sulfo-propane (BMSP)	5.6
histidine (HIS)	7.6
1,3-bis(*N*,*N*-dimethylamino)-2-*O*-sulfo-propane (BDMASP)	7.9
1,3-bis(*N*,*N*-dipropylamino)-2-*O*-sulfo-propane (BDPASP)	8.4
3-bis(1-piperidino)-2-*O*-sulfo-propane (BPSP)	8.7
methyl lysine (MeLYS)	9.9
tyramine (TYRA)	10.1
arginine (ARG)	10.6

1.6 Preparative-scale IET devices

1.6.1 Binary IET devices

A membrane-based preparative IET instrument known as the Gradiflow BF200IET [33, 34, 38, 42-44] was introduced in 2002. The Gradiflow BF200IET has only two sample compartments with a membrane-to-membrane distance of 1 mm and an anode-to-cathode distance of less than 8 mm. Thus, high field strengths can be achieved in the

system, which leads to high electrophoretic velocities, and ultimately, short separation times. Since the sample solution is recirculated from cooled external reservoirs, the volume of sample that can be processed can be varied, and Joule heating issues are mitigated. Figure 8 shows the schematic of the Gradiflow BF200IET. Protein separation rates of 360 mg/hour have been reported for the BF200IET [38].

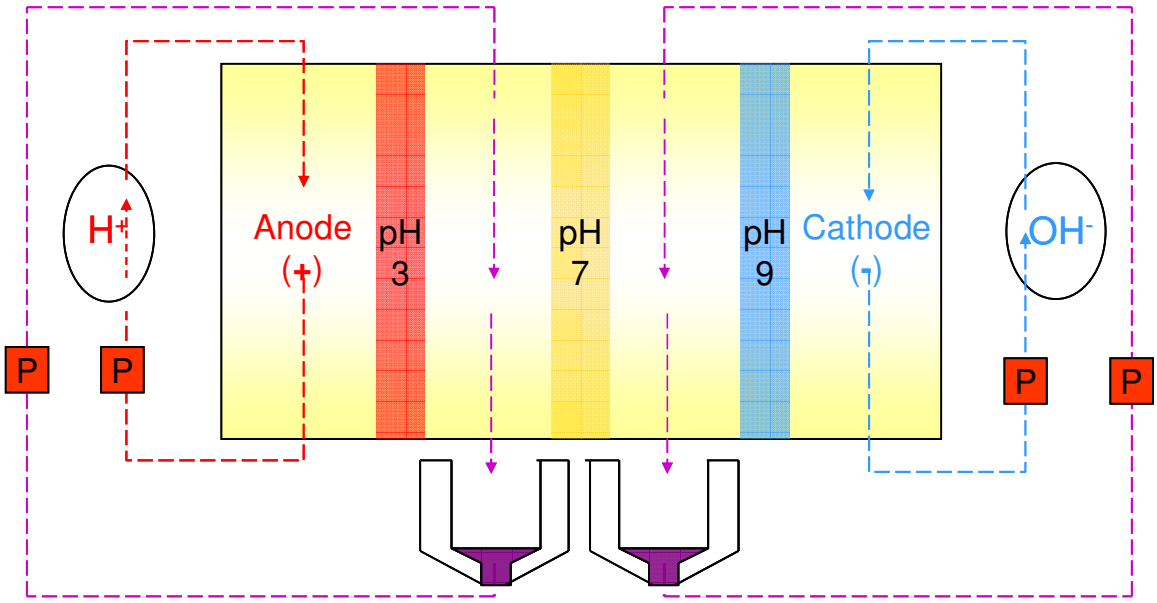

Figure 8. Schematic diagram of the Gradiflow BF200IET unit. Figure reproduced from [36].

Since there is only one separation membrane in the BF200IET, it can only be used to carry out binary separations. If an individual component is to be separated from a complex mixture, one must complete two sequential binary separations, using buffering membranes whose pH values differ slightly from each other. In order to eliminate this limitation, Shave and Vigh designed a new IET device called the Biflow [45]. The

Biflow contains two separation heads, connected to independent power supplies. The separation heads have the same optimized design as the Gradiflow BF200IET unit. Each head houses an anode and a cathode compartment, an anodic and a cathodic membrane, an anodic and a cathodic separation compartment, and a middle separation membrane. Figure 9 shows a schematic of the Biflow IET instrument.

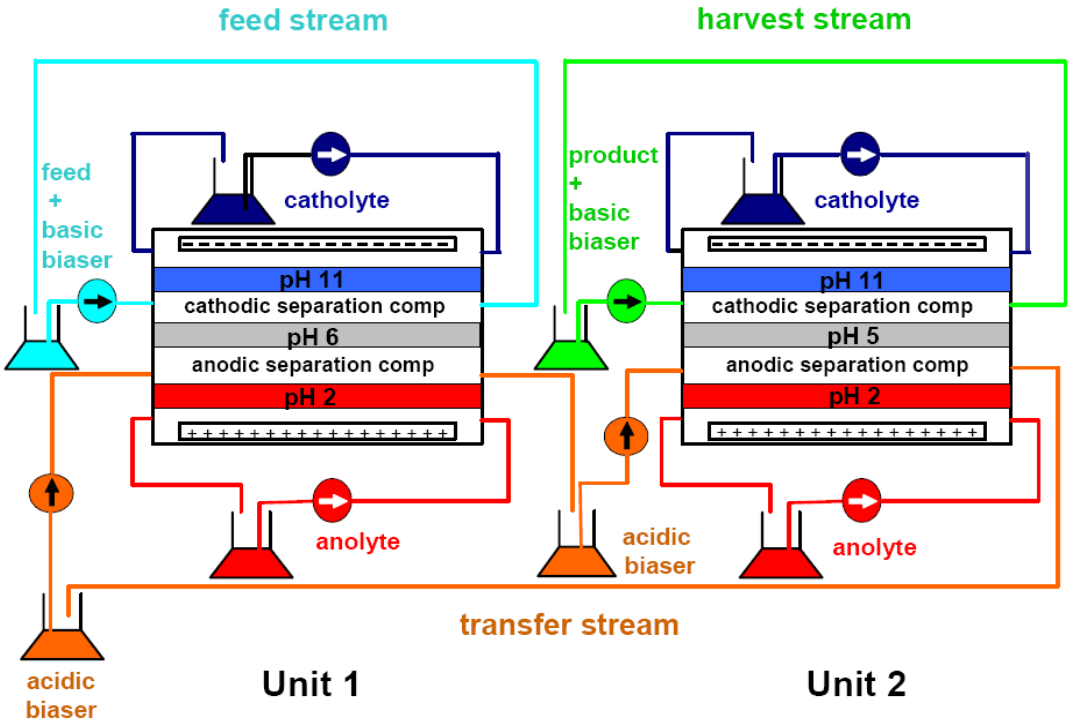

Figure 9. A schematic of the Biflow IET instrument. Figure reproduced from [45].

The electrode membranes in Units 1 and 2 typically buffer at the same pH value. The middle separation membranes in Units 1 and 2 buffer at different pH values. The pH spread of the separation membranes dictates the p*I* range (Δp*I*) of the product prepared. The cathodic separation compartment in Unit 1 contains the feed stream; the cathodic separation compartment in Unit 2 contains the harvest stream**.** A transfer stream travels

through both units. During a separation, the ampholytic components in the feed with p*I* values lower than the pH of the separation membrane in Unit 1 pass into the transfer stream and are shuttled into Unit 2 through an electrically insulating air-gap. In Unit 2, components with p*I* values higher than the pH of the separation membrane pass into the harvest stream. This principle of double, oppositely directed component transfer, which replaces the principle of exhaustive electrophoresis [46, 47] (where it takes a very long time to remove the last traces of contamination), results in a contamination-free product in the harvest stream.

1.6.2 Multicompartmental IET devices

The preparative IET instruments discussed above can only separate a complex mixture into two parts (BF200IET) or produce a single, pure component (BiFlow). Often, it would be desirable to obtain multiple, pure components from a complex feed mixture. The objective of the multicompartmental IET devices is to achieve such separations.

The ZOOM® Fractionator (Figure 10) was developed by Zou and Speicher, and released commercially by Invitrogen (Carlsbad, CA) [48, 49]. The sample compartments of the ZOOM are made of Teflon. Each compartment has a 0.5 cm center-to-wall distance and holds 0.64 mL solution. The length of each compartment (*i.e.*, the approximate inter-membrane distance) is 1.4 cm. The anode-to-cathode distance is 20 cm. The device can be used to obtain, simultaneously, up to 7 fractions. However, due to poor dissipation of Joule heat, the maximum electric power that can be applied is limited to 1 watt. The

device has been used to prefractionate, in 4 hours, up to 50 mg of *E. coli* lysate prior to two-dimensional gel electrophoretic analysis [48].

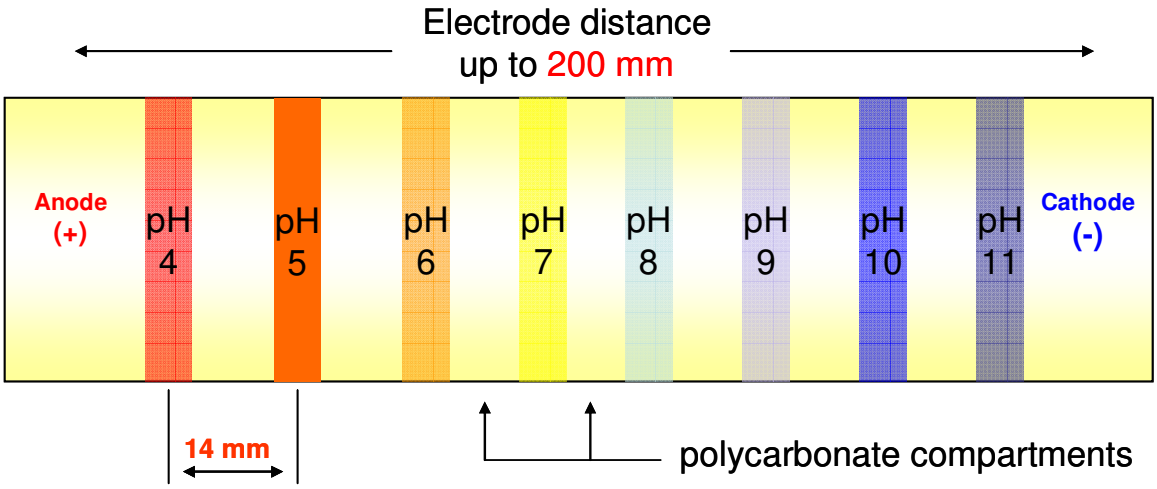

Figure 10. A schematic diagram of the ZOOM® Fractionator. Figure reproduced from [50].

A similar MCE instrument, called the IsoelectriQ^2 (IQ^2) was developed by Proteome Systems (Sydney, Australia) [49, 50]. It can hold up to 7 polycarbonate compartments, each one with an inter-membrane distance of 2.2 cm and a volume of 5 ml. The anode-to-cathode distance is 22.2 cm [51, 52]. The sample solution is constantly agitated with magnetic stir bars located at the bottom of each compartment to provide mixing and improved Joule heat removal. A protein load of 5-50 mg is recommended. Separations are usually done in 24-48 hours, with a maximum power of 1 watt. A schematic diagram of the MCE used in the IQ^2 system is shown in Figure 11.

The plastic materials (Teflon for the ZOOM, and polycarbonate (Lexan) for the IQ^2) limit the power that can be used for the separation, because these materials do not facilitate efficient heat transfer. This leads to a long fractionation time.

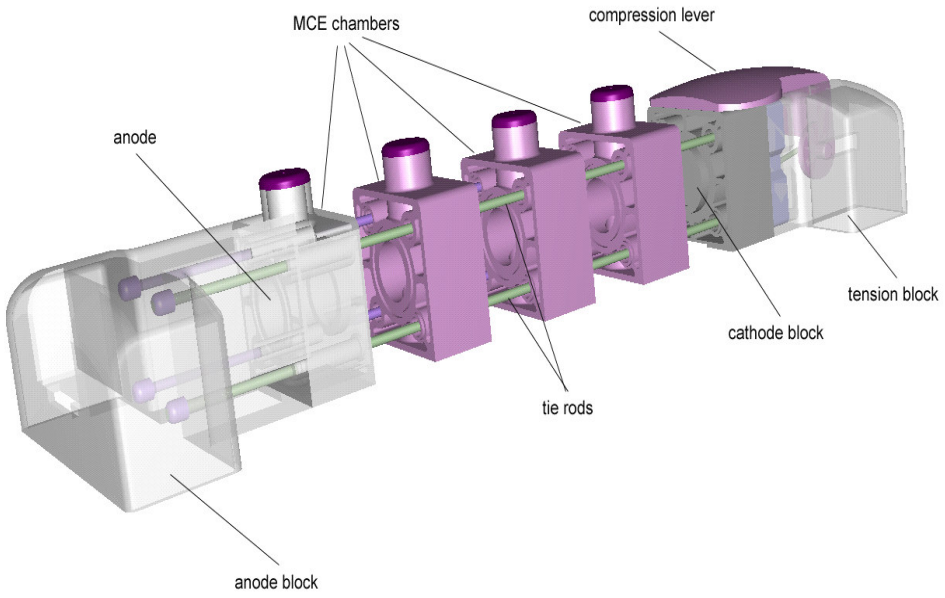

Figure 11. A schematic diagram of the MCE used in the IQ^2 system. Figure reproduced from [49].

The Isoprime (Fig. 12) [53, 54] is an IET instrument made with a variable number of compartments. Each sample compartment holds about 5 ml solution. A larger volume sample can be processed by recirculating the solutions through the separation compartments from outside reservoirs. The Isoprime proved that preparative-scale IET separations are feasible; however, the system had significant drawbacks that affected the rate of separation. The relatively large separation compartments resulted in a membrane-to-membrane distance of 10 mm, which caused long separation times.

Moreover, since the Isoprime can have up to eight separation compartments, each 10 mm in length, the anode-to-cathode distance is long. Consequently, very high potentials have to be applied to maintain high field strengths. The maximum power, however, that can be applied to the system is limited by the rate with which Joule heat is dissipated. Therefore, the long inter-membrane distance, combined with the limited field strength that can be applied result in long separation times (up to 24 hrs for 10-100 mg proteins).

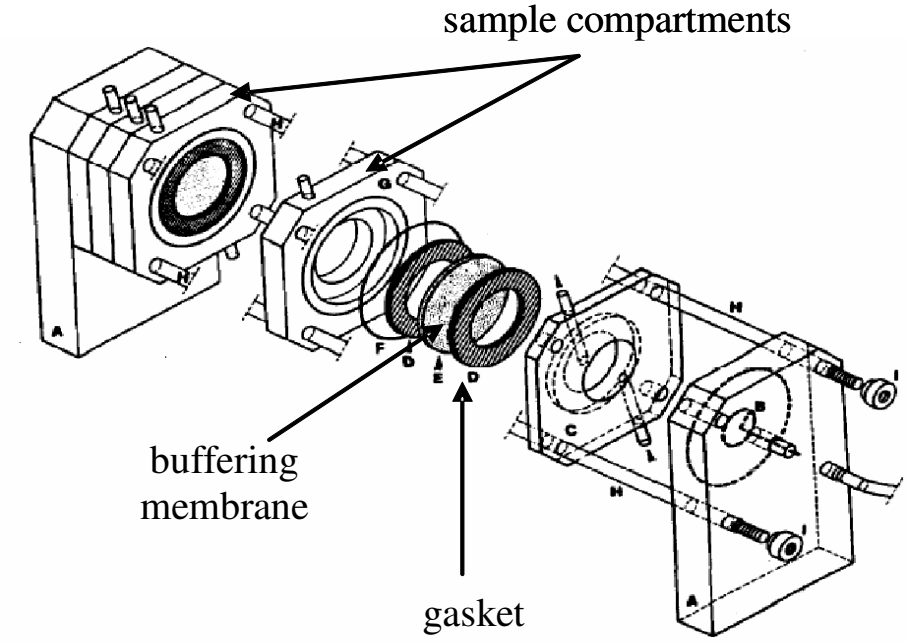

Figure 12. The IsoPrime preparative MCE. Anode-to-cathode distance is up to 100 mm. Figure reproduced from [53].

1.6.3 A multicompartmental electrolyzer for size-based electrophoretic separations

A multicompartmental electrolyzer, the MEDUSA was designed to carry out size-based and charge-sign based fractionation of proteins [55]. The separation unit contains the anode and cathode compartments and up to twelve separation compartments (Figure 13).

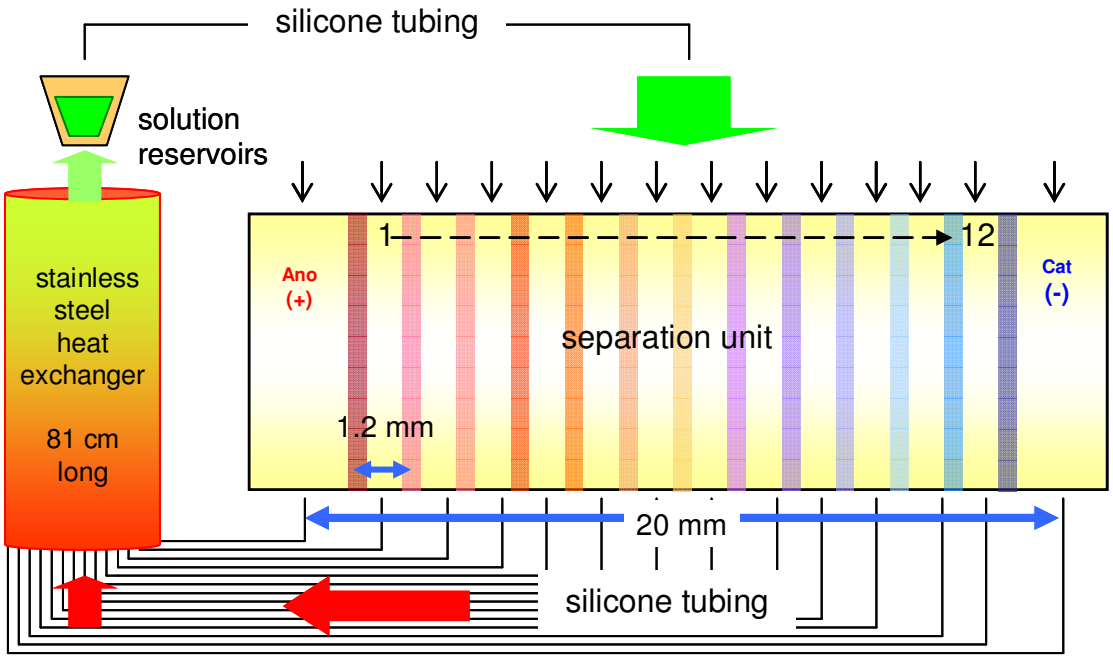

Figure 13. A schematic diagram of the MEDUSA.

The electrode compartments and separation compartments are formed by grids (Figure 14), each about 1.2 mm thick, and polyacrylamide membranes that are as thin as 0.15 mm and have nominal permeation limits ranging from 5,000 Da to 800,000 Da. Silicone gaskets are used to provide a seal between the electrode compartments and the separation unit. The anolyte, catholyte and sample solutions are recirculated through the compartments from outside reservoirs through an 81-cm long stainless steel cooling cylinder that is located in front of the separation unit.

The exploded view of the unit is shown in Figure 15. An electric field orthogonal to the flow direction drives the sample components across the polyacrylamide separation membranes.

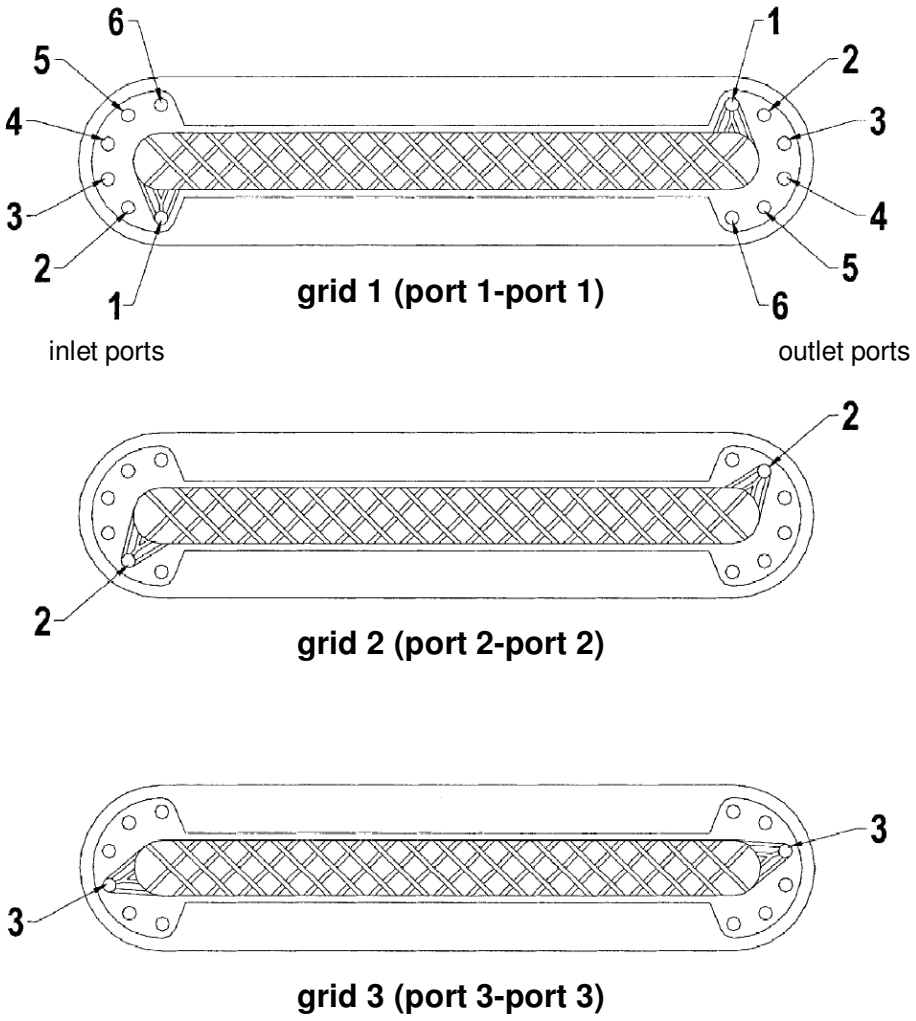

Figure 14. The MEDUSA grids that provide support for the separation membranes and form the separation compartments. Figure reproduced from [55].

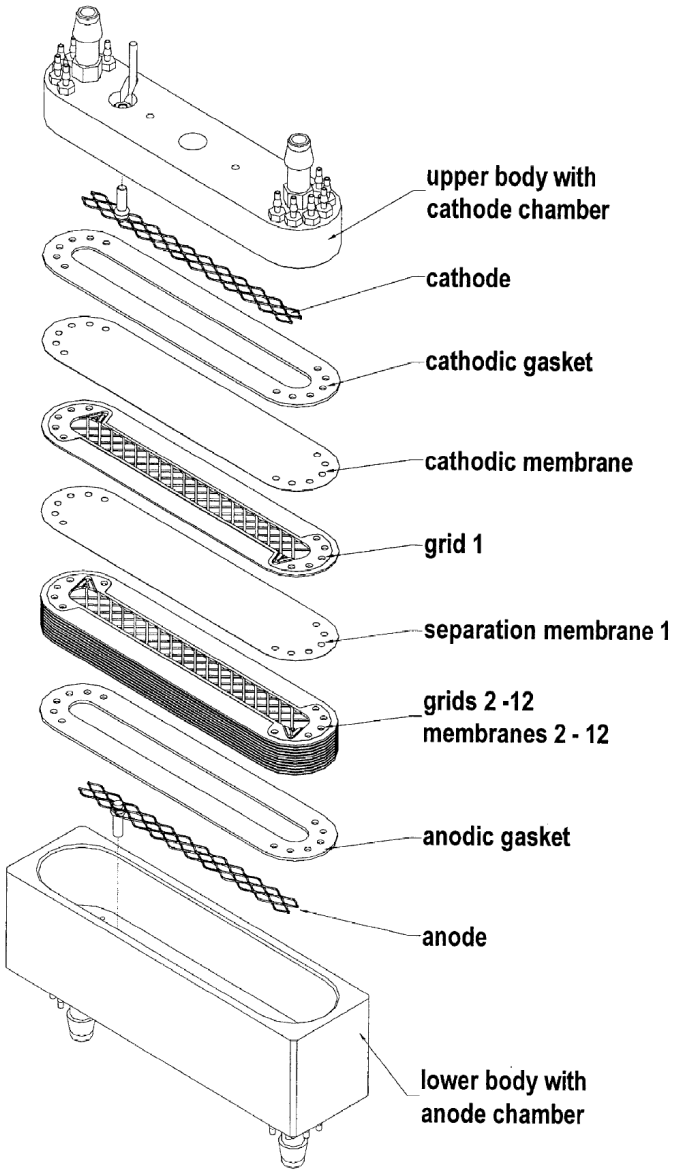

Figure 15. Exploded view of the MEDUSA separation unit. Figure reproduced from [55].

We realized that the MEDUSA instrument could also be utilized for the IET separation of multiple components in a single run, similarly to the operation of the Isoprime. However, it had to be redesigned to meet the needs of IET, including the elimination of pressure-driven flow across the membranes and improvement of Joule heat removal.

1.7 Surface-modified capillaries for capillary electrophoretic analysis of the fractions produced by IET

Overall success of the preparative-scale separations critically depends on the availability of analytical methods that can be used to monitor the quality of the preparative separation. For electrophoretic preparative separations, capillary electrophoretic (CE) methods, including isoelectric focusing (cIEF), zone electrophoresis (cZE) and isotachophoresis (cITP), with or without mass spectrometric detection (CE-ESI-MS), are the most appropriate monitoring methods.

CE separations are carried out mostly in fused silica capillaries. There are four to five silanol groups per nm^2 on the hydrated silica surface [56, 57], their pK_a values range from 2 to 9 [57]. As the pH of the background electrolyte (BGE) is increased, the silanol groups dissociate and create fixed negative charges on the surface. These charges lead to the formation of a double layer of counter-ions: an inner Stern layer and an outer Gouy – Chapman layer. When the separation potential is applied across the capillary, cations in the diffuse Gouy – Chapman layer move towards the cathode, bring along

their hydrate layer and create a bulk flow, called the electroosmotic flow (EOF), in the capillary [58]. If the fixed charges on the inner wall of the capillary are positive, then an EOF towards the anode is observed.

In 1969 Giddings predicted [59] and in 1981, Jorgenson and Lukacs experimentally verified [60] that peak resolution in CE, defined as

$$R_S = \frac{1}{2}\frac{abs(t_2 - t_1)}{\sigma_2 + \sigma_1} \qquad (1)$$

where t_1 and t_2 are the migration times and σ_1 and σ_2 are the peak widths at 61 % of the peak height for analytes 1 and 2, vary with the magnitude of the EOF as

$$R_s = 0.177\left(\mu_1^{eff} - \mu_2^{eff}\right)\left(\frac{V}{D_{AV}\left(\mu^{AV} + \mu^{EOF}\right)}\right)^{1/2} \qquad (2)$$

where μ_1^{eff} and μ_2^{eff} are the effective mobilities of analyte 1 and 2, μ^{AV} is their average mobility, D_{AV} is their average diffusion coefficient, μ^{EOF} is the mobility of the electroosmotic flow, and V is the applied potential.

Thus, whenever μ_1^{eff} and μ_2^{eff} are not equal, the magnitude of R_s can be increased or decreased, as needed, by controlling the magnitude of μ^{EOF}. This dependence is true with the assumption that peak dispersion is caused only by longitudinal diffusion, such that time-based peak variance is:

$$\sigma^2 = \frac{2Dt}{\left(\mu^{obs} E\right)^2} \qquad (3)$$

where L_D is the length of the capillary from the injector to the detector, E is the field strength, and μ^{obs} is the observed mobility of the peak.

If separation selectivity, α, is defined as:

$$\alpha = \frac{\mu_1^{eff}}{\mu_2^{eff}} \tag{4}$$

where the effective mobility of a component, μ^{eff}, is calculated from the observed mobility, μ^{obs}, and μ^{EOF} as:

$$\mu^{obs} = \mu^{eff} + \mu^{EOF} \tag{5}$$

and if the normalized EOF mobility, β, is defined as:

$$\beta = \frac{\mu^{EOF}}{\mu_2^{eff}} \tag{6}$$

where μ_2^{eff} is the mobility of the slower analyte, then the peak resolution equation for an analyte pair becomes [61]:

$$R_s = \left(\frac{EL_D}{8}\right)^{1/2} \frac{abs(\alpha-1)(\alpha+\beta)^{1/2}(1+\beta)^{1/2}}{(\alpha+\beta)^{3/2}(D_2)^{1/2}+(1+\beta)^{3/2}(D_1)^{1/2}} \left(\mu_2^{eff}\right)^{1/2} \tag{7}$$

Whenever $\alpha \neq 1$ and β approaches -1, R_s approaches infinity. Thus, by effectively controlling β, through the precise control of μ^{EOF}, one can optimize peak resolution.

According to Smolukowsky [62]:

$$\mu^{EOF} = \frac{-\varepsilon\psi_0}{\eta} \quad (8)$$

where ε is the electrical permittivity of the solvent, ψ_0 is the electrical potential in the shear plane at the capillary-solution interface, and η is the viscosity of the solution. ψ_0 is related to the surface charge density, σ^*, as:

$$\sigma^* = \varepsilon\kappa\psi_0 \quad (9)$$

where κ is the inverse of the double layer thickness that depends on both ε and the ionic strength of the solution. Thus, Equation 4 can be written in terms of the surface charge density as:

$$\mu^{EOF} = \frac{\sigma^*}{\kappa\eta} \quad (10)$$

or

$$\mu^{EOF} = \frac{\kappa^{-1}\sigma^*}{\eta} \quad (11)$$

According to Eq. 11, the magnitude of μ^{EOF} can be controlled by manipulating either the thickness of the double layer, κ^{-1} (by changing the ionic strength of the BGE), the viscosity of the BGE, η (by adding a polymer to the BGE), or the charge density on the capillary wall, σ^* (by controlling the degree of dissociation of the silanol groups or by depositing charged groups onto the surface) [63].

Fujiwara and Honda decreased the magnitude of μ^{EOF} by increasing the ionic strength of the BGE which reduced the thickness of the double layer (κ^{-1}), and by adding an organic

modifier which decreased the permittivity *(ε)* of the BGE [64, 65]. Both measures had undesirable side effects: the higher ionic strength of the BGE worsened the Joule heating effects, which mandated the use of lower field strengths and resulted in lower R_s values, while the presence of organic solvents in the BGE hurt the solubility of their ionic analytes.

Herren [66] and Mazzeo [67] suppressed the EOF by adding soluble polymers, such as methylcellulose to the BGE to increase its viscosity (η). However, there was no net gain in R_s, because the effective mobilities of the analytes also decreased commensurably [68].

The bulk of the efforts focused on finding techniques that altered the surface charge density (σ^*) on the capillary wall by depositing (i) noncharged (neutral) moieties to suppress the EOF, or (ii) positively or negatively charged moieties to generate a desired EOF. Deposition was achieved either by adsorbing appropriate molecules (*e.g.*, alkylamines, surfactants, or polymers) [69-74] or by covalently attaching a polymer network [14, 57, 66, 68, 75-79] to the inner capillary wall.

1.7.1 Surface modification by adsorbed molecules

The surface modifiers can be deposited either dynamically or statically. Though the adsorbed molecules alter μ^{EOF}, their surface concentration typically cannot be varied at will to tune the magnitude of μ^{EOF}. In the dynamic mode, the additive molecules are

always present in the BGE and are adsorbed onto the surface in a dynamic equilibrium [80]. In the static mode, the capillary is rinsed, prior to CE analysis, with a solution that contains the adsorbing molecules to saturate the wall; the adsorbing molecules are not present in the actual BGE. The adsorbed agents can be small molecules [81-85], surfactants [86-92] or polymers [70, 93-100].

1.7.1.1 Small molecules as adsorbed agents

A wide variety of amines have been employed as BGE additives to reduce or reverse the EOF (and to reduce the extent of protein adsorption). Oligoamines, such as spermine and tetraethylenepentamine [84] interact strongly with the silanols groups on the capillary wall, thus, at sufficiently high concentrations, they can reverse the sign of the surface potential and the direction of the EOF.

1.7.1.2 Surfactants as adsorbed agents

Cationic surfactants such as cetyltrimethylammonium bromide (CTAB), didodecyl-dimethylammonium bromide (DDAB), and 1,1,2,2-tetrahydroperfluoroalkylpyridinium chloride reverse the sign of the surface charge, and thus, reverse the direction of the EOF. Atomic force microscopy (AFM) studies [89] found that CTAB (a surfactant that contains a single long alkyl chain) forms spherical aggregates on the silica wall, while the double-chained surfactant DDAB forms a uniform bilayer that covers the entire surface. Thus, DDAB inhibits the adsorption of cationic proteins more effectively than CTAB, but it interferes with the separation of anionic proteins. Anionic and cationic

surfactants tend to be strongly denaturing, this limits their utility when the native conformation of proteins need to be maintained during CE analysis [101]. Zwitterionic surfactants, such as 1,2-dilauroyl-*sn*-phosphatidylcholine (DLPC), a double-chained phospholipid were recently employed to form smooth bilayers as statically adsorbed coatings. As a zwitterion, DLPC binds neither the acidic nor the basic proteins.

1.7.1.3 Polymers as adsorbed agents

Both uncharged and charged polymers can be used as polymeric adsorbed agents. Uncharged, hydrophilic poly(vinyl alcohol) (PVA), hydroxypropylmethylcellulose (HPMC), hydroxyethylcellulose (HEC) and dextran have been tested as EOF suppressants during the separation of basic proteins [95]. They proved to be ineffective as dynamic coatings above pH 5. Though more hydrophobic polymers such as poly(vinylpyrrolidone) (PVP) or poly(*N,N*-dimethylacrylamide) (PDMA) formed more stable adsorbed coatings, they interacted with the hydrophobic regions of proteins [70, 102, 103].

The majority of the charged polymeric agents used for control of the EOF are cationic polymers. Polybrene and polyarginine have created anodic EOFs and were used for the efficient separation of basic proteins [99], but the polyarginine coating was only stable in the $4 < pH < 9$ range. The polyethyleneimine (PEI) coating was stable over a wider

pH range: 3 < pH < 11, but it was adsorbed irreversibly on the silica wall and led to poor separation efficiencies [43].

If an anionic surface is required for the analysis, the adsorbed coatings are employed in successively deposited multiple ionic layers. A polycation, such as Polybrene is first deposited on the negatively charged silica surface to form a base layer. Then, a polyanion, such as dextran sulfate is deposited onto the base layer to create a negatively charged surface [101, 104].

The adsorbed coatings are temporally unstable and the coatings are not sufficiently reproducible, thus their utility is limited. Their presence in the BGEs may interfere with the CE separation itself, or with further downstream analysis, such as mass spectrometry [79].

1.7.2 Surface modification by covalently attached polymers

The covalently attached polymeric coatings protect the silica matrix against chemical attack by the BGE, shield the silanol groups and hinder the undesirable analyte - silica surface interactions [105]. Polymeric coatings can be obtained by covalent attachment of a pre-formed polymer to the wall or by *in situ* creation of a polymer. Pre-formed polymers are introduced into the capillaries as viscous solutions and are grafted to the wall through appropriate reactive groups. Alternatively, a thin layer of the pre-polymer

is deposited onto the wall, then the film is thermally or chemically crosslinked to immobilize it.

In situ coating methods usually involve three steps: (i) pretreatment of the silica surface, (ii) attachment of reactive groups to the silica surface (intermediate layer), and (iii) incorporation of the reactive surface groups into the polymer that is formed from monomers that fill the capillary. Like the adsorbed coatings, the covalently attached coatings can also be noncharged (neutral) or charged (anionic or cationic) to bring about the desired μ^{EOF} value.

1.7.2.1 Covalently attached noncharged polymers

The polymers used for this class of coatings include poly(vinyl alcohol) [95, 106], dextran [107, 108], celluloses [107, 109, 110], polyethers [57, 111-114], poly(ethylene glycol) [106, 115, 116], poly(vinylpyrrolidone) [117, 118], polyacrylamide [65, 75] and polyacrylamide derivatives [68, 78, 119-124].

1.7.2.1.1 Covalently attached pre-formed polymers

Hjertén and Kubo in 1993 reported the use of cellulose- and dextran-coated capillaries for protein analysis [107]. 40 and 500 kDa polysaccharides were first derivatized with allyl glycidyl ether to obtain allyl polysaccharides. Next, the 15- cm long capillaries were pretreated with NaOH and HCl, then bifunctionalized with γ-methacroyl-oxypropyltrimethoxy silane [68]. A 0.7 %(w/v) solution of the allyl polysaccharide

(buffered at pH 7), was mixed with a 10 %(w/v) aqueous solution of the initiator ammonium persulfate (APS), deareated, mixed with a 5 %(v/v) solution of the catalyst *N,N,N′,N′*-tetramethyl-ethylenediamine (TEMED) and filled into the bifunctionalized capillary. Polymerization was allowed to proceed for 17 hours. A high performance liquid chromatographic (HPLC) pump was used to displace the highly viscous phase from the capillary. The coatings were stable for 16 days in a pH 12, 5 %(w/v) SDS solution. No EOF mobility measurements were reported.

In 1995, Mechref and El Rassi described a simpler method using commercially available materials [108]. The coating procedure involved three major steps: the silica surface was first bifunctionalized with a 10 %(v/v) solution of γ-glycidoxypropyltrimethoxysilane at 96°C for 20 minutes, then dextran was covalently attached to the epoxy-layer in the presence of BF_3 catalyst, finally the dextran chains (45, 71, or 150 kDa) were crosslinked with a mixture of 10 %(v/v) 200 kDa poly(ethylene glycol) diglycidyl ether and 10 %(v/v) 200kDa PEG in dry dioxane containing 1 %(v/v) BF_3 for 2 hours.

EOF stability studies were conducted by monitoring the migration time of dimethyl sulfoxide after the coated capillaries were exposed to pH 2 and pH 12 solutions for 10 minutes, before each run, for 5 days. The most stable coatings were obtained with the 150 kDa dextran chains. For this coated capillary, the μ^{EOF} values were in the (2.28 – 9)

x 10^{-5} $cm^2V^{-1}s^{-1}$ range as the pH was varied from 5 to 10. Figure 16 shows the dependence of μ^{EOF} on the pH of the BGE:

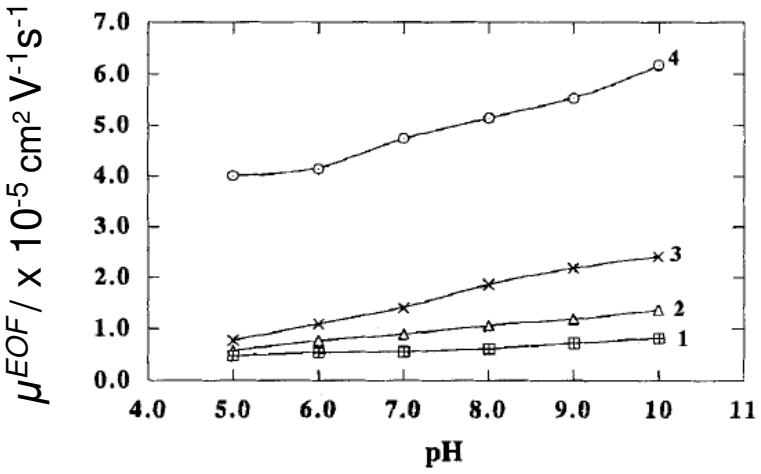

Figure 16. μ^{EOF} as a function of the pH of the BGE. Capillary: 47 cm total length (40 cm effective length) x 50 µm ID. BGE: 0.025 M phosphate buffer at different pH values; applied potential: 25 kV. Curves: 1, 150 kDa dextran; 2, 71 kDa dextran; 3, 45 kDa dextran; 4, untreated fused-silica capillary. Figure reproduced from [108].

A PVA-based coating was prepared by Gilges in 1994 [95] using the device shown in Figure 17 [125]. The 1.2 m long, 50-µm ID capillary to be coated and the serially connected, 3-m long, 50-µm ID throttle capillary were filled by a 10 %(w/w) water solution of 50 kDa PVA.

The coating solution was slowly discharged from the first capillary by 0.15 MPa N_2, depositing a homogenous polymer film onto the wall. The thin film was then thermally immobilized at 140 °C, for several hours, under a gentle stream of nitrogen.

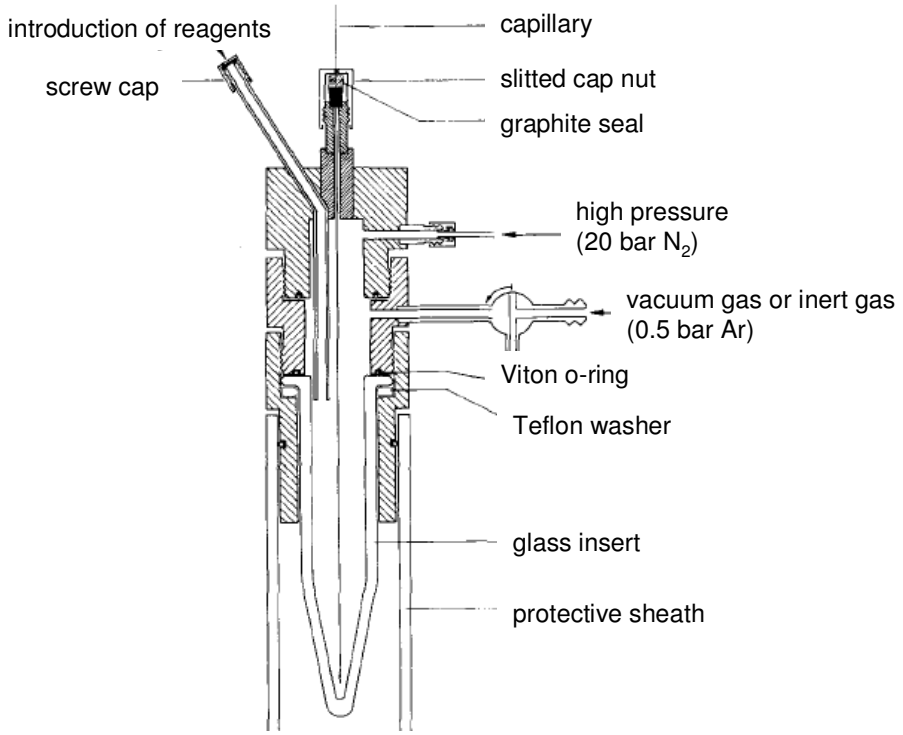

Figure 17. Device used for reproducible introduction of reagents into the capillary under an inert atmosphere. Figure reproduced from [125].

In the 5 < pH < 9 range, the average μ^{EOF} was 1.2 x 10^{-5} $cm^2V^{-1}s^{-1}$. At pH 8.5, loss of efficiency was observed after 40 runs, and the capillary could not be regenerated by their rinsing procedures.

1.7.2.1.2 Covalently attached *in situ* formed polymers

In 1995, Liu covalently anchored an epoxy polymer to the capillary wall and then cross-linked the film with ethylenediamine [113]. The coating procedure involved 3 steps: (1) the capillary was sequentially flushed with 1M NaOH, 0.1 M HCI, and deionized water, then dried in a gas chromatographic oven at 100°C for 1 hour while purging with

nitrogen gas (inlet pressure: 400 kPa); (2) the capillary was filled with a solution of 5 % γ-glycidoxypropyltrimethoxy silane in dichloromethane and allowed to react for 3 hours; then the capillary was rinsed with dichloromethane for 10 minutes and heated at 100°C for 2 h while purging with nitrogen gas (inlet pressure: 400 kPa); and finally, (3) a thin film of bisphenol A diglycidyl ether (DEBA) in dichloromethane was deposited on the pretreated capillary wall and then cross-linked with ethylenediamine. The solvent residue was removed in a gas chromatographic oven by purging the capillary with nitrogen gas (inlet pressure: 100 kPa) at room temperature for 2 hours, then the temperature was raised to 100°C for 1 hour. Figure 18 shows the schematic for the reaction.

They tested 10 %, 50 %, and 80 % solutions of the epoxy polymer as coating solutions. The best coating was obtained with the 80 % solution. Though the reported lifetime of the coating was more than 2 months, μ^{EOF} varied in the (5 to 30) x 10^{-5} $cm^2V^{-1}s^{-1}$ range for the 3 < pH < 10 BGEs, because the coatings could not completely mask the silanols groups. Other epoxypolymer based capillary coatings showed similarly varying μ^{EOF} values [57, 111, 112].

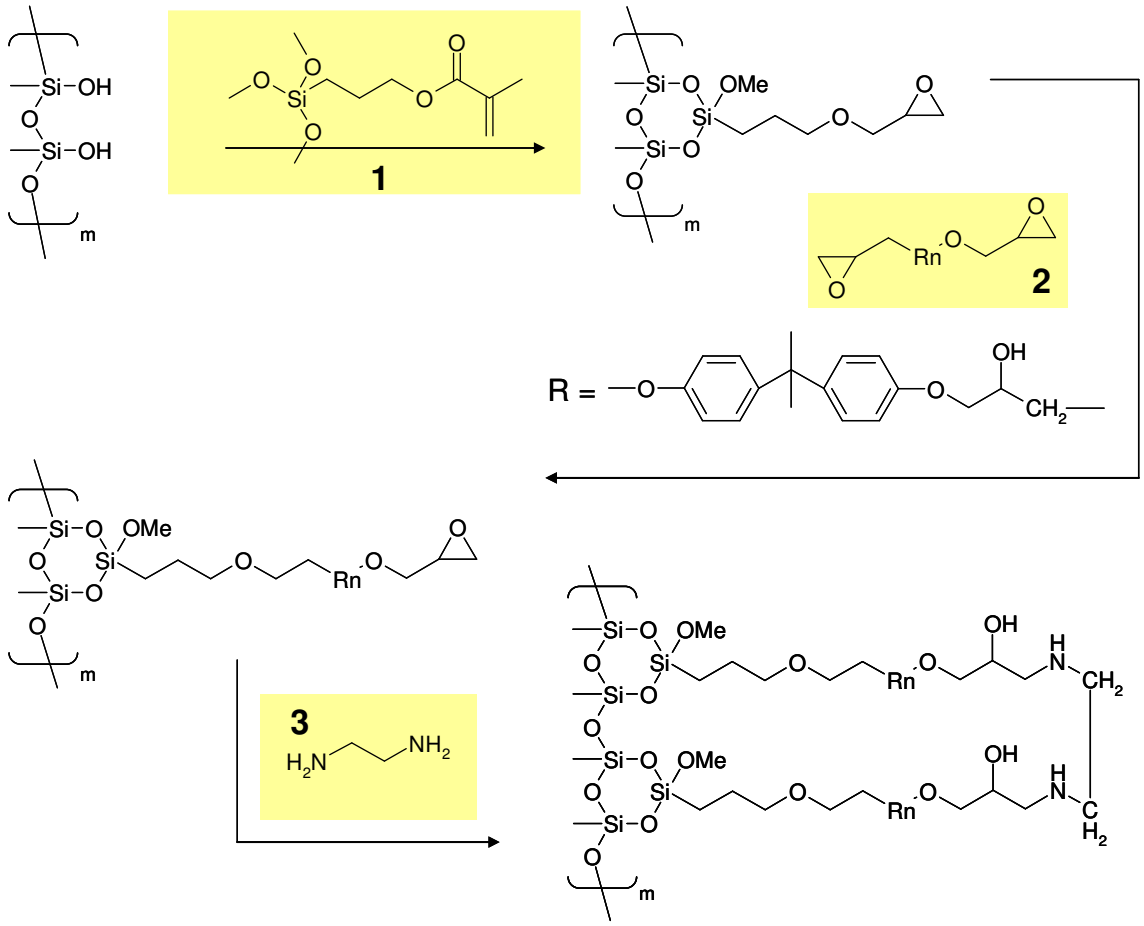

Figure 18. Schematic for the reactions involved in the preparation of crosslinked epoxy polymer coating. (1) Bifunctionalization with γ-glycidoxypropyltrimethoxysilane; (2) reaction with bisphenol A diglycidyl ether; (3) crosslinking with ethylenediamine. Figure reproduced from [113].

El Rassi in 1991 reported "fuzzy" and "interlocked" poly(ethylene glycol) coatings [115]. The fuzzy coating had two layers: a crosslinked glycidoxypropylpolysiloxane sublayer covalently attached to the inner surface of the capillary, and a hydrophilic polyether top layer. The interlocked coating did not have this crosslinked layer. The polyether fuzzy coatings were prepared by first filling the fused silica capillaries with an

aqueous solution of 10 % (v/v) γ-glycidoxypropyltrimethoxysilane and allowing them to react at 96°C for 40 minutes. Then, the capillaries were filled with 0.01 M HCl and heated at 95°C for 40 minutes. After washing successively with water and dioxane, the capillaries were flushed with a dioxane solution that contained 1 %(v/v) BF_3. Next, the capillaries were filled with an equimolar solution of poly(ethylene glycol) (PEG) diglycidyl ether (600 kDa) and PEG 2000 or PEG 600 in dioxane. For the preparation of the polyether interlocked coatings, dimethylformamide (DMF) solutions containing PEG 200 were filled into the bifunctionalized capillaries and allowed to react at 100°C for 1 hour.

The fuzzy coatings exhibited lower EOF than the interlocked coatings, because the additional crosslinked polysiloxane sublayer shielded the surface silanols better. As the pH of the BGE was increased from 4 to 7, the μ^{EOF} increased from 8 x 10^{-5} to 15 x 10^{-5} $cm^2V^{-1}s^{-1}$ for the fuzzy coatings, and from 8 x 10^{-5} to 40 x 10^{-5} $cm^2V^{-1}s^{-1}$ for the interlocked coatings. The coated capillaries were stable for several weeks when operated at pH 6.0 or below, and for more than 80 hours when used in the $6.5 < pH < 7.0$ range.

The polyacrylamide (PAA) coatings are the most popular polymeric coatings. Hjertén made the first surface modified capillaries to suppress EOF for the analysis of small molecules by using a non-crosslinked linear polyacrylamide coating [68]. The coating protocol involved the typical 3-step methodology: (1) capillary pretreatment with base,

acid, and water rinses; (2) bifunctionalization with γ-(trimethoxysilyl)propyl-methacrylate (BindSilane reagent); and (3) forming of the polymeric coating *via* free radical polymerization involving the grafted functional groups and the monomers. Polymerization was continued overnight and the unattached polymer chains were rinsed out of the capillary. Figure 19 shows the reaction scheme.

The capillary pretreatment and bifunctionalization steps are typically rugged procedures (see above). The actual polymerization step is the critical step where the conditions such as temperature, concentration of the monomer, catalyst and initiator, and their relative ratios, dictate the quality of the coating. Several studies on the factors that affect polymerization kinetics have been reported [57, 126-134].

A recent study was conducted by Cifuentes [129]. The most reproducible coatings were made when the solutions (monomer, catalyst, and initiator) were degassed for at least 30 minutes and polymerized at room temperature. A catalyst-initiator (*N*,*N*,*N*′,*N*′-tetramethylethylenediamine - ammonium persulfate) ratio of 1.5 at millimolar concentrations (e.g., 2.95 - 1.96 mM) and an acrylamide concentration of 0.56 M gave a coating that insured the best peak shape for lysozyme and α-chymotrypsinogen.

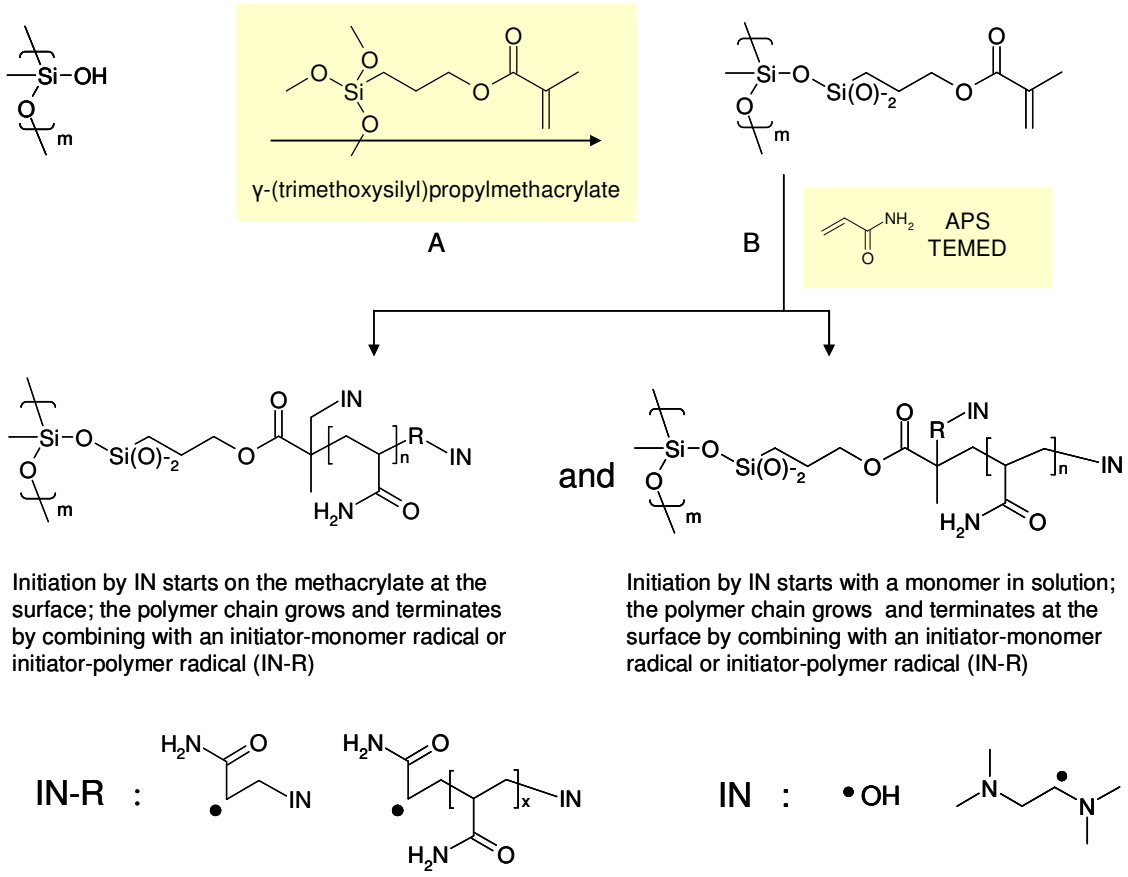

Figure 19. Linear polyacrylamide coating. The pretreated capillary is (A) bifunctionalized with γ-(trimethoxysilyl)propylmethacrylate and then (B) the covalently attached polymer network is made *in situ via* free radical polymerization of the acrylamide monomers [135].

The linear polyacrylamide coatings have limited stability at alkaline pH. Greaves reported [136] that microscopically, silica surfaces are rough, and nanometer-scale cavities are ubiquitous. These cavities are not efficiently covered by linear polyacrylamide and the exposed anchored polyacrylamide chains are prone to hydroxide attack at high pH. This results in hydrolysis and degradation of the coating, leads to an increase in EOF and band broadening of proteins after a few days of use.

The stability of polyacrylamide coatings has been improved [119, 137, 138] by crosslinking acrylamide (AA) with *N,N'*-methylenebis(acrylamide) (MBA) and providing multiple anchors for the polymeric matrix as shown in Figure 20.

The preparation procedure for the crosslinked coating is similar to that of the linear polyacrylamide, except that *N,N'*-methylenebis(acrylamide) is mixed with acrylamide and copolymerized *in situ* as in Hjerten's method [68].

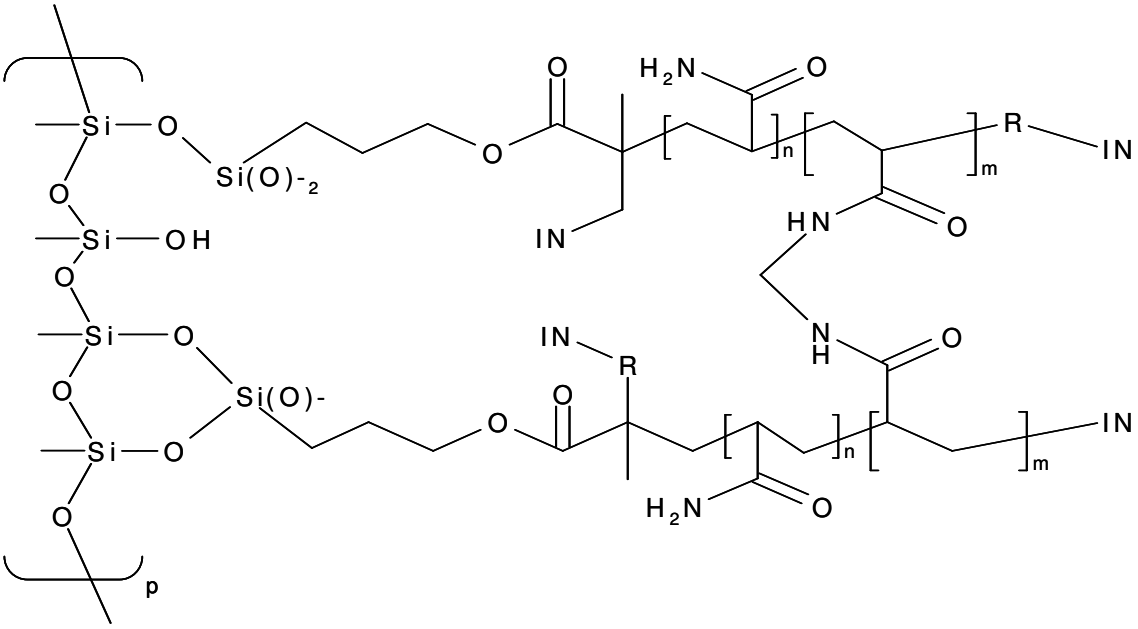

Figure 20. Crosslinked polyacrylamide with multiple anchoring points can stay immobilized even when one or more of the Si-O-Si bonds are severed. For 4 %T, 0.2 %C, n = 499, m = 1. IN-R: (1) initiator-monomer radical (terminator), where the monomer is AA or MBA; or (2) initiator-polymer radical (terminator), where the polymer is $–[AA]_r–[MBA]_s–$ and r and s depend on the composition of the coating solution.

The coatings made by Lin in 2004 [137] suppressed the EOF and were stable under alkaline conditions. They designed a device that was used to carry out their protocol (Figure 21).

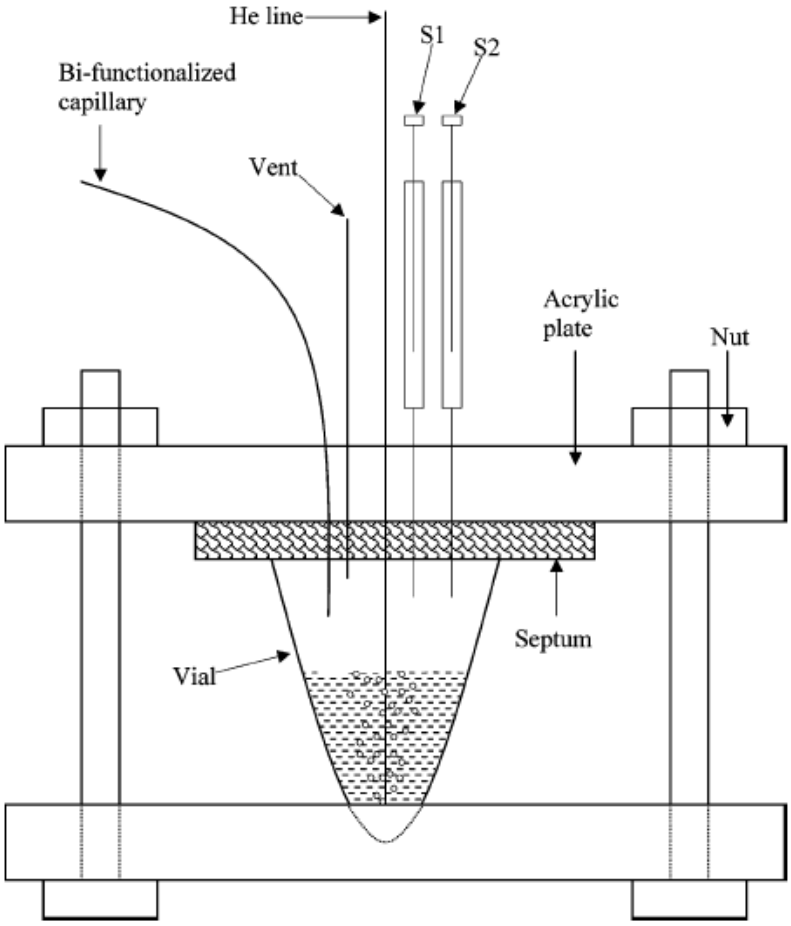

Figure 21. Device for making crosslinked polyacrylamide coatings in capillaries. S1: syringe for APS introduction; S2: syringe for TEMED introduction [137].

It consisted of a 2-mL vial (to contain the coating solution) covered by a septum and held together by two 1/4-inch-thick acrylic plates. There were five 1-mm-diameter holes across the top acrylic plate providing access for the 5 lines needed: (1) helium gas line port to purge the solution and remove any dissolved oxygen; (2) syringe port for initiator

(APS) introduction; (3) syringe port for catalyst (TEMED) introduction; (4) port for vent line; and (5) port for the capillary to be coated. Their best coatings were made with a mixture of 4 %T and 0.2%C. They reported μ^{EOF} values as low 0.1 x 10^{-5} $cm^2V^{-1}s^{-1}$ in a pH 9 BGE. The capillaries were tested in IEF and zone analysis of proteins. Migration times were reproducible for 240 runs. The capillaries were exposed to a 200 mM arginine solution (pH 10.36) for 2 hours and then used for cIEF analysis. No changes in the cIEF profile were observed when compared to their control capillaries.

1.7.2.2 Covalently attached charged polymers

Covalently attached charged polymers can either be positively charged generating an anodic EOF, or negatively charged generating a cathodic EOF. Most coating methodologies use free radical polymerization.

1.7.2.2.1 Covalently attached cationic polymers

In 1997, Liu and Hartwick introduced capillaries with a poly(aminoethylmethacrylate) (PAEM) [139] and with a poly(diallyldimethylammonium) (PDADMAC) [140] coating. The fused silica capillaries were first pretreated and bifunctionalized according to Hjerten's method [68]. A solution containing 10 % 2-aminoethyl methacrylate hydrochloride (for the PAEM capillaries) and 10 % diallyldimethylammonium chloride (for the PDADMAC capillaries) was mixed with a certain volume of 3 mg/mL TEMED and 1 mg/mL APS solutions (actual volumes not reported) and immediately pumped through their activated capillaries (no coating time reported). After polymerization, the

capillaries were rinsed with deionized water and left to dry overnight at 30-40 °C. Figure 22 and Figure 23 show the synthesis schemes for PAEM and PDADMAC respectively.

For PAEM-coated capillaries, μ^{EOF} decreased from -45 x 10^{-5} to -30 x 10^{-5} $cm^2V^{-1}s^{-1}$ as the pH of the BGE was increased from 3 to 7. Relative standard deviation (RSD) for μ^{EOF} (3 capillaries) was about 3 %. After 45 hours of exposure to BGEs of 3 < pH < 7.2, in an electric field of 250 V/cm, μ^{EOF} at pH 4.5 was in the -46.8 x 10^{-5} to -46.6 x 10^{-5} $cm^2V^{-1}s^{-1}$ range. After another 18 hours of exposure, μ^{EOF} decreased to -26 x 10^{-5} $cm^2V^{-1}s^{-1}$.

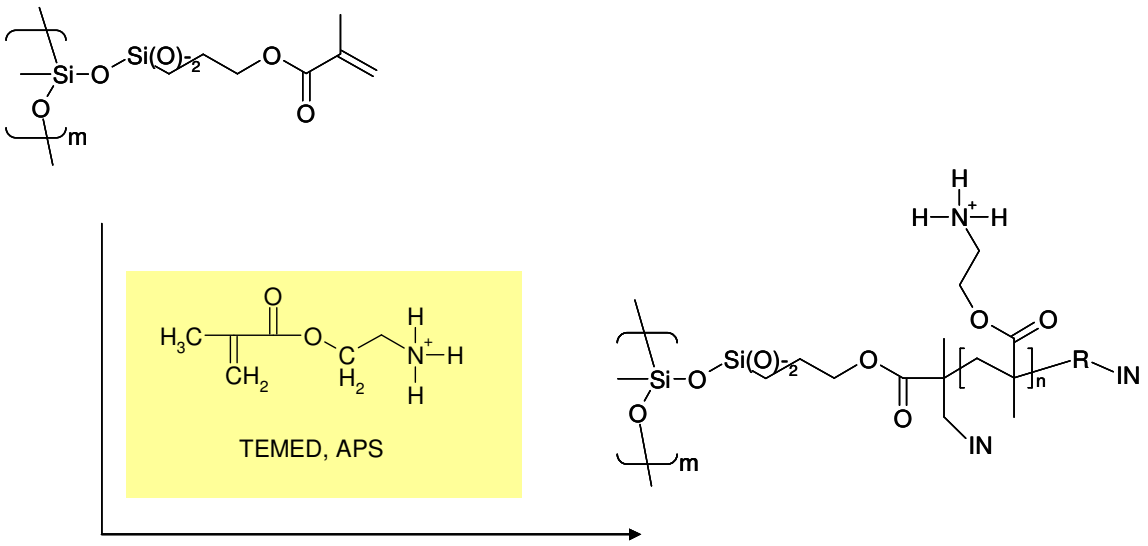

Figure 22. Synthesis of PAEM-coated capillaries *via* free radical polymerization. Figure reproduced from [139].

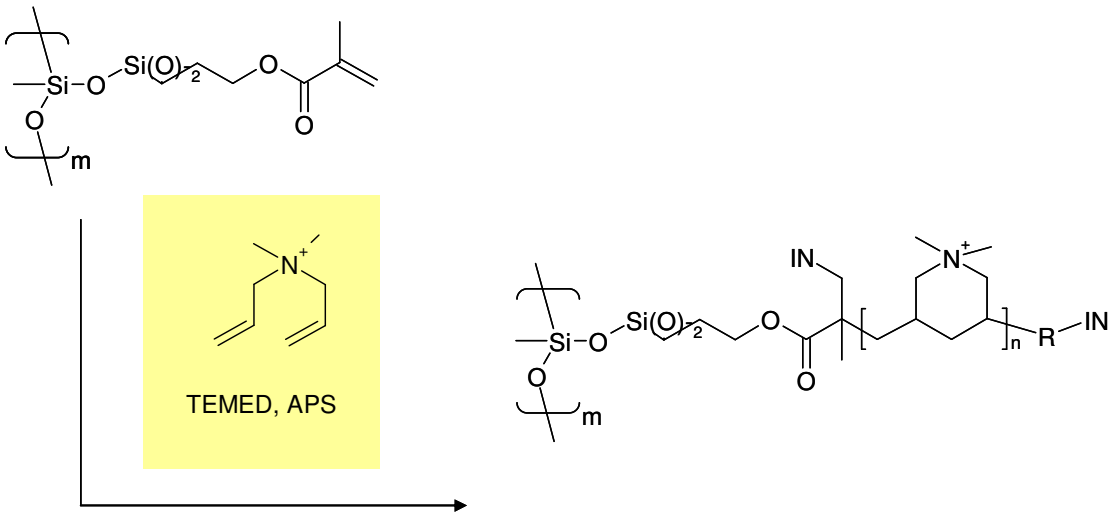

Figure 23. Synthesis of PDADMAC-coated capillaries *via* free radical polymerization. Figure reproduced from [140].

For the PDADMAC-coated capillaries, μ^{EOF} decreased from -59 x 10^{-5} to -20 x 10^{-5} $cm^2V^{-1}s^{-1}$ as the pH of the BGE was increased from 2 to 8.5. The capillaries were subjected to the same stability tests as the PAEM-coated capillaries: at pH 4, the initial μ^{EOF} was -57 x 10^{-5} $cm^2V^{-1}s^{-1}$ with an RSD of 2.3 % (3 capillaries).

In 1997, Srinivasan produced capillary columns with permanent positively charged walls [141]. The fused silica capillaries were first pretreated and bifunctionalized according to Hjerten's method [68]. Next, a cationic prepolymer was formed by dissolving 2 %(w/w) acrylamide and 1.8 %(w/w) (methacrylamidopropyl)trimethylammonium chloride in water, degassing the solution, mixing with 0.2 %(v/v) TEMED and 0.4 %(w/v) ammonium persulfate and allowing it to polymerize for 48 h at 10 °C. The resulting cationic polymer was precipitated with acetone and reconstituted in deionized water before use as a 4 % polymer solution. Into 10 mL of the polymer solution, 5 µL of

TEMED and 50 µL of a 10 %(w/w) ammonium persulfate in water were added. The capillary was filled with the solution, sealed at both ends with 2-cm pieces of Teflon tubing and placed in an oven at 80 °C for 18 h. The unattached portion of the polymer was rinsed off with deionized water. Figure 24 shows a schematic structure of the cationic polyacrylamide coating.

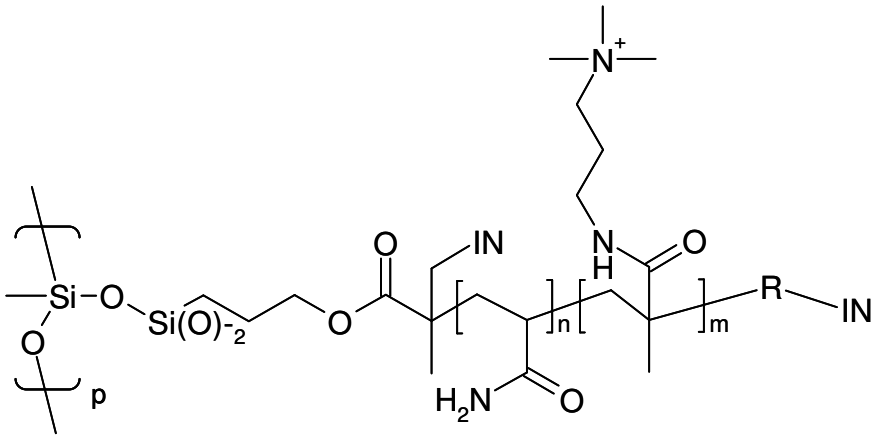

Figure 24. Possible schematic structure of the linear cationic polyacrylamide coating by Srinivasan [141], n: 1, m= 1.11.

They used the capillaries to separate (1) α-lactalbumin (from bovine milk), (2) carbonic anhydrase (from bovine erythrocytes), and (3) myoglobin (from horse skeletal muscle) and achieved average separation efficiencies of > 200,000 plates in 50-cm long capillaries with a 25 mM pH 7 phosphate buffer as the BGE. However, they didn't report any anodic EOF measurements or coating stability tests.

1.7.2.2.2 Covalently attached anionic polymers

In 1994, Sun, *et al.* [63] developed negatively-charged linear polyacrylamide coatings. They prepared 2 monomer solutions, degassed and neutralized with concentrated NaOH to pH 7. Solution A contained 0.386 M of 2-acrylamido-2-methyl-1-propanesulfonate (AMPS) in deionized water. Solution B contained 0.386 M acrylamide in deionized water. The capillary was pretreated and bifunctionalized according to Hjerten [68]. 5 mg of ammonium persulfate and 5 μL of TEMED were added to 5 ml of solution A and 5 mL of solution B. The mixed solution was immediately filled into the pretreated capillary and left there for 1 hour. The capillary was rinsed with water and dried with air before use. Figure 25 shows a schematic structure of the negatively charged linear polyacrylamide coating.

They made capillaries having μ^{EOF} in the 25 x 10^{-5} to 55 x 10^{-5} $cm^2V^{-1}s^{-1}$ range. For a particular capillary, μ^{EOF} varied from 50 x 10^{-5} to 54 x 10^{-5} $cm^2V^{-1}s^{-1}$ as the pH of the BGE was increased from 2 to 9. RSD for 3 capillaries was 1.7 %. The capillaries were stable for only up to 18 days in $3 < pH < 9$ BGEs, and only for 60 hours if an electric field of 288 V/cm was applied.

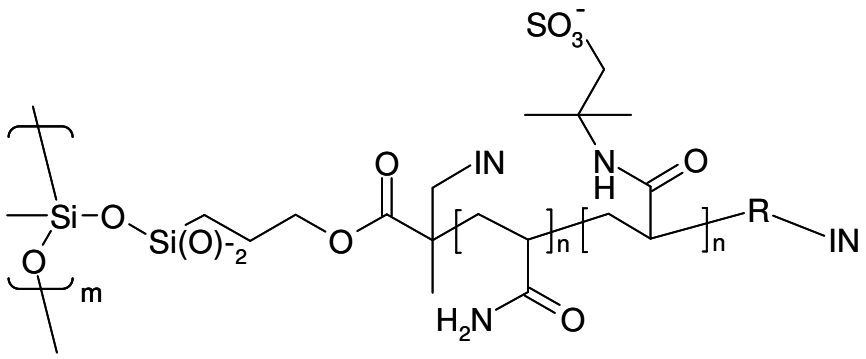

Figure 25. Possible structure of the negatively charged linear polyacrylamide coating [63].

After this survey of the pertinent literature, it can be concluded that the objectives of the capillary wall coatings were limited: (1) for neutral coatings: the lessening of band broadening of target analytes by preventing electrostatic interactions with the dissociated silanol groups, and the suppression of EOF for cIEF separations; and (2) for charged coatings: improving separation efficiencies of analytes that have the same charge as that of the surface coating *via* electrostatic repulsion, and providing a sweeping mechanism to move the analytes toward the detector.

Another objective of this dissertation is to develop capillaries with covalently attached charged groups to provide 3 specific qualities: (1) the capillaries were to have a specific μ^{EOF} value (low to high value) such that one can choose which capillary to use for a particular analysis; (2) the capillaries with specific μ^{EOF} values were to have constant μ^{EOF} over a wide pH range; (3) and the capillaries were to be durable over a wide pH range.

2 REDESIGN OF THE MEDUSA TO ACCOMMODATE PREPARATIVE – SCALE ISOELECTRIC TRAPPING PROTEIN SEPARATIONS

2.1 Redesign principle and objectives

This section describes the redesign of the MEDUSA, a preparative-scale multi-compartmental electrolyzer (MCE) to make it suitable for IET separations. Three main areas of concern had to be addressed: (i) the sealing system, (ii) configuration of the liquid flow path and (iii) the cooling system.

2.1.1 Sealing system design

The twelve compartments in the MEDUSA were formed from a series of grids. The grids were assembled in a separation unit that was equipped with 12 inlet and outlet ports to direct flow into each separation compartment. Six of the twelve separation compartments had their inlet and outlet connections at the anodic side of the separation unit. The other six separation compartments had their inlet and outlet connections at the cathodic side of the separation unit. The 6 anodic compartments were formed by the first set of six different grids. The 6 cathodic compartments were formed by the second identical set of six different grids. Three of the six different grids that made up one set are shown in frontal view in Figure 26; the other three grids of the set are mirror images of the ones shown. Each grid was 1.2-mm thick, 0.13 cm wide and 13.7 cm long, resulting in a compartment volume of about 2.14 mL [55].

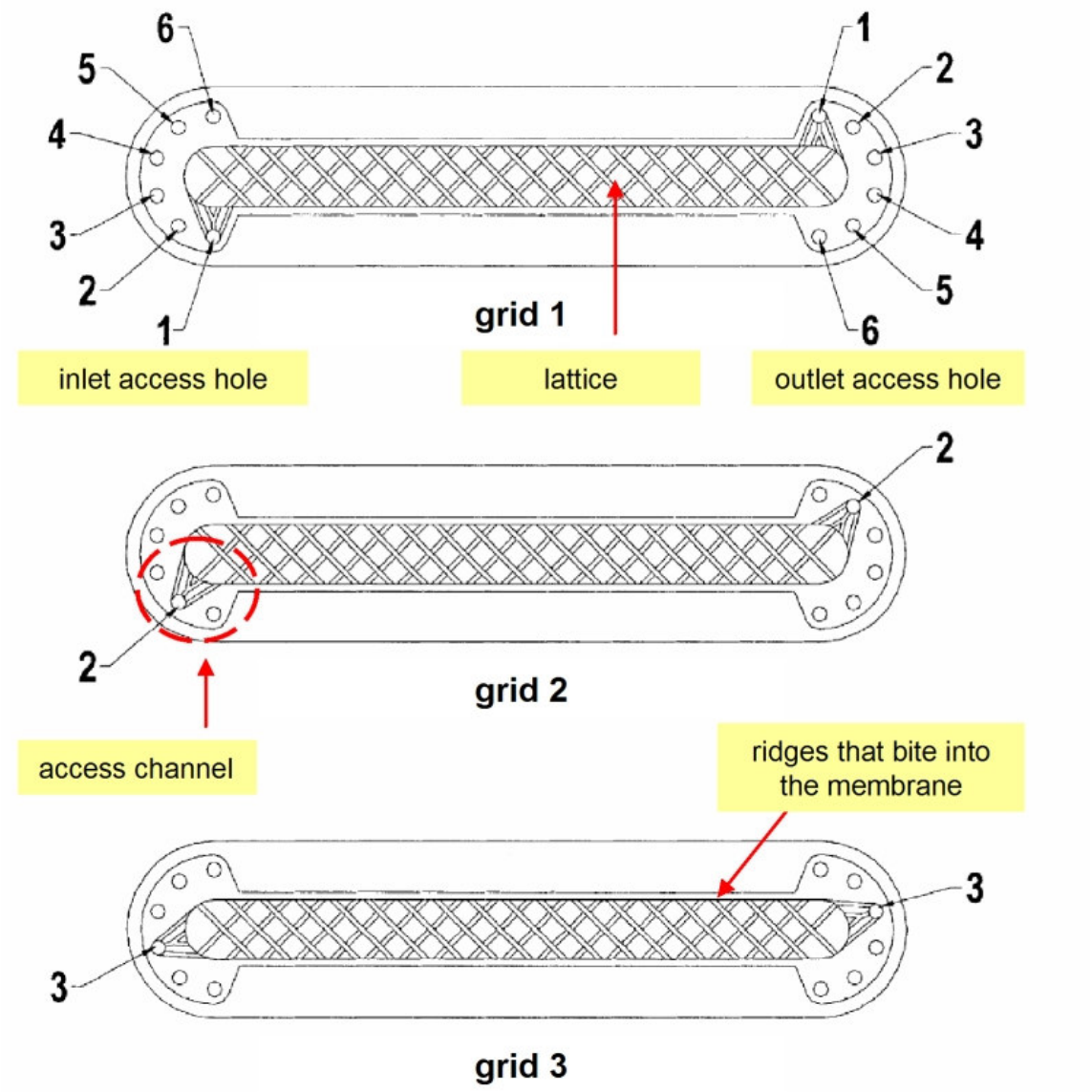

Figure 26. MEDUSA grids form the compartments. Figure modified from [55].

In order to ease the assembly process, the original grids were made smaller than the housing. This made precise alignment of the inlet and outlet ports and the access holes of the grids difficult. The misaligned holes created flow restrictions in the separation unit, which in turn, led to uneven pressure drop along the grids and caused detrimental pressure-driven flow across the membranes.

The grids had elevated ridges (about 0.1 mm high) along the periphery of the channel that bit into the membranes when the separation unit was compressed to seal. Unfortunately, these ridges caused more harm than did good: if a first sealing attempt failed (a frequent case), the bite marks on the membranes led to leaks in the next sealing attempt.

The original MEDUSA grids also possessed a lattice made of two sets of offset “ribs” that ran at 45° and 135° with respect to the long axis of the grid. The objective of this lattice was to support the membranes and provide a weaving liquid flow path to mitigate membrane fouling. Since the uneven, weaving flow could be co-directional or counter-directional to the electric field, this nonseparative transport could compromise the separative electrophoretic transport process.

To eliminate these limitations, a new grid system has been designed that allows one to: (1) seal the separation unit on the first attempt, (2) preserve the integrity of the membranes, and (3) minimize undesirable convective flow effects.

2.1.1.1 Membrane supports (compartments) and gaskets

Poly(vinyl acetate) (PVAC) sheets were used to manufacture the membrane supports that replace the original MEDUSA grids. The 0.5 mm thick PVAC sheets were laser-cut to provide self-aligning, snug fit in the separation unit (Figure 27), guaranteeing that the holes in the PVAC membrane supports and the inlet/outlet ports of the separation unit are in registry. The PVAC membrane supports have a smooth, level surface (no ridges): thus, they do not bite into the membranes as the system is compressed to seal. The membrane supports do not contain a lattice, thus convective flow orthogonal to the membranes is minimized.

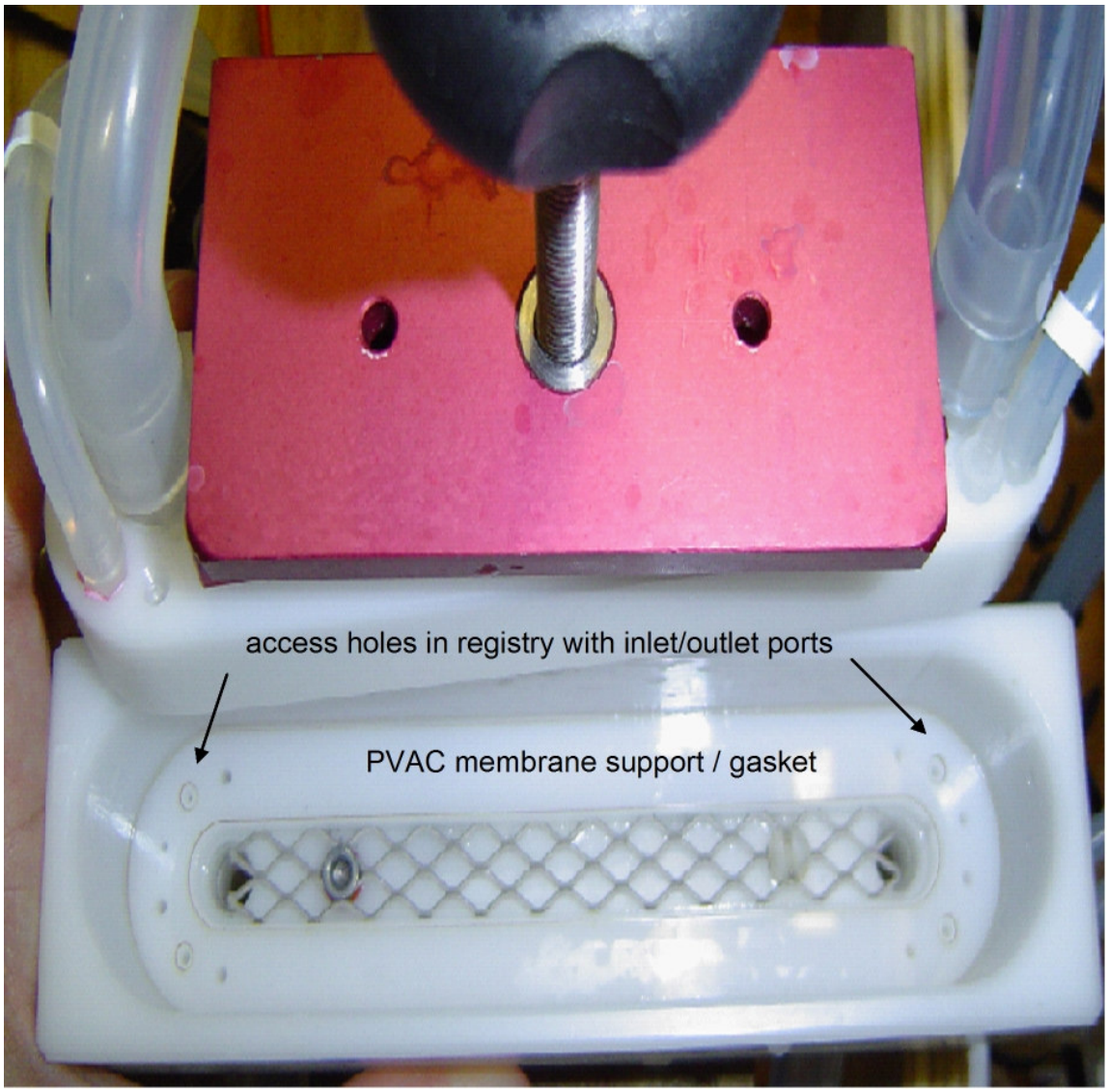

Figure 27. The PVAC membrane supports and gaskets have a snug fit in the separation unit insuring registry of the inlet/outlet ports and the access holes.

0.5 mm thick silicone gaskets were laser cut to form and help to seal the compartments. The 6 anodic compartments are formed by the first set of six pairs of PVAC membrane support and silicone gasket combinations. The 6 cathodic compartments are formed by the second identical set of six pairs of PVAC membrane support and silicone gasket combinations. Three pairs of the PVAC support and silicone gasket combinations used to make the first 3 compartments are shown in frontal view in Figure 28.

The membrane support-gasket combinations are designed such that each compartment is isolated from the next compartment. In Figure 28, it can be seen that the membrane support-gasket combination used to make compartment 2 does not contain the access holes of compartment 1. The membrane support-gasket combination used to make compartment 3 does not contain the access holes of compartments 1 and 2, *etc*. This seal design significantly decreases the probability of leaks between the compartments that occur *via* the access holes, and overall, provides a better seal between the compartments.

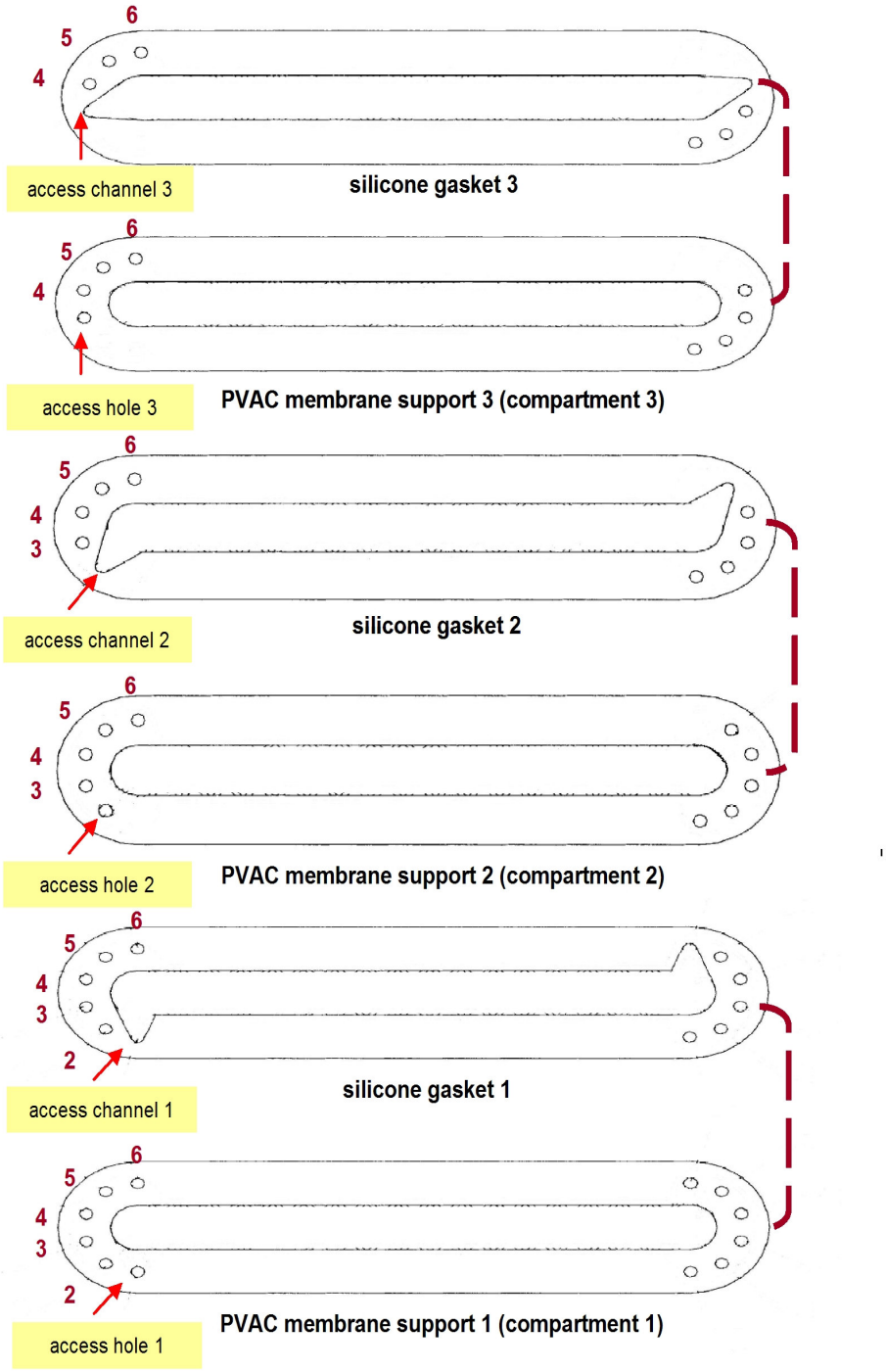

Figure 28. Specific PVAC membrane support and silicone gasket combinations make and seal the compartments.

The assembly of the elements forming a single compartment is illustrated in Figure 29. A full compartment is formed by four elements: a silicone gasket with access holes – a buffering membrane – a silicone gasket with access channel and access holes – a PVAC membrane support.

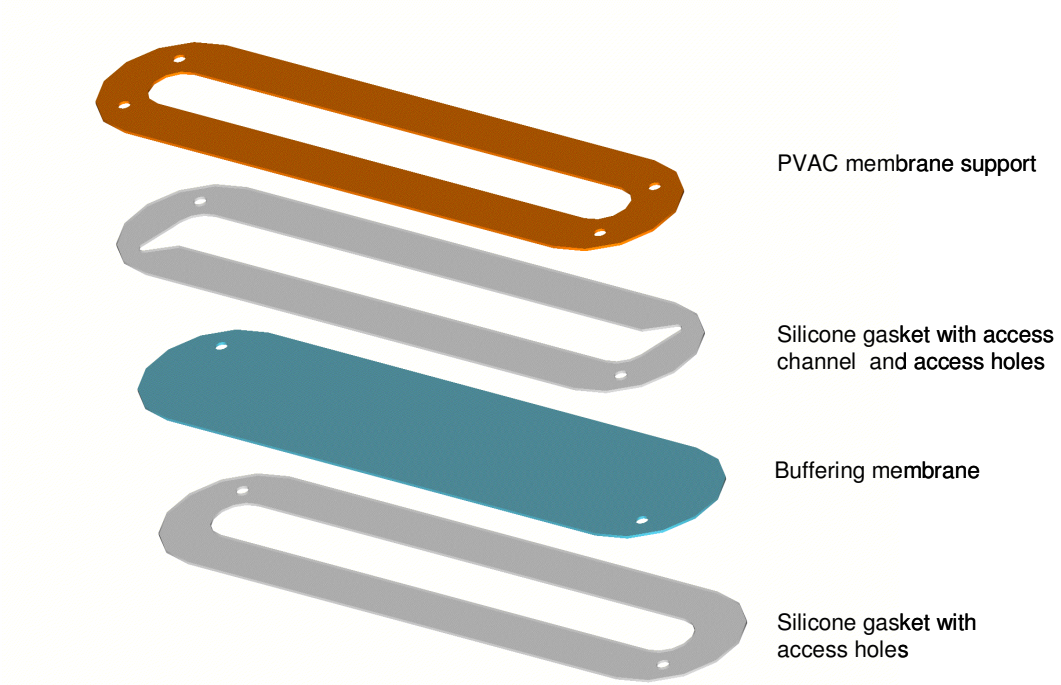

Figure 29. A separation compartment formed from four elements.

The membrane-to-membrane distance in the new compartment design is about 1.5 mm. This translates to a maximum anode-to-cathode distance of about 25 mm (assuming that the separation unit contains an anode compartment, twelve separation compartments and a cathode compartment).

2.1.2 Configuration of the liquid flow path and design of the cooling system

The configuration of the liquid flow path and the design of the cooling system design in the original MEDUSA were tied together, because the cooling apparatus of the instrument, a stainless steel tube-in-a-tube heat exchanger was an integral part of the liquid flow path. The following sections describe the configuration of the liquid flow path in the redesigned MEDUSA, the new cooling system, and the simultaneous optimization of both elements.

2.1.2.1 Configuration of the liquid flow path

The plumbing system of the MEDUSA contained three main components: the separation unit, the stainless steel heat exchanger and the interconnecting silicone tubing. Centrifugal pumps recirculated the solutions through the solution reservoirs and the separation unit. Figure 30 shows a schematic of all the elements *vis-à-vis* each other, and the direction of liquid flow.

The stainless steel heat exchanger was 81 cm long and was situated at the outlet of the separation unit. This heat exchanger had flow lines for the 12 sample solutions and the 2 electrolyte solutions. All sample lines had an internal diameter of 2 mm; the electrolyte lines had an internal diameter of about 10 mm. Figure 31 shows an image of the stainless steel heat exchanger.

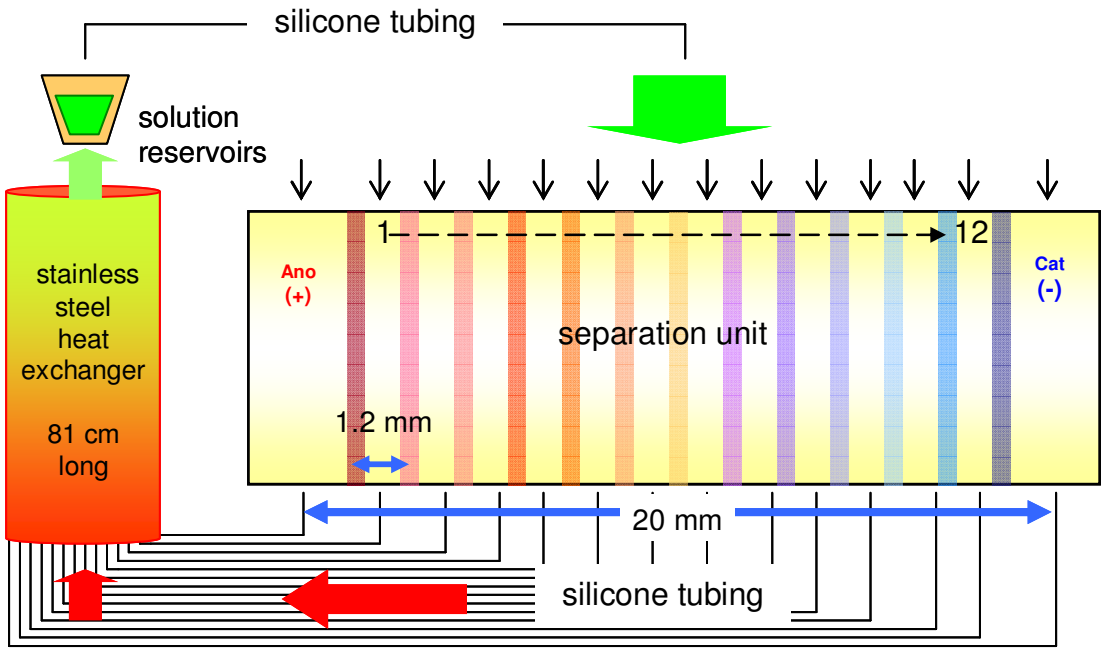

Figure 30. Schematic diagram of the MEDUSA preparative-scale multicompartmental electrolyzer. Arrows indicate the liquid flow direction.

All inter-connecting silicone tubes for the sample solutions had an internal diameter of 2 mm and a length of over 100 cm. The silicon tubes for the electrolyte solutions had an internal diameter of about 10 mm and a length of about 50 cm.

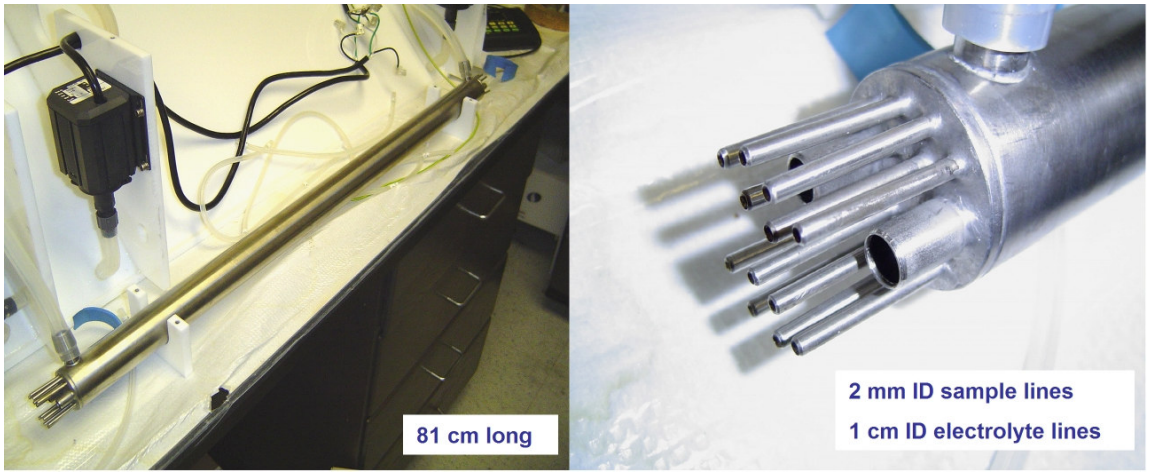

Figure 31. The stainless steel heat exchanger of the MEDUSA.

The placement of the stainless steel heat exchanger at the outlet of the separation unit, and the long length of silicone tubing associated with it, however, created significant backpressure in the separation compartments, resulting in pressure gradients and bulk liquid transport across the membranes. This trans-membrane flow disrupted the electrophoretic migration of the analytes and caused uncontrollable volume changes which led to failed IET separations. Moreover, the heat exchanger added a 12-mL volume to each sample loop and provided a large surface area for analyte adsorption and loss.

2.1.2.2 Performance of the stainless steel heat exchanger

Joule heat generated during electrophoresis was removed through the stainless steel heat exchanger that was supplied with coolant liquid from a chiller. Temperature monitoring experiments were conducted to test the cooling efficiency of the heat exchanger. Figure 32 shows the liquid flow path in the MEDUSA and sampling points 1-5 along the liquid flow path.

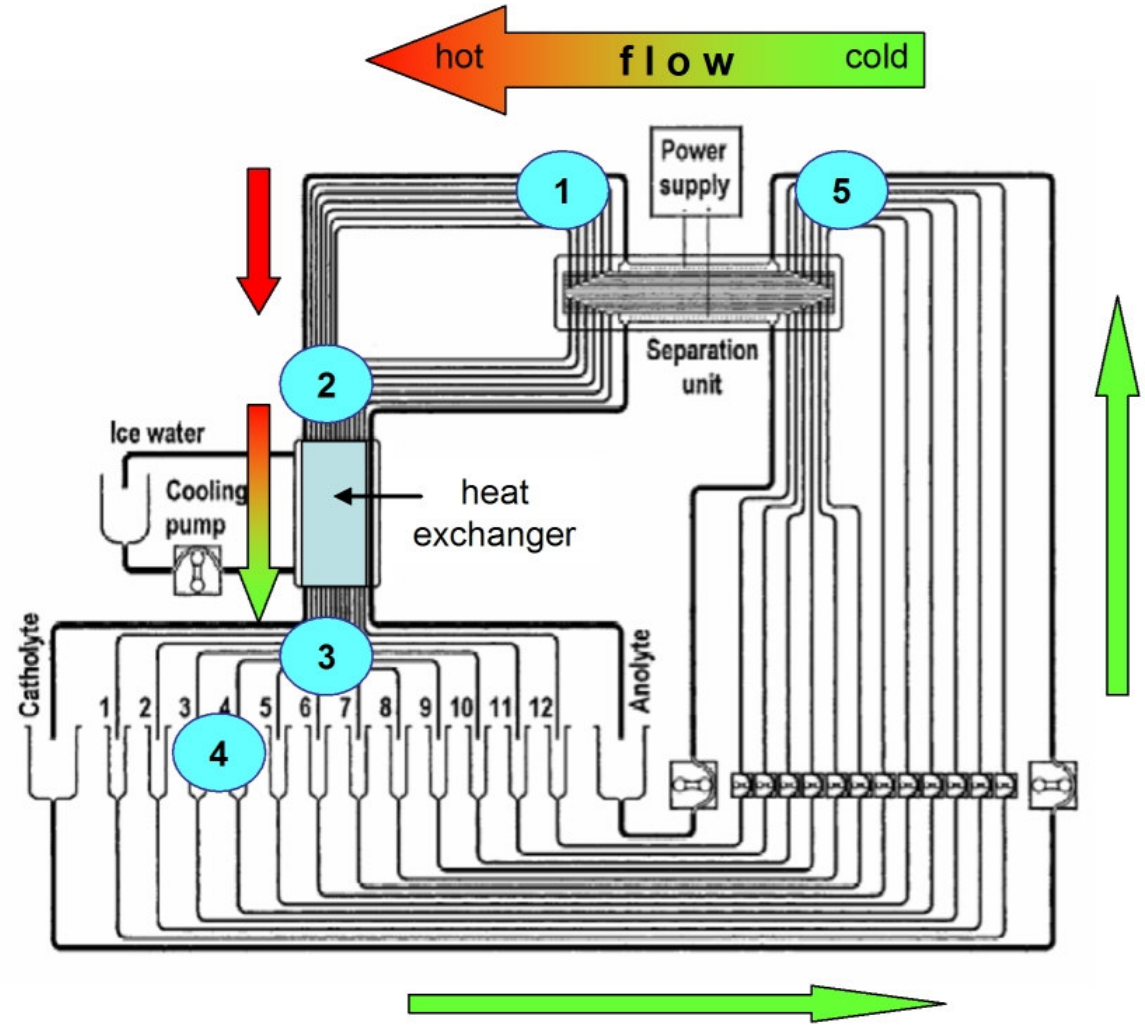

Figure 32. Testing of the cooling efficiency of the stainless steel heat exchanger of the MEDUSA. Arrows indicate the direction of flow and numbers 1-5 are the sampling points along the flow path. Figure modified from [55].

Sampling point 1: liquid taken directly from the outlet ports of the separation unit, 2: liquid taken before the stainless steel heat exchanger, 3: liquid taken immediately after the stainless steel heat exchanger, 4: liquid taken from the solution reservoirs, and 5: liquid taken before the inlet ports of the separation unit.

The set-up used for this experiment contained an anode compartment, 4-separation compartments and a cathode compartment. A 10 mM H_3PO_4 solution titrated to pH 7 with LiOH was used as the background electrolyte. 15 mL of this solution was recirculated at a rate of 60 mL/min with a peristaltic pump through each separation compartment. 100 mL of same solution was recirculated at a rate of 2 L/min with a centrifugal pump through each electrode compartment. The flow rate of the recirculated coolant was 2.8 L/min; its temperature was 0 °C.

The anolyte and catholyte had shorter residence times in the electric field than the sample solutions and acted as heat sinks inside the separation unit during electrophoresis.

Table 2 shows the temperature of the recirculated solutions at the different sampling points along the liquid flow path when 0 W and 60 W of power were applied to the system. The test was continued for 4 hours and readings were taken every 30 minutes. Even with no power applied to the system, the solutions picked up ambient heat, aided by the long sample solution lines of the original MEDUSA. Table 2 lists the results from the cooling efficiency tests.

Table 2. Cooling efficiency tests for the original MEDUSA. The average temperature of the solution was monitored at different sampling points.

Original MEDUSA	T ℃	
Solution sampling point	**0 W**	**60 W**
1: from separation unit	5	8
2: going into steel heat exchanger	6	9
3: from steel heat exchanger	2	2
4: in sample reservoir	3	3
5: going into separation unit	4	4

The stainless steel heat exchanger was able to remove Joule heat, but it contributed a large dead volume and created deleterious flow resistance that disturbed the IET separation.

2.1.2.3 Redesign of the liquid flow path and the cooling system

To minimize the dead volume and the flow resistance, the stainless steel heat exchanger was replaced with glass solution reservoirs that had cooling jackets supplied with a stream of thermostated ethylene glycol – water solution from a chiller. The anolyte, sample solutions and catholyte immediately cascaded into these cooled glass reservoirs as they exited the separation unit (Figure 33). This design minimized the dead volume in the system, minimized flow resistance and the accompanying trans-membrane bulk flow, provided efficient Joule heat removal and controlled the temperature of the buffering membranes. (This is important, because the pKa values of the buffering

species in the membranes change with temperature and in turn, affect the outcome and/or the reproducibility of the separations.)

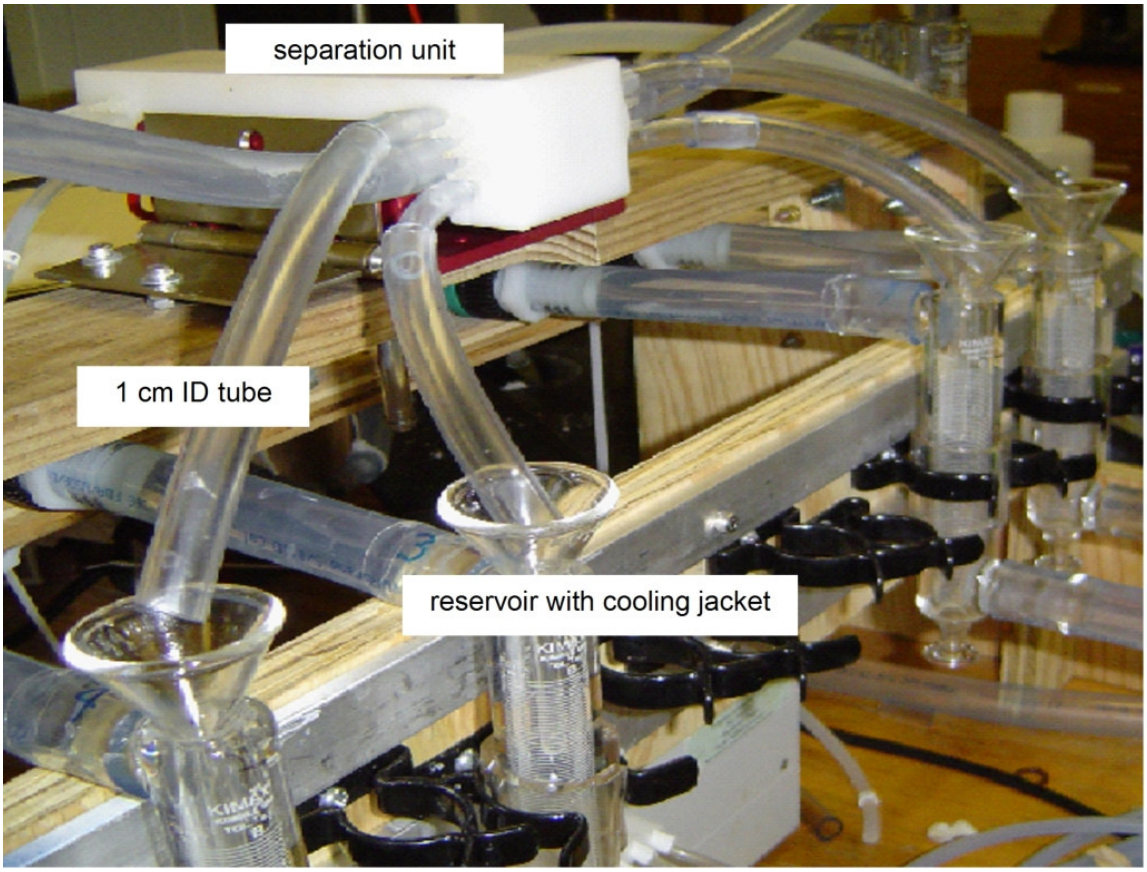

Figure 33. In the redesigned MEDUSA instrument, reservoirs with cooling jackets are used to collect the solutions as they cascade out of the separation unit.

Figure 34 illustrates the coolant plumbing system and the adjustable valves (V) that insure that all cooling jackets are supplied with the coolant at the same flow rate.

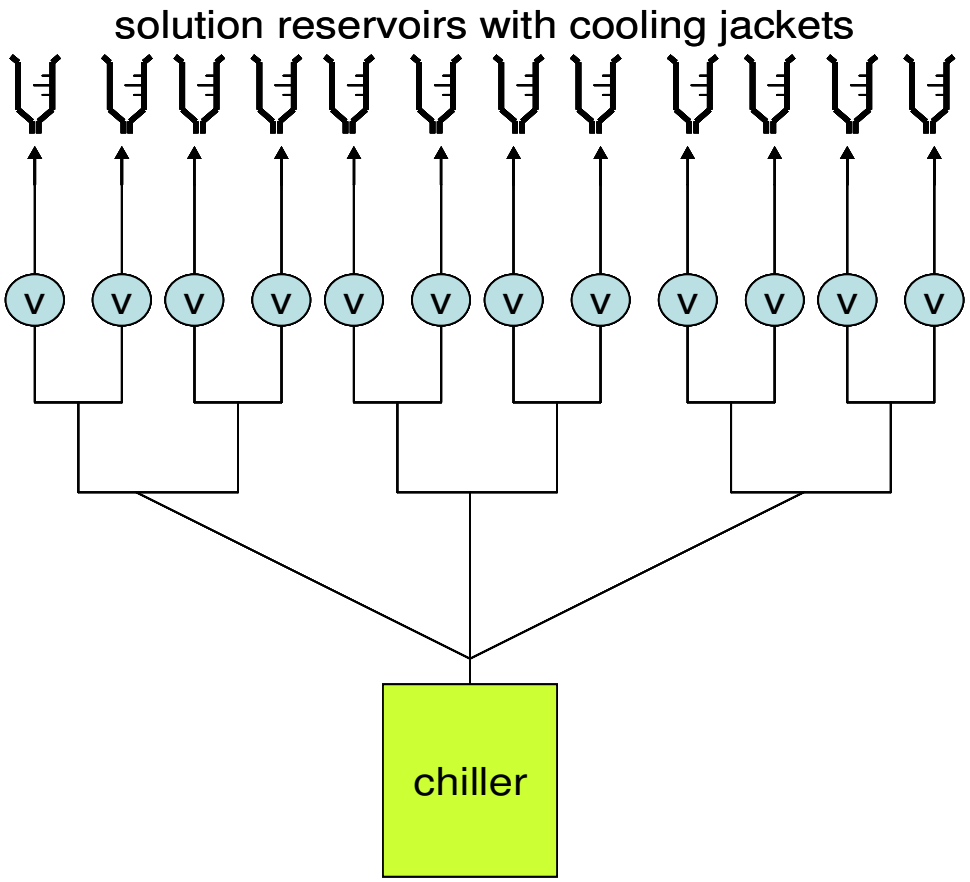

Figure 34. Schematic of the coolant plumbing system in the redesigned MEDUSA.

A new wooden instrument frame holds all the elements in close proximity, minimizing the length of the inter-connecting tubing and reducing the total dead volume to 5 mL/compartment. Figure 35 shows an image of the redesigned MEDUSA instrument.

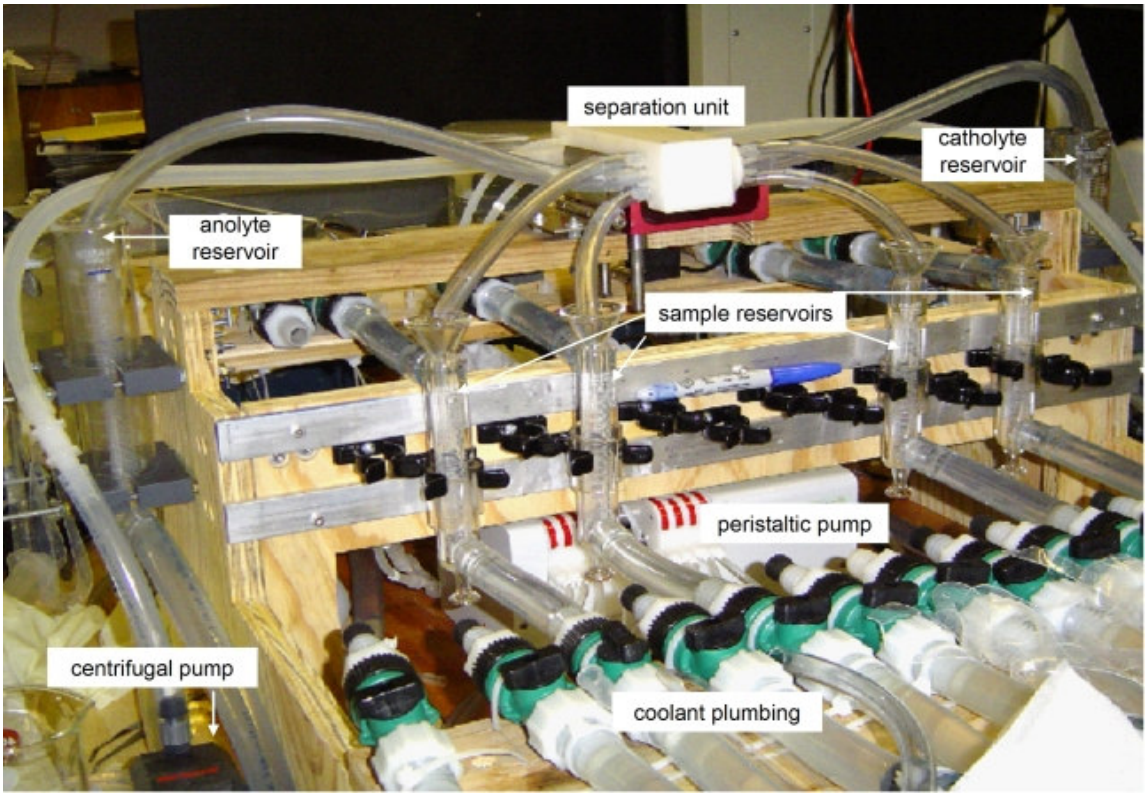

Figure 35. Digital image of the redesigned MEDUSA. A wooden instrument frame accommodates the elements. All reservoirs have cooling jackets.

The cooling efficiency of the redesigned MEDUSA system was evaluated using the same procedure as for the original MEDUSA system. Temperature readings in both the 0 W and 60 W experiments were taken every 30 minutes for 4 hours. The sample solutions were recirculated at a flow rate of 60 mL/min; their jackets were cooled at a flow rate of 1.6 L/min. The anolyte and catholyte were recirculated at a flow rate of 2 L/min; their jackets were cooled at a flow rate of 2.8 L/min. The coolant was maintained at a temperature of 0 °C. Despite the higher flow rates, the anolyte and catholyte could only be cooled to 5 °C, indicating that heat exchange in glass reservoirs was limited. Table 3 shows the temperature readings for all sampling points. The redesigned instrument has smaller dead volume, lower flow resistance, yet it provides the adequate cooling needed.

Table 3. Cooling efficiency in the redesigned MEDUSA. The average temperature of the liquid was monitored at different sampling points.

Redesigned MEDUSA	**T ℃**	
Solution sampling point	**0 W**	**60 W**
from separation unit	3.5	12
in glass reservoirs with cooling jackets	3	6
before separation unit	3	6.5

3 FAST, PREPARATIVE IET SEPARATIONS IN A MULTICOMPARTMENTAL ELECTROLYZER: DEMONSTRATION OF POSSIBLE APPLICATIONS FOR THE REDESIGNED MEDUSA

The IET technique and its associated infrastructure have been developed simultaneously by different researchers in our group. Since development of the redesigned MEDUSA has been completed ahead of the other tasks, only a small fraction of the required auxiliary materials (buffering membranes, p*I* markers and pH-biasers) was available, limiting us to a few, demonstrative applications.

3.1 Four-compartment IET separation of low molecular weight ampholytes

3.1.1 Background and objective

The redesigned MEDUSA instrument was first used, in the 4-separation compartment arrangement, for the IET separation of a mixture of 3 low molecular weight (< 500 dalton) ampholytes that had different p*I* values. The mixture of ampholytes was loaded into one compartment, separated and kept trapped for up to two hours.

3.1.2 Instrument set-up, materials, and method

The 4 separation compartments of the redesigned MEDUSA contained the low molecular weight ampholytes (structures shown in Figure 36): meta-amino benzoic acid (MABA, approximate p*I* 3.9), histidine (HIS, approximate p*I* 7.5), and labetalol (LAB, approximate p*I* 8.3), all from SIGMA, St. Louis, MO, USA. Five PVA-based buffering membranes whose pH values bracket the p*I*s of the probes were used to make the

compartments. The membrane that buffered at pH 2 was placed directly adjacent to the anode compartment, the membranes that buffered at pH 6, 7, 8.2 and 12 made separation compartments 1, 2, 3 and 4, having the most basic membrane (pH 12) immediately before the cathode compartment. 10 mM solutions of isoelectric buffers whose p*I* values fall between the pH values of the buffering membranes were used as pH-biasers [38-41] in the separation compartments: aspartic acid (ASP, approximate p*I* 2.7), carnosine (CAR, approximate p*I* 8.1), lysine (LYS, approximate p*I* 9.9), and arginine (ARG, p*I* 10.6). The anolyte was a 30 mM benzenesulfonic acid solution (BSH, pH 1.52), the catholyte a 100 mM benzyltrimethylammonium hydroxide (BTMAOH, pH 13) solution. Their UV-absorbance allowed us to monitor if any acid or base invasion occurred during the IET separation.

The flow rates through the separation compartments were set at 30 mL/min, the flow rates through the anode and cathode compartments were 2 L/min. After the separation unit was assembled, water was recirculated through each compartment and the water volumes were monitored for at least 30 minutes to assure that there were no leaks between the compartments. After the system passed the leak test, the appropriate solutions were filled into the compartments as shown in Figure 37.

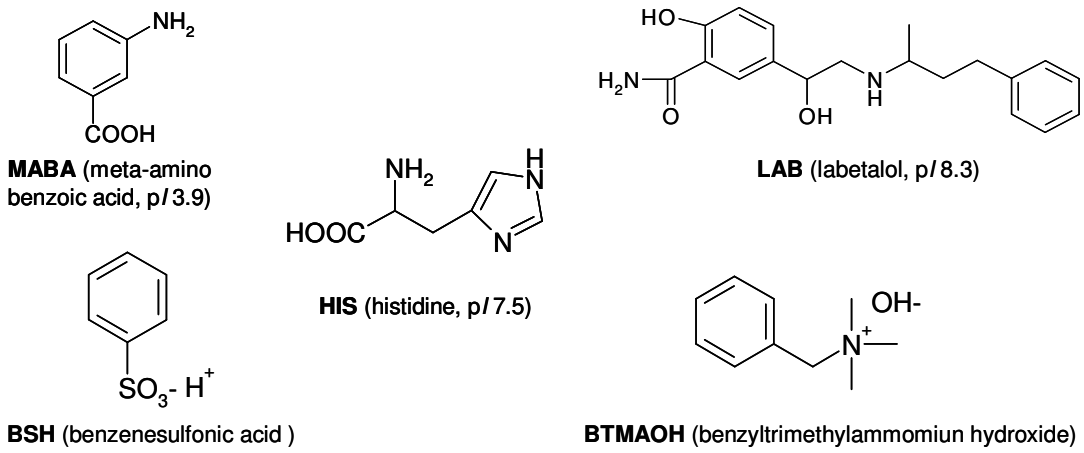

Figure 36. Structures of the low molecular weight analytes, anolyte and catholyte used for this experiment.

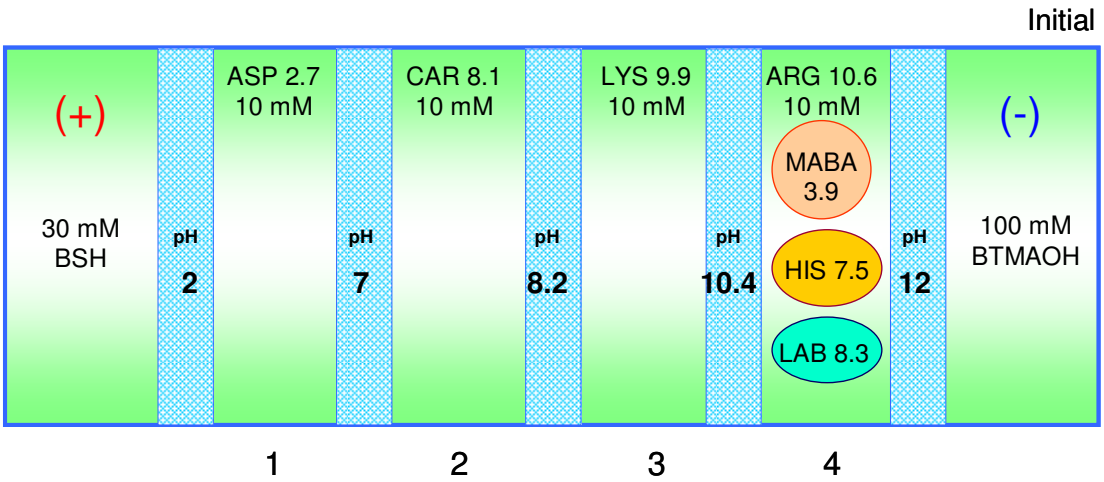

Figure 37. Initial set-up of the redesigned MEDUSA instrument for the separation of 3 small ampholytes.

Upon application of 60 W of power from a Thermo Electron EC1000-90 power supply, the compartments were sampled every 5 minutes for the first 15 minutes, then every 30 minutes up to 2 hours. Capillary electrophoretic analysis by a P/ACE 2000 instrument (Beckman-Coulter, Fullerton, CA) of the aliquots collected from the respective compartments was used to confirm that IET was achieved. The UV detector of the

P/ACE 2000 was set at 214 nm. The capillary used had a 25 µm internal diameter, 20 cm length to the detector (L_d), and a 26.7 cm total length (L_t). A 20 mM boric acid solution titrated with lithium hydroxide to pH 9.25 was used as the BGE. A potential of 25 kV was employed with positive polarity at the detector side of the capillary. Normalized peak areas from the initial feed solution and from subsequent samples were calculated to see if any sample was lost.

3.1.3 Results and discussion

Figure 38 illustrates the final conditions of the IET experiment.

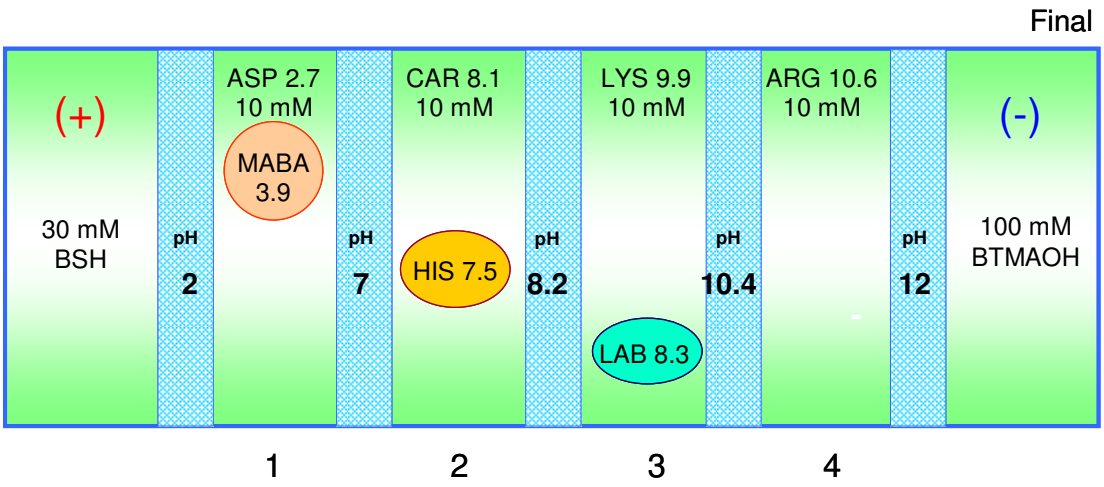

Figure 38. Final conditions. The three ampholytes are trapped by buffering membranes having pH values that bracket the p*I* values of the ampholytes.

During separation, volume changes occurred in each compartment: as the ampholytes migrated, they carried water of hydration. Table 4 shows the volume changes, including the 1 mL aliquots taken from the anolyte and catholyte and the 0.5 mL aliquots taken from solutions in the 4 separation compartments, as a function of time. Volume loss in the anode and cathode compartments was due to sampling only. The volume changes were included in the analyte recovery calculations.

Table 4. **Volume of solution left in each compartment as a function of separation time.**

Sampling Time min	**Anolyte** mL	**Comp 1** mL	**Comp 2** mL	**Comp 3** mL	**Comp 4** mL	**Catholyte** mL
0	100	10	10	10	10	100
5	99	10.5	10.5	9.5	7.5	99
10	98	10	10	9	5	98
15	97	9.5	9.5	8	5	97
30	96	9	9	7.5	4.5	96
60	95	8.5	8.5	7	4	95
90	94	8	8	6.5	3.5	94
120	93	7.5	7.5	6	3	93

Figure 39 shows the electropherograms for the initial and final samples taken during the IET separation. Initially, all the analytes were in compartment 4. At the end, no analyte was detected in compartment 4, as predicted. In compartment 3 only LAB is seen; in compartment 2, HIS and the UV-absorbing pH-biaser CAR are detected; in compartment 1, only MABA is seen. Benzenesulfonate ion (BS^-) and benzyltrimethylammonium ion ($BTMA^+$) remained in the anode and cathode compartment, respectively. There is no detectable cross-contamination between the compartments indicating that the IET separation was successful and the components were trapped for at least 2 hours, the duration of the experiment.

The normalized peak areas (nA) were calculated using Caesar 4.0 for Windows software (Analytical Devices, Inc., Alameda, CA) and are listed in Table 5 at four sampling points: (i) at t = 0 (before potential was applied); (ii) at t = 10 minutes (when the CE traces indicated that the separation might have been finished); (iii) at t =15 minutes (to see if the separation was indeed finished); (iv) and finally, at t = 120 minutes (to see if the analytes remained trapped). Table 5 also lists the corresponding volume correction factors and the corrected peak areas used to calculate the difference from the original feed solution (% Diff from Feed).

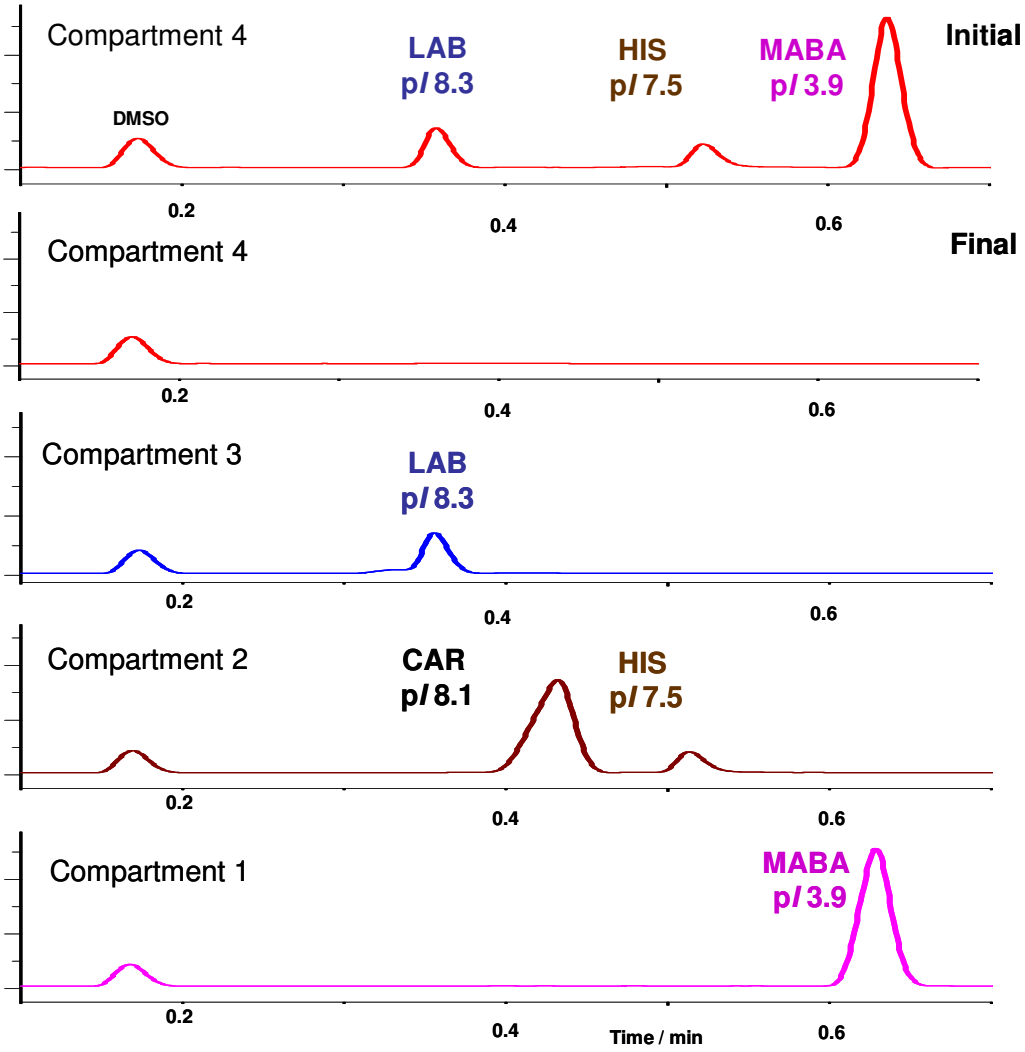

Figure 39. Electropherograms for the samples taken during the IET separation. The ampholytes were separated and trapped between buffering membranes whose pH values bracket their isoelectric points.

Table 5. Normalized peak areas (nA) for the detectable analytes in Compartment 1-4 at 3 different sampling time points. The corrected peak areas were obtained with the Vol Factor. The differences between the peak areas of the analytes at t = 0 and at the specific sampling time are also shown (% Diff from Feed).

t = 0 minutes						
Compartment	**MABA (pI 3.9)**	**HIS (pI 7.5)**	**CAR (pI 8.1)**	**LAB (pI 8.3)**	**BS-**	**BTMA+**
Anolyte					1.93E-03	
1						
2			1.11E-03			
3						
4	1.17E-03	1.79E-04		2.99E-04		
Catholyte						3.14E-04

t = 10 minutes									
Compartment	**MABA (pI 3.9)**	**HIS (pI 7.5)**	**CAR (pI 8.1)**	**LAB (pI 8.3)**	**BS-**	**BTMA+**	**Vol Factor**	**Corrected nA**	**% Diff from Feed**
Anolyte					1.93E-03		1	1.93E-03	0
1	1.04E-03						1.11	1.15E-03	1.7
2		1.63E-04					1.11	1.81E-04	1.1
			1.05E-03				1.11	1.16E-03	4.5
3				3.00E-04			1	3.00E-04	0.3
4	no analytes detected								
Catholyte						3.17E-04	1	3.17E-04	1.0

Table 5. Continued.

t = 15 minutes									
Compartment	**MABA (pI 3.9)**	**HIS (pI 7.5)**	**CAR (pI 8.1)**	**LAB (pI 8.3)**	**BS-**	**BTMA+**	**Vol Factor**	**Corrected nA**	**% Diff from Feed**
Anolyte					1.94E-03		1	1.94E-03	0.5
1	1.02E-03						1.12	1.14E-03	2.6
2		1.66E-04					1.12	1.86E-04	3.9
			1.06E-03				1.12	1.18E-03	6.3
3				3.27E-04			0.94	3.07E-04	2.7
4	no analytes detected								
Catholyte						3.16E-04	1	3.16E-04	0.6

t = 120 minutes									
Compartment	**MABA (pI 3.9)**	**HIS (pI 7.5)**	**CAR (pI 8.1)**	**LAB (pI 8.3)**	**BS-**	**BTMA+**	**Vol Factor**	**Corrected nA**	**% Diff from Feed**
Anolyte					1.94E-03		1	1.94E-03	0.5
1	1.07E-03						1.15	1.23E-03	5.1
2		1.52E-04					1.15	1.75E-04	2.2
			1.03E-03				1.15	1.18E-03	5.9
3				2.85E-04			0.92	2.62E-04	12.4
4	no analytes detected								
Catholyte						3.16E-04	1	3.16E-04	0.6

The average %Diff from Feed for the 3 sampling time points for the sample solutions is 2.9 % indicating adequate sample recovery.

The anolyte and catholyte were also sampled and analyzed the same way as the sample solutions. No analyte peaks were detected in their CE traces and no BS^- or $BTMA^+$ were detected in the separation compartments.

3.2 Four-compartment IET separation of chicken egg white proteins

3.2.1 Background and objective

In 2001, Desert, *et al.* used SDS-PAGE, native-PAGE, isoelectric focusing (IEF), and 2-dimensional electrophoresis (2DE) to analyze chicken egg white (EW) [142] and compared the results with values previously reported in literature [143-150] as shown in Table 6.

Column 1 lists the identified EW proteins. Column 2, 3, and 4 lists the p*I* values of the proteins from the lowest to the highest value obtained from the literature, IEF, and 2D-PAGE experiments, respectively. Column 5 lists the percentage of the particular protein in chicken EW. Finally, column 6, 7, and 8 list the molecular weight (MW) values obtained from the literature, SDS-PAGE analysis, and 2D-PAGE analysis, respectively.

Table 6. List of proteins identified in chicken egg white. Different techniques were used to determine their relative amounts and isoelectric points. Table adapted from [142]. Columns 2 and 6 contain values taken from the literature. nd: not determined.

EW Protein	p*I* (Lit.)	IEF p*I*	2D-PAGE p*I*	% of Total Protein	MW (Lit.) (kDa)	SDS-PAGE (MW kDa)	2D-PAGE (MW kDa)
ovomucoid				11	28	38	36
O5	3.83	4.0	4.4				
O4	4.01	4.1	4.5				
O3	4.17	4.3	4.6				
flavoprotein	4.2	nd	nd	0.8	29.2	38	nd
ovomucoid							
O2	4.28	4.4	4.7				
O1	4.41	4.5	4.9				
ovalbumin				54	45	50	44
A1	4.75	4.8	5.2				
A2	4.89	4.9	5.3				
A3	4.94	5.0	5.4				
ovoinhibitor	5.1	7.0	nd	0.1-1.5	49	nd	nd
ch21 protein	5.19	nd	5.6	nd	18	23	23
ovoglobulin		5.3-6.1	nd		49	nd	nd
G2	5.5			4			
G3	5.8			4			
ovotransferrin			7.0	12 - 13	77.7	74	81
fe2-ovtf	6.2	6.4					
fe-ovtf	6.6	6.6					
apo-ovtf	7.2	6.8					
avidin	10	nd	nd	0.05	68.3	19	nd
lysozyme	10.5			3.5	14.3	14	

Ovomucoid and flavoprotein can be highly glycosylated, up to 25 % and 15 % [147], respectively. Glycoproteins migrate more slowly in SDS-electrophoresis than nonglycoproteins, because the carbohydrate moieties do not bind SDS [143].

Since chicken egg white is readily available, inexpensive and has proteins whose p*I* values cover a broad range ($3.8 < pI < 10.5$), it was chosen to further test the capabilities of the redesigned MEDUSA.

In the first experiment, the chicken egg white proteins were separated into 4 fractions with p*I* ranges: $3.83 < pI < 5.8$, $6.2 < pI < 6.6$, $6.7 < pI < 7.2$, and $8.2 < pI < 10.5$. In a succeeding experiment, 2 ovoglobulin isoforms (p*I* 5.5 and p*I* 5.8) were isolated from a mixture that also contained ovotransferrin isoforms (p*I* 6.2, 6.6 and 7.2), avidin (p*I* 10) and lysozyme (p*I* 10.5).

3.2.2 IET separation of chicken egg white into four fractions

3.2.2.1 Instrument set-up, materials, and method

Ovomucoids (MUC, p*I* 3.8-4.4), ovalbumins (ALB, p*I* 4.7-5.4), ovoglobulins, (GLOB, p*I* 5.5-5.8) ovotransferrins (TRANS, p*I* 6.2-7.5), and lysozyme (LYZ, p*I* 10.5) are the major proteins of interest in chicken egg white. Membranes buffering at pH 2, 6, 7, 8.2, and 12 were used to form the four separation compartments. The separation was done under pH-biased conditions [38]. 10 mM each of aspartic acid, (ASP, p*I* 2.8), carnosine (CAR, p*I* 8.06), and lysine (LYS, p*I* 9.9) were used as pH biasers in compartments 1, 3,

and 4 respectively. For compartment 2, 4-hydroxy-3,5-bis(morpholinomethyl)benzoic acid (HBMMB p*I* 6.2) was used as the biaser: it was isolated from technical grade 4-hydroxy-3-methylmorpholino benzoic acid (HMMB p*I* 5.8) by a prior two-compartment IET separation [36]. Egg white, dissolved in a glutamic acid (GLU, p*I* 3.2) solution was fed into compartment 1.

The separation was started in constant current mode, at 75 mA. As the separation progressed, the potential increased until at 60 minutes it reached the 999 V limit of the power supply. From that point on, the power supply was operated in constant potential mode, at 999 V. As the separation progressed further, the current decreased and the potential remained constant at 999 V.

Figure 40 illustrates the initial set-up of the IET experiment. 5-mL aliquots were taken from each compartment every 10 minutes for 2 hours. The fractions were separated by SDS-PAGE and stained with Coomassie Blue.

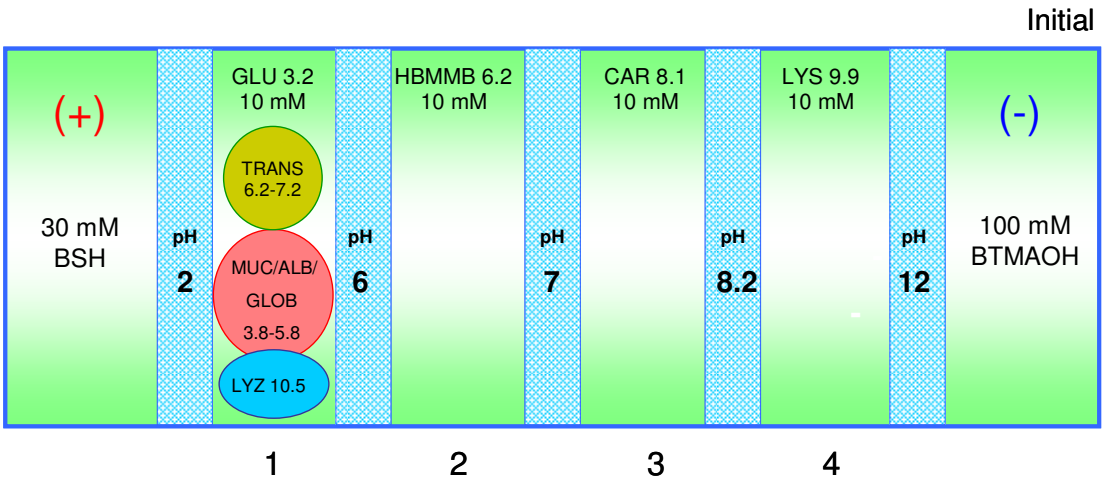

Figure 40. Initial set-up of the 4-compartment IET separation of major chicken egg-white proteins.

3.2.2.2 Results and discussion

Figure 41 illustrates the final conditions for the 4-compartment IET separation of chicken egg white proteins. The isoforms of ovomucoid, ovalbumin and ovoglobulin ($3.8 < pI < 5.8$) were trapped in compartment 1, between the membranes buffering at pH 2 and pH 6; the ovotransferrin isoforms ($6.2 < pI < 7.2$) were trapped in compartments 2 and 3, between the membranes buffering at pH 6, 7 and 8.2; lysozyme (pI 10.5) was trapped in compartment 4 bounded by membranes buffering at pH 8.2 and pH 12.

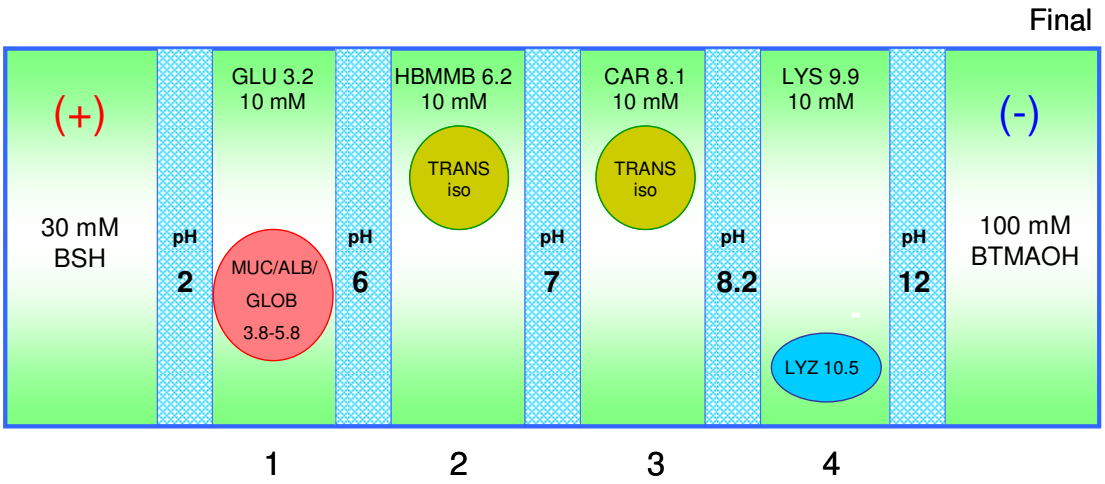

Figure 41. Final conditions of the 4-compartment IET separation of egg white proteins.

The SDS-PAGE image shown in Figure 42 is divided into 5 lanes for easier visual interpretation of results: samples taken from separation compartments 1-4 were in the first 4 lanes (from left); the molecular weight standards were in the 5th lane. The lanes are divided by black lines labeled with the pH value of the corresponding buffering membrane used in the IET separation. Red horizontal lines are also drawn across the SDS-PAGE image to help visual alignment of the molecular weight standards and the protein bands.

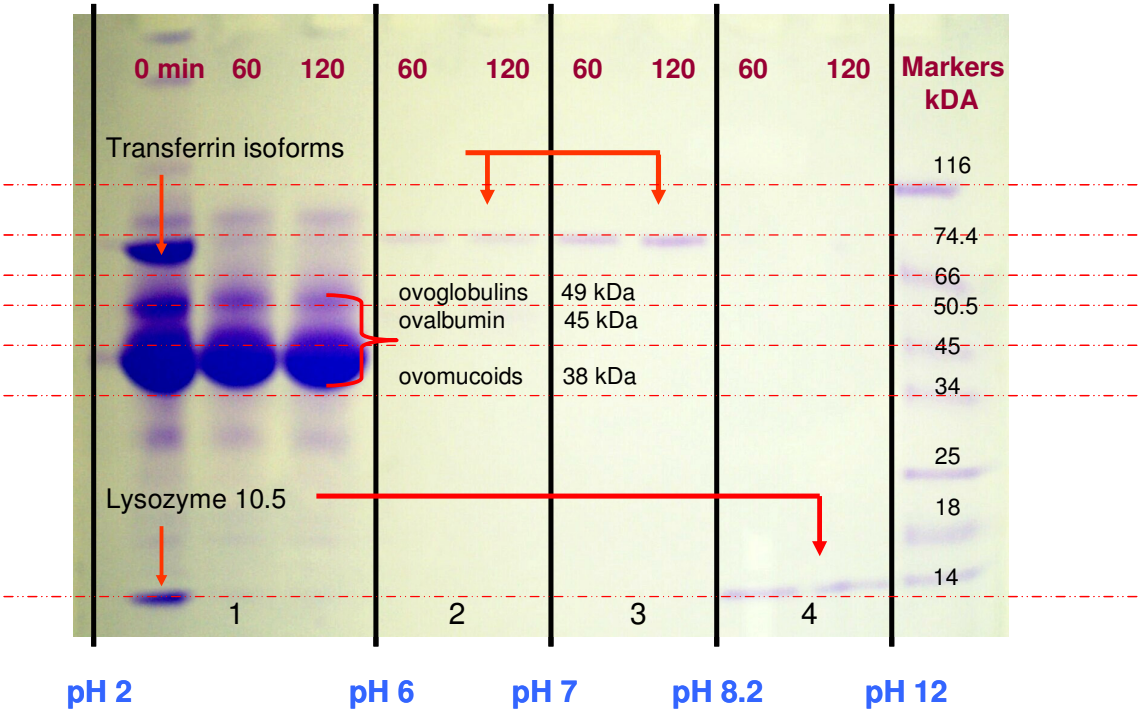

Figure 42. SDS-PAGE analysis of the fractions collected from compartments 1-4 at 0, 60, and 120-minute. Proteins were stained with Coomassie Blue.

Lane 1 has 3 sub-lanes designated 0, 60, and 120 min corresponding to the 0-, 60-, and 120-minute fractions taken. Lanes 2-4 only have 2 sublanes corresponding to the 60- and 120-minute fractions. In Lane 1, sublane 1 (designated 0 min) is the chicken egg white feed showing at 74 kDa the ovotransferrins; between 34-50 kDa, the ovoglobulins, ovalbumins, and ovomucoids (unresolved); and at 14 kDa, lysozyme. In the 60-min sublane, only the ovoglobulins, ovalbumins, and ovomucoids are visible. In Lanes 2 and 3, the ovotransferrin isomers are seen while in Lane 4, only lysozyme is present. The intensities of the bands in the 60- and 120-min lanes are similar, indicating that the IET

separation was practically completed in 60 minutes, and that no significant sample loss occurred while trapping was continued for another hour.

3.2.3 Isolation and concentration of ovoglobulin isoforms

3.2.3.1 Instrument set-up, materials, and method

With the availability of a newly synthesized PVA-based buffering membrane of pH 5.6 [151], another 4-compartment IET separation of the 5.2 < p*I* < 10.5 chicken egg white fraction was carried out to simultaneously isolate and concentrate the isoforms of ovoglobulin (p*I* 5.2 and 5.8, representing 4 %(w/w) of the protein content of chicken egg white). The mixture also contained the isoforms of ovotransferrin (6.2 < p*I* < 6.8 and p*I* 7.2, 13 %(w/w)), avidin (AVI, p*I* 10, 0.5 %(w/w)) and lysozyme (p*I* 10.5, 3.5 %). The 5.2 < p*I* < 10.5 egg white fraction (10 g in 500 mL aqueous solution) was loaded into compartment 3 with 10 mM CAR (p*I* 8.1) as the pH biaser. 10 mL of a 10 mM aqueous solutions of GLU (p*I* 3.2), HBMMB (p*I* 6.2), and LYS (p*I* 9.9) were used as pH biasers in compartments 1, 2, and 4 respectively. 100 mL of a 30 mM solution of benzenesulfonic acid and 100 mL of a 100 mM solution of benzyltrimethylammonium hydroxide were used as the anolyte and catholyte.

Figure 43 shows the initial set-up. The separation was started in constant current mode, at 75 mA. As the separation progressed, the potential increased until at 60 minutes it reached the 999 V limit of the power supply. From that point on, the power supply was

operated in constant potential mode, at 999 V. As the separation progressed further, the current decreased and the potential remained constant at 999 V.

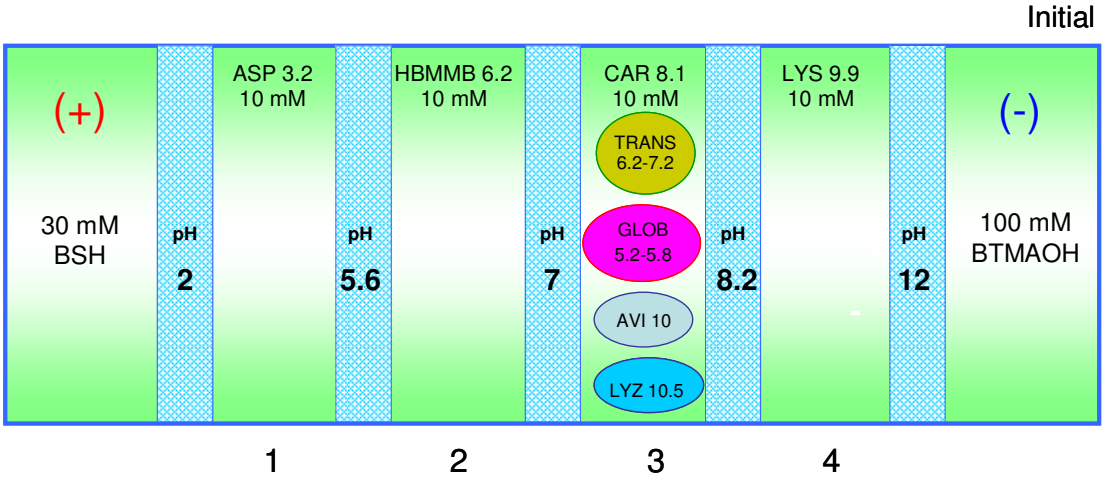

Figure 43. Initial set-up of the redesigned MEDUSA for the isolation and concentration of ovoglobulin isoforms.

During the course of the separation, 0.5-mL aliquots were collected from each compartment every 15 minutes for 240 minutes. The aliquots were analyzed by SDS-PAGE and detected by silver staining.

3.2.3.2 Results and discussion

Figure 44 illustrates the final conditions of the IET separation. The isoforms of ovoglobulin were separated from each other by the new pH 5.6 PVA-based buffering membrane and were located in compartments 1 and 2, respectively. The ovotransferrin isoforms were also separated by the pH 7 membrane and were located in compartments 1 and 2. Finally, avidin and lysozyme were separated from the rest and trapped in compartment 4.

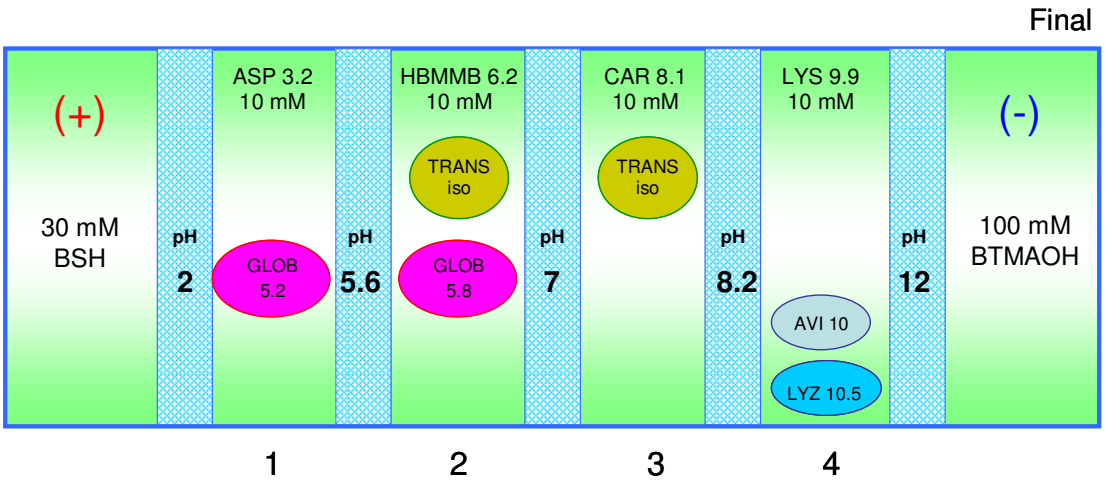

Figure 44. Final conditions in the redesigned MEDUSA after the isolation and concentration of the ovoglobulin isoforms.

The silver stained SDS-PAGE image shown in Figure 45 is divided into 7 lanes for easier interpretation of the results: the left outermost lane contain the molecular weight standards and an empty lane that serves as reference that tells us if a band is real or just an artifact; the second lane from the left and the outermost right lanes correspond to fractions taken from the anolyte (A) and catholyte (C); the middle 4 lanes represent the fractions taken from the 4 separation compartments: 1, 2, 3-FEED, and 4. The lanes are divided by black lines that are labeled with the pH of the corresponding buffering membrane used in the IET separation. Red horizontal lines are also drawn across the SDS-PAGE image to help with the alignment of the molecular weight standards and the protein bands. The sublanes (30-240 minutes) in Lane 1 contain the ovoglobulin isoform (p*I* 5.2) that became trapped and enriched there. The sublanes in Lane 2, contain an ovoglobulin isoform (p*I* 5.8) and ovotransferrin isoforms ($6.2 < pI < 6.6$). In the sublanes in Lane 3, the intensity of the ovotransferrin band is slowly decreased as the

other isoforms ($6.2 < pI < 6.8$) are transferred to compartment 2. The p*I* 7.2 isoform of ovotransferrrin is left trapped in compartment 3. Meanwhile, over time, lysozyme is transferred to compartment 4. Avidin is also present and concentrated in Lane 4: it can be found just below the 18 kDa marker indicating that under the analytical conditions used, avidin dissociated into its monomers of 15.6 and 15.9 kDa [142, 150, 152].

The sample load was 10 g of chicken egg white. Since the average concentration of the ovomucoid isomers is 4 % w/w in egg white [142] and transfer was complete in 120 minutes (as indicated by the SDS-PAGE image and conductance measurements), the fractionation rate achieved in the redesigned MEDUSA is about 200 mg/hour for this protein. This production rate compares very well with the rates reported for a binary IET separation of chicken egg white proteins using the Twinflow [38] and is better than reported production rates by the Isoprime MCE [54].

Figure 46 shows the conductance values measured over the 240-minute separation time. For compartments 1, 2, and 3, conductance starts to level-off at 120 minutes. This most probably signifies that almost all of the proteins that needed to be trapped in those compartments are already there. In compartment 4, there is still a slight increase in conductance from 120 minutes to 240 minutes. This is because, as seen in Lane 3 of Figure 10, lysozyme has not yet been completely transferred to compartment 4 in 240 minutes.

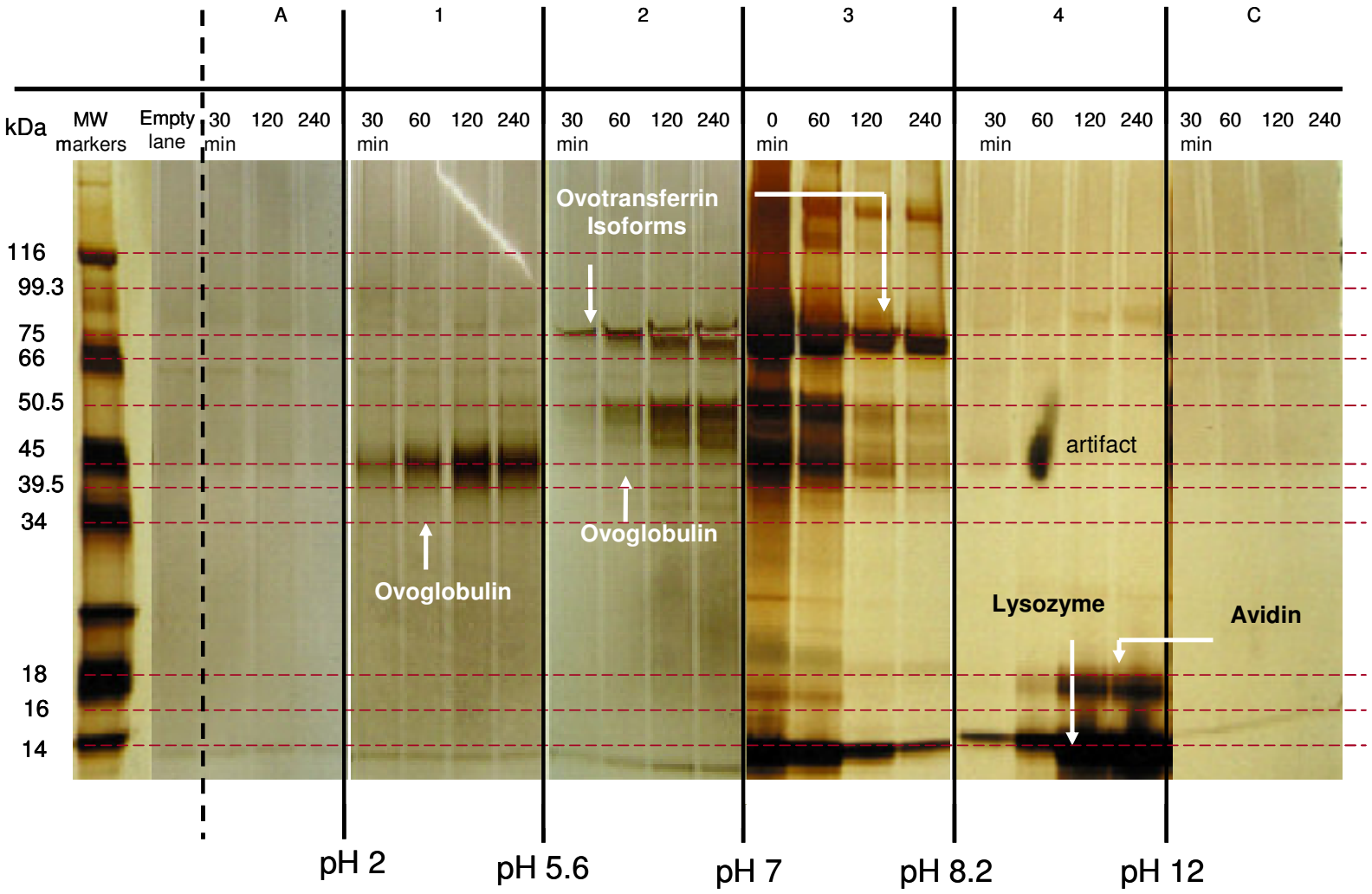

Figure 45. SDS-PAGE separation of the IET fractions obtained from chicken egg white (silver-stained image).

Figure 47 shows the pH values of the fractions taken over time: they do not change much over the entire time course of the IET separation indicating that the separation was achieved under ideal pH-biased conditions, without acid or base invasion.

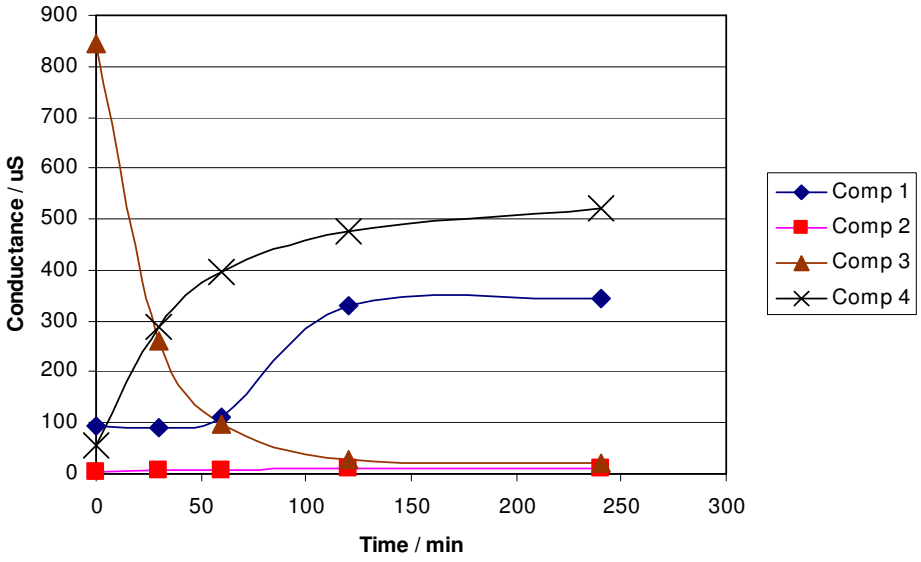

Figure 46. Conductance of the aliquots taken over the time course of the IET separation of chicken egg white proteins.

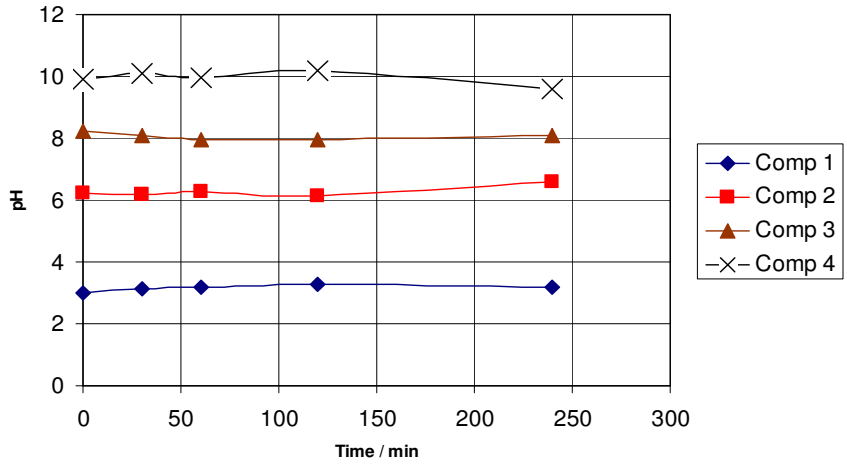

Figure 47. pH of the aliquots taken over the time course of the IET separation of chicken egg white proteins.

3.3 Six-compartment IET separation of low molecular weight ampholytes

3.3.1 Background and objective

In order to characterize the performance of the redesigned MEDUSA in the 6 separation compartment arrangement, eleven low molecular weight ampholytes were separated and trapped. Three of the ampholytes had p*I* values very close to the pH values of the respective buffering membranes.

3.3.2 Instrument set-up, materials, and method

The anolyte was a 30 mM solution of BSH (pH 1.52), the catholyte a 100 mM solution of BTMAOH (pH 13). Separation compartment 1 contained 4-aminophenyl butyric acid (APBA, approximate p*I* 5.2), tyramine (TYRA, approximate p*I* 10), and UV-absorbing derivatives of aspartic acid (MK 1-4, $2.1 < pI < 2.6$). Separation compartment 2 contained aspartic acid (ASP, approximate p*I* 2.8). Compartment 3 contained 1,3-bis(4-

morpholino)-2-*O*-sulfo-propane (BMSP, approximate p*I* 5.8), compartment 4 contained histidine (HIS, approximate p*I* 7.5). Compartment 5 and 6 contained lysine (LYS, approximate p*I* 9.9) and arginine (ARG, approximate p*I* 10.6), respectively. The solutions were recirculated at a flow rate of 30 mL/min. The anolyte and catholyte were recirculated at a flow rate of 2 L/min. After a successful leak test, a power of 60 W was applied. 0.5-mL aliquots were taken every 5 minutes for the first 15 min and then every 15 min for 4 hours. Figure 48 shows the structures of the ampholytes. Figure 49 illustrates the initial set-up.

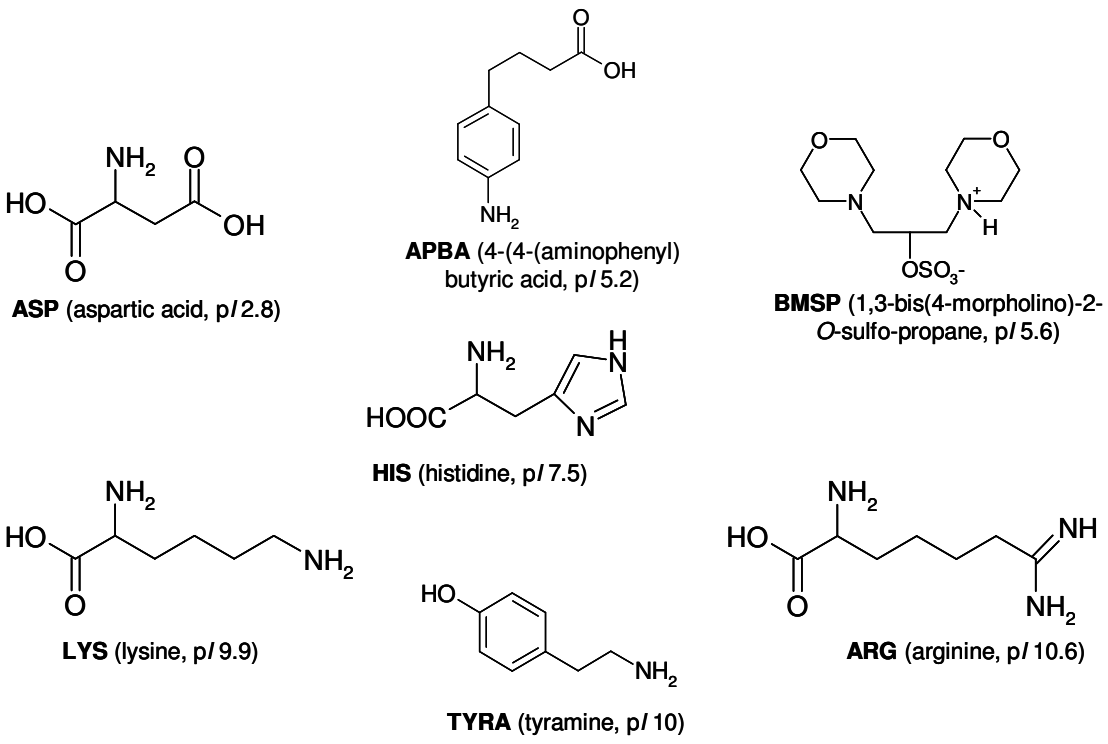

Figure 48. Structures of the low molecular weight ampholytes used for this experiment.

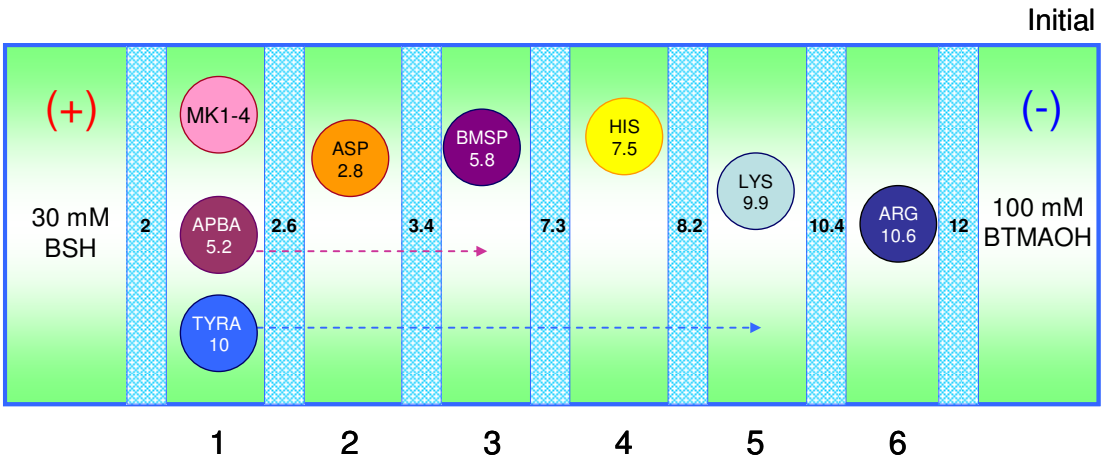

Figure 49. Initial setup of the 6-compartment IET separation of low molecular weight ampholytes. Arrows predict the movement of analytes into their respective compartments.

3.3.3 Results and discussion

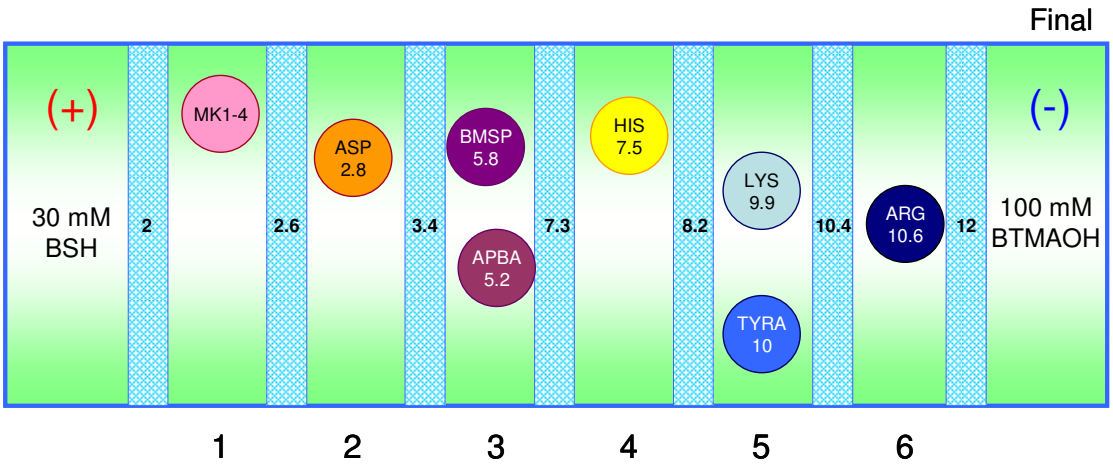

Figure 50. Final conditions. 6-compartment IET separation of low molecular weight ampholytes.

Figure 50 illustrates the final conditions of the separation. Aliquots taken during the course of the IET separation were analyzed by CE at 214 nm. Fractions taken from compartment 1, 2, 3, 5 and 6 were analyzed with a 10 mM phosphoric acid BGE titrated with lithium hydroxide to pH 7, at 10 kV, with negative polarity at the detector side. Fractions from compartment 4 were analyzed with a 10 mM phosphoric acid BGE titrated with lithium hydroxide to pH 9.25, at 10 kV, with negative polarity at the detector side.

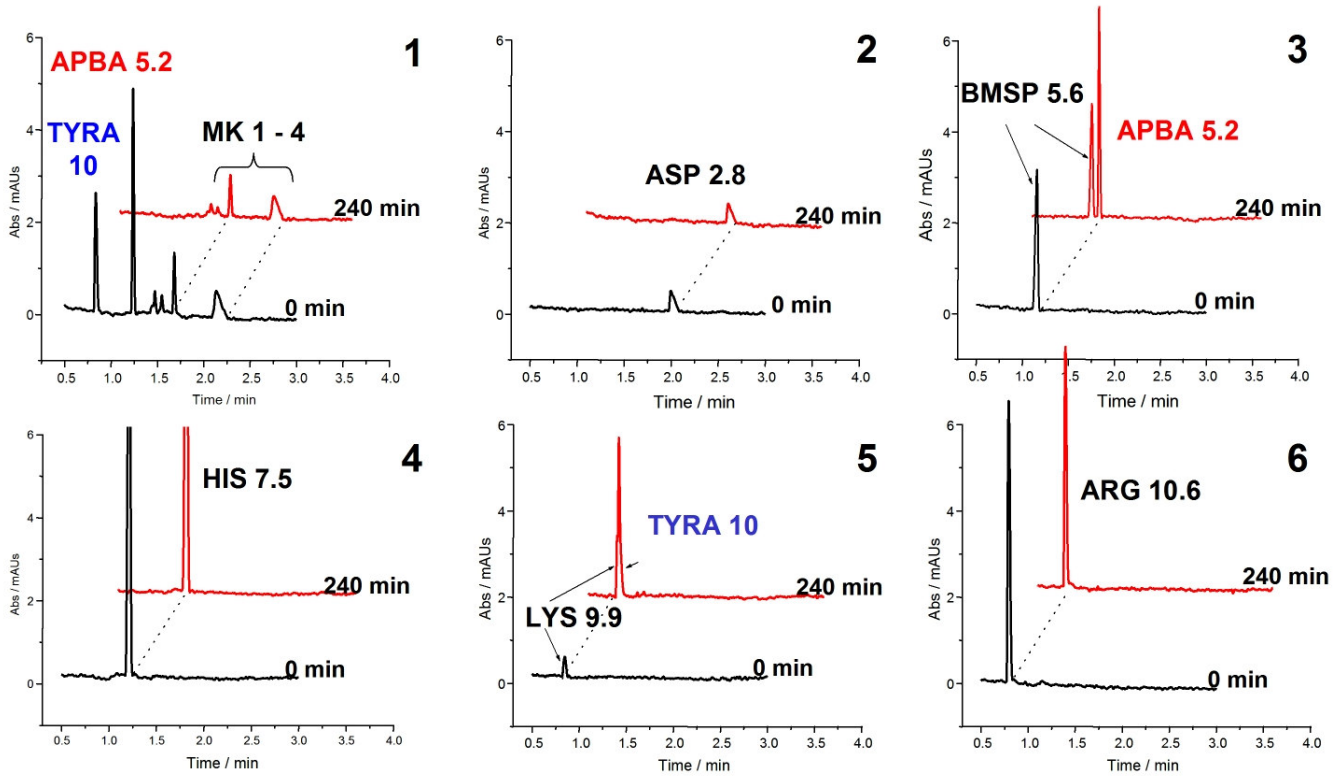

Figure 51. CE analyses of the sample fractions. Each graph is an offset overlay of the initial analysis at 0 minutes and the final analysis at 240 minutes of run time**.**

Figure 51 shows the electropherograms for the different compartments at separation time t = 0 minutes and at t = 240 minutes. The separation was finished within t = 10 minutes but the 10 min electropherograms are not shown. In compartment 1, at t = 0 minutes, all analytes are present: APBA, TYRA and MK 1-4. At t = 240 minutes, only MK 1-4 remained trapped in compartment 1. In Compartment 2, at t = 0 minutes and t = 240 minutes, only ASP is present. In Compartment 3, at t = 0 minutes, BMSP is present. At t = 240 minutes, BMSP and APBA are present. In compartment 4, at t = 0 minutes and at t = 240 minutes, HIS is present. In compartment 5, at t = 0 minutes, LYS is present. At t = 240 minutes LYS and TYRA are present. The mobilities of both analytes are very similar; however, the LYS can still be seen as a shoulder (to the left) next to the TYRA peak. Lastly, in compartment 6, at t = 0 minutes and at t = 240 minutes, ARG is present. As predicted, all probe analytes are in compartments that have buffering membranes with pH values that bracket their respective pI values.

Table 7 shows the peak areas for the ampholytes at t = 0, 10, 15, 120, and 240 min. The corrected peak areas were calculated as in the previous experiments, taking the volume changes into account. For MK 1 and MK 4 a recovery of 89.5 % ± 4.3 % and for ARG, a recovery of 78.8 % was calculated after 240 minutes of IET. For the other ampholytes, a recovery of 94.8 % ± 0.8 % is seen even after 240 minutes of trapping.

The losses can be attributed to isoelectric precipitation, because some of the buffering membranes have pH values that are very close to the p*I* values of the respective components. To confirm this hypothesis, the buffering membranes were soaked in deionized water and then the solutions were concentrated and analyzed by CE. Though the peak areas did not quantitatively account for all the missing material, they support the notion of isoelectric precipitation on the membrane.

3.4 Concluding remarks

This series of experiments demonstrated the utility of the redesigned MEDUSA for simultaneous fractionation of low molecular weight ampholytes and proteins. The redesigned MEDUSA could accommodate a large volume of feed mixture and could concentrate the low molecular weight ampholytes and proteins.

Table 7. Corrected peak areas of the ampholytes as a function of time and their % difference from their original values.

	0 min	10 min	% Diff	15 min	% Diff	120 min	% Diff	240 min	% Diff
Comp 1									
TYRA	1.996E-04								
APBA	1.292E-04								
MK 1	1.019E-05	9.016E-06	11.5	8.981E-06	11.9	8.801E-06	13.6	8.673E-06	14.9
MK 2	8.808E-06	8.231E-06	6.6	8.222E-06	6.7	8.140E-06	7.6	8.050E-06	8.6
MK 3	2.685E-05	2.591E-05	3.5	2.581E-05	3.9	2.564E-05	4.5	2.548E-05	5.1
MK 4	2.881E-05	2.562E-05	11.1	2.551E-05	11.4	2.514E-05	12.7	2.495E-05	13.4
Comp 2									
ASP	1.839E-05	1.775E-05	3.5	1.761E-05	4.2	1.740E-05	5.4	1.720E-05	6.5
Comp 3									
BMSP	1.559E-04	1.510E-04	3.1	1.497E-04	4.0	1.485E-04	4.7	1.477E-04	5.3
APBA		1.260E-04	2.5	1.251E-04	3.2	1.236E-04	4.3	1.232E-04	4.7
Comp 4									
HIS	6.392E-04	6.239E-04	2.4	6.229E-04	2.6	6.163E-04	3.6	6.110E-04	4.4
Comp 5									
LYS	4.014E-05	no resolution							
LYS-TYRA									
Comp 6									
ARG	6.321E-04	5.400E-04	14.6	5.370E-04	15.0	5.240E-04	17.1	4.980E-04	21.2

4 CAPILLARIES WITH CHARGED COATINGS ON THE INNER WALL: DESIGN AND MANUFACTURE

4.1 Objectives and principles

Capillaries with covalently attached anionic and cationic polymers on their inner walls have been developed to provide 3 specific qualities: (1) the capillaries were to have a specific EOF mobility (low to high value) such that one can choose which capillary to use for a particular analysis; (2) the capillaries with specific EOF mobilities were to have an EOF that was invariant in pH over a wide range; (3) and the capillaries were to be durable for extensive use over a wide pH range.

The manufacture of these charged coated capillaries involve 3 major steps: (1) pretreatment of the capillary; (2) bifunctionalization of the capillary surface; (3) coating of the capillary surface. The first 2 steps are the same for making capillaries either with anionic or cationic polymeric coatings. In the third step, the reagents used, their ratios and the reaction time differ with the two coating types.

The pretreatment and bifunctionalization processes are typically done on a long capillary (capillary stock) to maximize productivity. After pretreatment and bifunctionalization, the capillary is closed with rubber septa at both ends and stored at room temperature. 46.7-cm long portions of the pretreated and bifunctionalized capillary stock is then used in the coating procedures. The polymeric coating is formed by *in situ* free radical

polymerization of acrylamide and acrylamido derivatives, and the growing polymer is anchored onto the bifunctionalized capillary surface.

4.1.1 Instrumentation for filling the reagents into the capillary

The instrument used to deliver and mobilize all reagents (and gases) through the capillary is a P/ACE 2000 unit (Beckman Coulter, CA). This instrument is a key component in the successful manufacturing of the charged polymer-coated capillaries, because it offers online automation and offline direct control. Online automated control is achieved through the Gold Ver. 8.10 software whereby the user can program the delivery of reagents (or gas), their sequence, flow rate and duration Offline user control is made possible by the direct-control user-instrument interface.

The capillary to be treated is installed into the cartridge of the P/ACE 2000 and the loaded cartridge is used in all subsequent steps. All steps involved in the coating procedure are carried out at room temperature.

4.1.2 Pretreatment of the fused silica capillary

In the pretreatment step, the inner surface of the fused silica capillary is cleaned and hydrated to create an activated foundation for the reagents that will be immobilized to the surface.

A 6-m long, 50-µm ID fused silica capillary, assembled in a cartridge, and installed into the P/ACE 2000 instrument, is pretreated by rinsing (at 20 psi) sequentially with 1 M NaOH, deionized water, 0.1 M HCl, and DI water, for 1 hour each. Acetone is then flushed through the capillary for 2 hours. Finally, the capillary is dried with nitrogen gas at 20 psi for 3 hours at 25 °C.

4.1.3 Bifunctionalization of the pretreated fused silica capillary

A 50 % solution of 3-(trimethoxysilyl)propylmethacrylate (BindSilane) in acetone (v/v) acidified with acetic acid is used as the bifunctionalization reagent. The bifunctionalization reagent solution is rinsed through the capillary for 1 hour, followed by acetone for another hour. The procedure is repeated twice to maximize the concentration of the silylpropylmethacrylate anchor groups on the surface, though complete conversion of all silanol groups is likely not achieved. Finally, the capillary is dried overnight in a low pressure (0.5 psi) N_2 stream.

In acidic medium, 3-(trimethoxysilyl)propylmethacrylate, reacts *via* a condensation reaction with the free silanol groups on the capillary surface; the anchored methacrylate group can then be copolymerized with acrylamide [68]. Figure 52 shows the schematic of the bifunctionalization reaction.

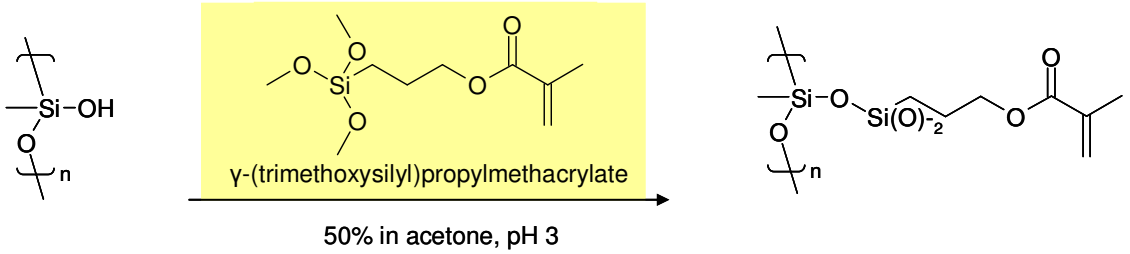

Figure 52. Schematic of the reaction of γ-(trimethoxysilyl)propylmethacrylate with the capillary surface (bifunctionalization).

4.1.4 Monomer-crosslinker solutions to form the immobilized polymer layers on the surface of the capillary

The monomer-crosslinker solutions used to form the immobilized polymer layers were all 3.2 %T and 0.2 %C. %T is defined as the total mass (*g)* of polymerizable monomers per 100 *g* solution; %C is defined as the mass (*g)* of crosslinker per 100 *g* of polymerizable monomers. A dilute (3.2 %) monomer concentration was chosen because the viscosity of this solution was low enough to permit relatively easy mobilization through the 46.7-cm, 50-µm ID capillaries (the P/ACE 2000 can only deliver a maximum of 20 psi pressure). 0.2 %C crosslinker was used because a lower concentration of crosslinker (0.1 %C) did not yield sufficiently durable coatings.

The monomer-crosslinker solutions contained a certain amount of charged monomer, neutral monomer, and crosslinker, where the ratio of charged monomer to non-charged monomer could be varied depending on the desired surface charge density for a particular coated capillary. To achieve a higher surface charge density (either negative

or positive) on the capillary, a solution with a higher amount of charged monomer (negative or positive) relative to the non-charged monomer was used.

The monomers used were: (i) negatively charged: 2-acrylamido-2-methyl-1-propanesulfonate ion, AMPS; (ii) positively charged: (3-acrylamidopropyl)trimethyl-ammonium ion, APTA; and (iii) non-charged: acrylamide, AA. The crosslinker used is *N,N′*-methylenebisacrylamide, MBA. The structures are shown in Figure 53.

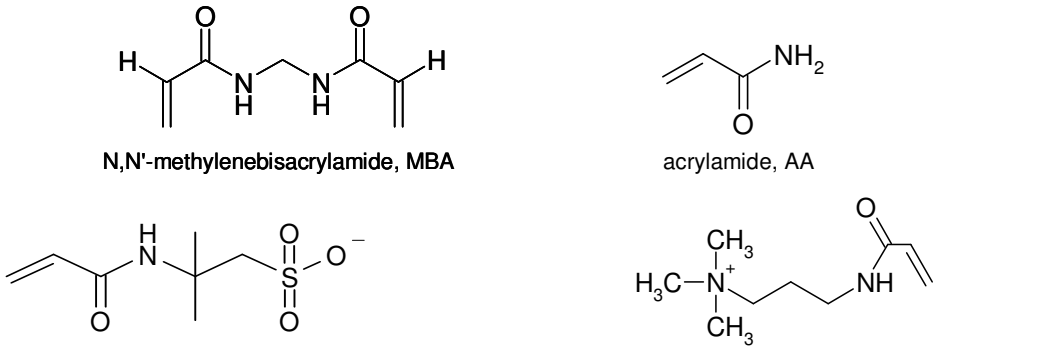

Figure 53. Structures of the monomers and crosslinker used to coat the bifunctionalized capillary surface.

The monomer-crosslinker solutions were mixed with a certain amount of catalyst, *N,N,N′,N′*-tetramethylethylenediamine, TEMED, then titrated to pH 6-7 with either tris-(hydroxymethyl)aminomethane, THAM (for the AMPS solution) or acetic acid, HOAc (for the APTA solution) to control hydrolysis of the amide functionalities and facilitate polymerization.

Typically, 100-g amounts of the solutions were prepared and stored at 5-8 °C in a refrigerator. For the coating reproducibility measurements, all capillaries were made with the same stock solution.

4.1.5 Purging of the monomer-crosslinker solution

In order to obtain reproducible coatings, the coating solution must be purged to eliminate any dissolved oxygen that acts as a radical scavenger and decreases the polymerization efficiency [127, 153]. Helium is used as the purging gas.

4 grams of the coating solution was carefully weighed into a 4-mL glass vial and covered with a screw-cap and rubber septum ensemble. Two stainless steel needles were inserted through the septum into the vial: (i) the purge needle reached through the coating solution all the way down to the bottom of the vial; (ii) the vent needle ended just above the coating solution. Helium was then delivered through the purge needle for 30 minutes to vigorously bubble through the solution and remove any dissolved oxygen. Figure 54 shows a schematic of the purging process.

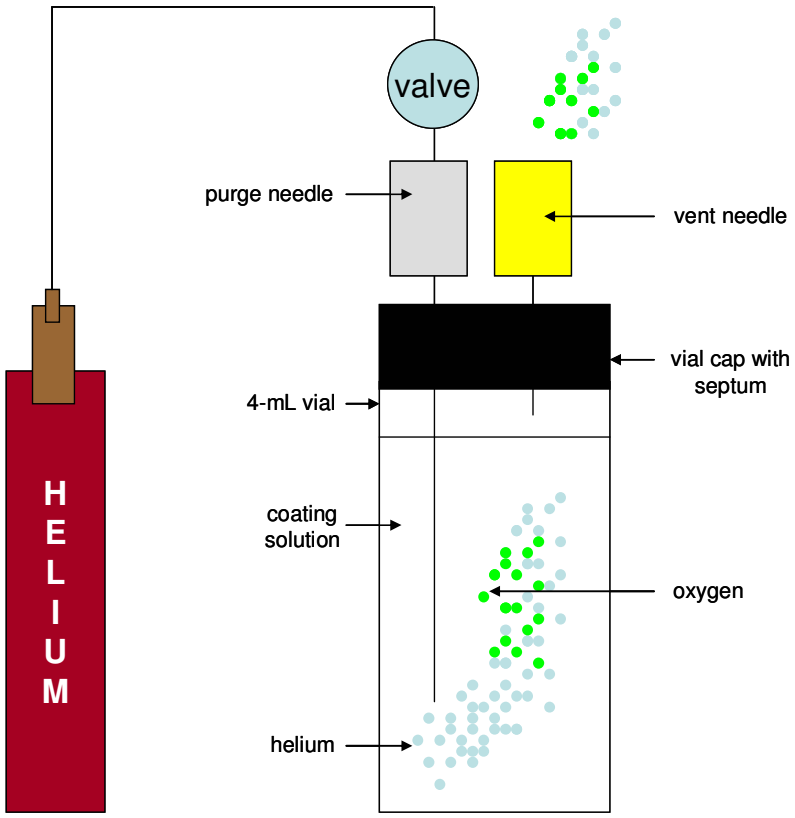

Figure 54. Schematic of the purging station for the removal of dissolved O_2 from the coating solution by helium gas.

4.1.6 General capillary coating procedure

A 46.7-cm L_t (total length), 40-cm L_d (length to the detector), 50-µm ID bifunctionalized capillary was first assembled into a P/ACE cartridge. The cartridge was then installed into the P/ACE instrument. While the coating solution was purged with helium, the capillary was flushed with nitrogen gas at 0.5 psi for 30 minutes to free the capillary of oxygen. In the meantime, a fresh 4 % ammonium persulfate solution, APS (the initiator solution), was prepared.

When the coating solution was ready, it was removed from the helium purging station and brought near the P/ACE, ready for addition of the initiator and delivery into the capillary. 10 μL of 4 %APS was injected into the coating solution through the septum. The solution was immediately shaken for about 2 seconds. The screw-cap and septum were removed from the vial and replaced with a rubber seal cap of the P/ACE to facilitate pressure-assisted injection of the reagents into the nitrogen-filled capillary. With the cap in place, the vial was placed onto the sample tray of the P/ACE and, using the user-instrument interface of the P/ACE, the coating solution was filled into the capillary.

The steps from the addition of the initiator to the filling of the solution into the capillary had to be done with controlled haste to minimize exposure to oxygen [127, 153]. Since the tip of the capillary was dipped far down into the solution, it was assumed that during the brief filling procedure, oxygen from air would not have diffused into the capillary affecting the reproducibility of polymerization.

The coating solution was flushed through the capillary for 2.5 minutes (this is the coating time). After that, deionized water, then nitrogen was immediately flushed through the capillary at 20 psi for 2 minutes each. Next, a gentle stream of nitrogen (0.5 psi) was passed through the capillary for 20 minutes and the polymeric layer was allowed to set for at least 6 hours before use.

4.2 Testing the quality of the coated capillaries

This section describes the general procedures used to test the quality of the coated capillaries. Each coated capillary was tested on 3 specific qualities: (1) the magnitude of the EOF generated over a wide pH range, (2) its long-term durability when exposed to low and high pH BGEs, and (3) the effect of the ionic strength of the BGE on the mobility of the EOF.

4.2.1 Determination of the μ^{EOF} by pressure mediated capillary electrophoresis

Pressure mediated capillary electrophoresis (PreMCE), developed by Williams and Vigh was used to determine the mobility of EOF, μ^{EOF} in the coated capillaries [154]. Specifically, a 2-band PreMCE method was used. The success of the method is predicated on precise pressure rinses which are available on the P/ACE 2000 (as with most commercial CE instruments). The PreMCE method eliminates problems inherent to the conventional mobility determination method such as a variable EOF during the run and migration through unthermostated regions of the capillary. Moreover, very low μ^{EOF} can also be measured quickly and reproducibly, especially important for capillaries with low permanent surface charge densities.

Figure 55 shows the typical sequence of steps involved in a 2-band PreMCE method for the determination of μ^{EOF}: (A) a band of a noncharged, UV-absorbing marker (neutral marker, *N*) is injected into the capillary; (B) the injected band of *N* is transferred for a certain amount of time (t_{trans}) using pressure (1.0 psi) such that *N* is in the thermostated

region of the capillary; (C) another band of *N* is injected; (D) this band of N is transferred into the capillary for another t_{trans} (both bands of *N* are now in the thermostated region); (E) electric potential (V) is applied across the capillary for a certain amount of time (t_{elec}); (F) a final band of *N* is injected; and (G) all bands of *N* are mobilized through the capillary, past the UV-detector, by pressure for a certain amount of time and the detector trace is recorded.

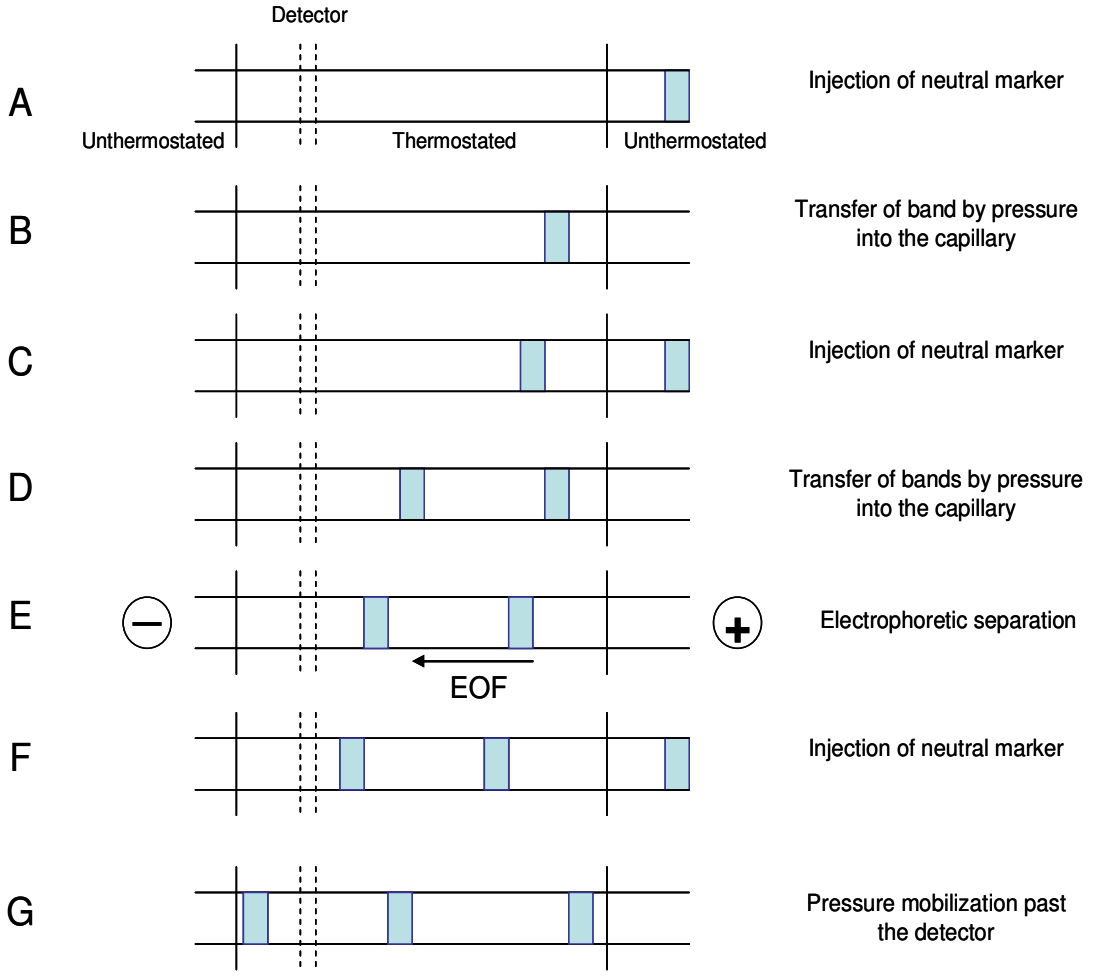

Figure 55. 2-band PreMCE method for the fast and accurate determination of the EOF mobilities. Figure reproduced from [154].

The coated capillaries tested all had a total length of 46.7 cm (L_t), a length to the detector of 40 cm (L_d), and an internal diameter (ID) of 50 μm. Taking the capillary dimensions into consideration, the following materials and conditions were specifically used for the method: *N* was dimethylsulfoxide (DMSO), t_{trans} = 75 seconds (with 1.0 psi), V = 10000 V, t_{elec} = 5 or 10 minutes (depending on whether high EOF or low EOF capillaries were tested; it is critical that the 2 bands of transferred *N* do not pass the detector during the electrophoresis step), and final mobilization time of 11 minutes (all 3 bands of *N* are seen in 10 minutes).

4.2.2 Testing the stability of μ^{EOF} in low and high pH BGEs

The durability of the coatings was tested by exposing the coated capillaries for extended periods of time to pH 2.71 and pH 9.25 background electrolytes. 10 μ^{EOF} determinations (as described above) were done everyday for the first 2 weeks and then every week thereafter for 4 months. Within this time frame, the capillaries were always stored with pH 2.71 or pH 9.25 buffers inside them.

4.2.3 The effect of the ionic strength of the BGE on μ^{EOF}

The higher the ionic strength of the BGE, the lower the μ^{EOF} becomes [76, 155-158]. Gas and co-workers used a unified equation to describe the ionic strength dependence of mobility in their PeakMaster program [159, 160] as follows:

$$\mu = \mu_1^0 - \left(B_1 z_1 \mu_1^0 \sum_{n-0}^{s} C_n R_1^n + B_2 / z / \right) \frac{\sqrt{\Gamma}}{1 + \frac{Ba}{\sqrt{2}} \sqrt{\Gamma}} \qquad (12)$$

where:

$$B_1 = \frac{e^3}{12\pi} \sqrt{\frac{N_{Av}}{(\varepsilon k T)^3}} \qquad (13) \qquad B_2 = \frac{e^2}{6\pi\eta} \sqrt{\frac{N_{Av}}{\varepsilon k T}} \qquad (14)$$

$$\Gamma = \sum_{l=1}^{s} \Gamma_l, \Gamma = c_l z_l^{\ 2} \qquad (15) \qquad B = \sqrt{\frac{2e^2 N_{Av}}{\varepsilon k T}} \qquad (16)$$

u_l^0: limiting ionic mobility, z_l: relative charge of the l-th ionic species, c_l: concentration of the l-th ionic species, e: elementary charge, N_{Av}: Avogadro constant, ε: permittivity of the solution, η: viscosity of the solution, k: Boltzmann constant, T: absolute temperature, $R_l^{(n)}$: n-th component of vector R_l, C_n: n-th member of a series, a: diameter of the ion, and s: the overall number of all ionic species.

We have realized that it is the ion in the diffused Guoy-Chapman layer that brings about the electroosmotic flow and thus, we extended Eq. 12 and used it to model the dependence of the μ^{EOF} on the ionic strength of the BGE.

A slightly simplified form of this equation has been used to fit the μ^{EOF} values measured in different ionic strength BGEs as follows:

$$\mu^{EOF} = a - b \frac{\sqrt{\Gamma}}{1 + c\sqrt{\Gamma}} \qquad (17)$$

where ***a*** and ***b*** are constants that depend on the physical, electronic, and thermodynamic properties of the bulk solution, ***c*** is a constant that depends on the electronic and thermodynamic properties of the ion, as well as its hydrodynamic diameter, in the diffused Guoy-Chapman double layer, and **Γ** is the ionic strength of the BGE used.

BGEs with ionic strengths in the 10 mM to 100 mM range were used in capillaries coated with both anionic and cationic polymers and, for reference purposes, in untreated fused silica capillaries. The Origin Ver. 5.1 software package (Microcal, Northampton, MA) was employed for the non-linear least square fitting procedure.

4.3 Manufacture of capillaries coated with an anionic polymer

Capillaries coated with an anionic polymer were made *via* free radical copolymerization of 2-acrylamido-2-methyl-1-propanesulfonate, AMPS, acrylamide, AA, *N,N'*-methylenebis(acrylamide), MBA and the methacrylate anchor group on the bifunctionalized surface of the fused silica capillary. The next sections describe the procedures in the design and manufacture of these capillaries and the results in their quality tests.

4.3.1 Design, materials and methods

Coating solutions with different AMPS/AA ratios (all 3.2 %T, 0.2 %C) were used to manufacture capillaries with different negative surface charge densities. Freshly-prepared concentrated stock solutions of the polymerizable reagents were mixed in appropriate volumes to yield the desired amounts needed to make each AMPS-coated capillary. Table 8 lists the actual amounts of AMPS, AA, MBA, and TEMED added to each coating solution. 10 μL of 4 %APS was used to initiate the polymerization of 4-g aliquots taken from each coating solution.

In Table 8, %AMPS was calculated as $100 * m_{AMPS}/(m_{AMPS} + m_{AA} + m_{MBA})$. 13 stock solutions were made yielding 13 capillaries with different EOF mobilities. From here onward, each solution and capillary will be designated by the %AMPS value used. Every capillary was prepared using the same procedure described in Sections 4.1.5 and 4.1.6. Figure 56 shows a possible schematic structure for a crosslinked, 18 %AMPS-coated capillary.

Table 8. Composition of the coating solutions used to prepare the immobilized anionic polymers. 10 µL of 4 %APS was also added to the 4-g aliquots taken from each stock solution to initiate the polymerization.

100-g stock solution (3.2 %T, 0.2 %C)					4-g aliquot
m_{MBA}	m_{AA}	m_{AMPS}	%AMPS	vol_{TEMED}	$vol_{4\ \%APS}$
g	*g*	*g*	*%*	*µL*	*µL*
0.0064	3.12	0.077	2.41	50	10
0.0064	3.05	0.155	4.83	50	10
0.0064	2.97	0.235	7.34	50	10
0.0064	2.87	0.330	10.3	50	10
0.0064	2.62	0.576	18.0	50	10
0.0064	2.40	0.800	25.0	50	10
0.0064	2.24	0.960	30.0	50	10
0.0064	2.08	1.12	35.0	50	10
0.0064	1.98	1.22	38.1	50	10
0.0064	1.76	1.44	45.0	50	10
0.0064	1.28	1.92	60.0	50	10
0.0064	0.640	2.56	80.0	50	10
0.0064	0.320	2.88	90.0	50	10

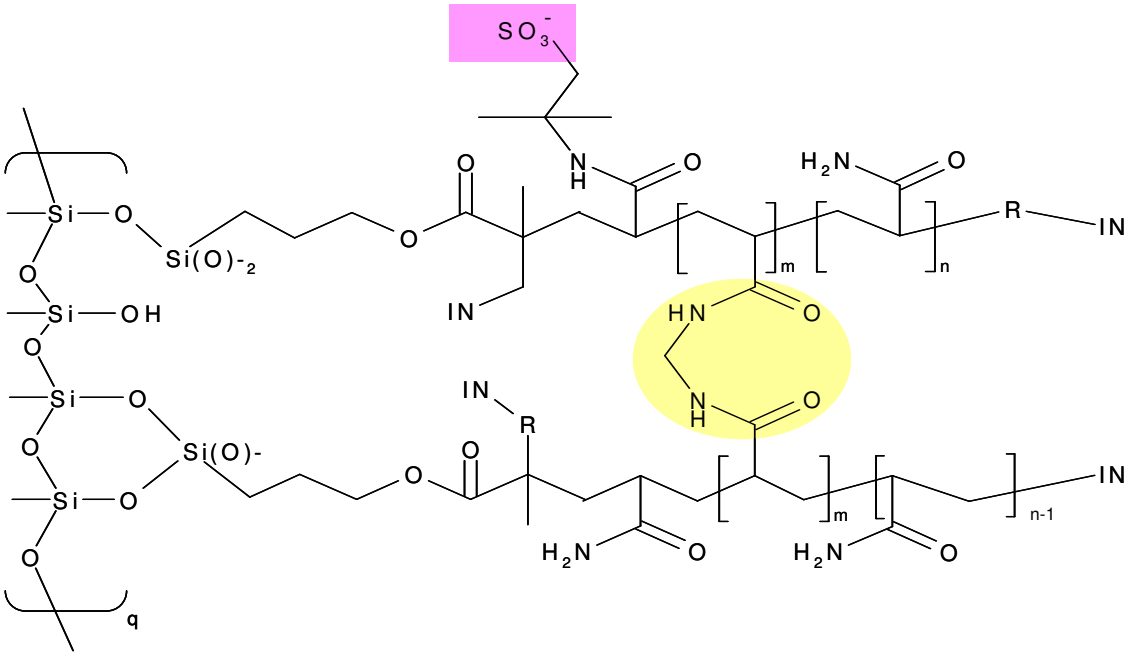

Figure 56. Possible schematic structure of the surface of an AMPS-coated capillary. For an 18 %AMPS-coated capillary (0.58g AMPS in 3.2 g AMPS+AA+MBA) at 3.2 % T, 0.2 %C, there should be 0.011 MBA (m) per 4.55 AA (n) and 1 AMPS. IN-R: (1) initiator-monomer radical (terminator), where the monomer is AMPS, AA, or MBA; or (2) initiator-polymer radical (terminator), where the polymer is $-[AMPS]_r-[AA]_s-[MBA]_t-$ and r, s, and t depend on the composition of the coating solution.

4.3.2 μ^{EOF} as a function of %AMPS

Following preparation, each capillary was immediately tested to determine μ^{EOF} in low and high pH BGEs. If the coating was well prepared, μ^{EOF} would be constant over the entire pH range. However, if there were residual exposed silanol groups (their pKa values can range from 2 to 9 [57]), μ^{EOF} would increase with increasing pH of the BGE.

Table 9 lists the μ^{EOF} values for the 13 AMPS-coated capillaries in 12.6 mM H_3PO_4 titrated with LiOH to pH 2.71 and 20 mM H_3BO_3 titrated with LiOH to pH 2.71 BGEs. Both BGEs have ionic strengths equal to 10 mM as calculated by the PeakMaster program 5.1 [161]. Figure 57 is a graphical representation of Table 9.

Table 9. μ^{EOF} for the AMPS-coated capillaries in low and high pH BGEs.

%AMPS	μ^{EOF} / 10^{-5} cm^2 $V^{-1}s^{-1}$	
	pH 2.71	pH 9.25
2.41	2.63	3.50
4.83	5.46	6.50
7.34	8.19	9.40
10.3	10.3	11.3
18.0	13.0	14.5
25.0	16.7	17.8
30.0	18.2	19.5
35.0	20.3	21.8
38.1	21.9	23.4
45.0	23.4	24.9
60.0	29.0	29.9
80.0	34.0	34.6
90.0	34.9	35.4

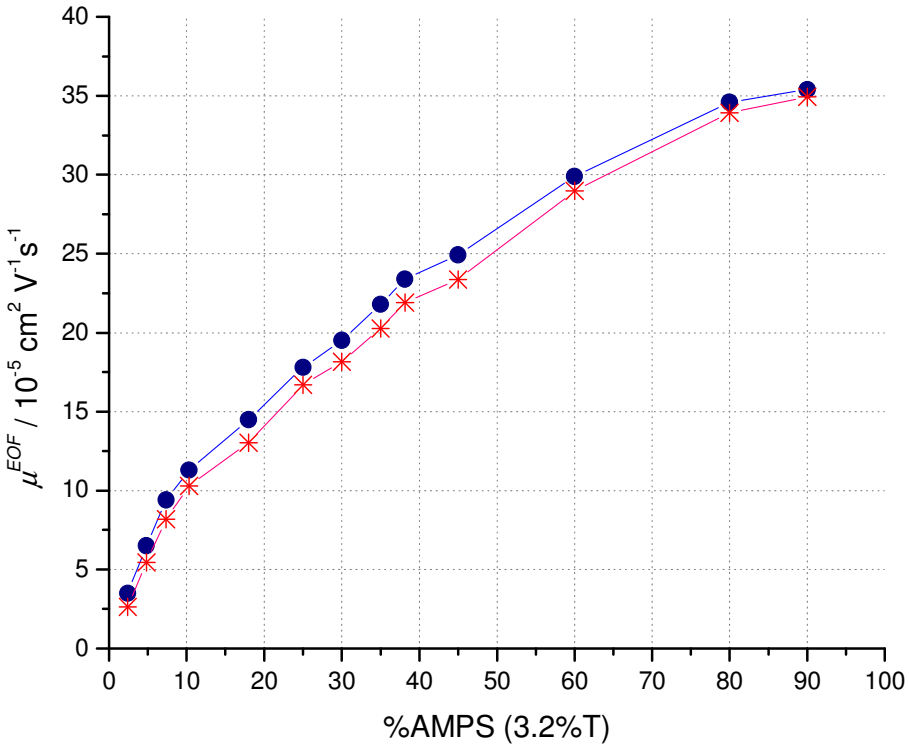

Figure 57. Graph of μ^{EOF} for the AMPS-coated capillaries in the low and high pH BGEs. Both BGEs have ionic strengths of 10 mM.

4.3.3 μ^{EOF} as a function of the pH of the BGE

Next, μ^{EOF} was determined in 4 BGEs whose pH span the 2.71 < pH < 9.25 range for 4 AMPS-coated capillaries. It is important that in comparing μ^{EOF} values at different pH values, the counter-ion responsible for EOF be the same for all BGEs. The magnitude of μ^{EOF} is a function of the mobility of this counter-ion. Theoretically, assuming that all other parameters are constant, different counter-ions (with different mobilities) will give different EOF mobilities [160, 162].

Four different 10 mM ionic strength buffers were prepared carefully. 12.6 mM phosphoric acid was titrated with LiOH to pH 2.71, 20 mM acetic acid (CH_3COOH) was titrated with LiOH to pH 4.72, 20 mM 4-(2-hydroxyethyl)-1-piperazineethanesulfonic acid (HEPES) was titrated with LiOH to pH 7.46, and 20 mM boric acid (H_3BO_3) was titrated with LiOH to pH 9.25, respectively, as shown in Table 10, making Li^+ as the common counter-ion. Using the PeakMaster 5.1 program [161], the theoretical μ^{eff} (effective mobilities) of the Li^+ counter-ions in the different BGEs were calculated.

Table 10. List of BGEs used in the determination of μ^{EOF} for the AMPS-coated capillaries. All BGEs have ionic strengths of 10 mM as calculated by the PeakMaster 5.1 program.

BGEs	Counter-ion	PeakMaster
		μ^{eff} / 10^{-5} cm^2 V^{-1} s^{-1}
12.6 mM H_3PO_4 titrated with LiOH to pH 2.71	Li^+	36.7
20 mM CH_3COOH titrated with LiOH to pH 4.72	Li^+	36.6
20 mM HEPES titrated with LiOH to pH 7.46	Li^+	36.6
20 mM H_3BO_3 titrated with LiOH to pH 9.25	Li^+	36.6

The 2 sets of 4 capillaries chosen were 2.41, 30, 60, and 90 %AMPS. The results obtained for these capillaries represent the entire %AMPS range used. Table 11 lists the dependence of μ^{EOF} (average values) for the representative capillaries at different pH values in the 2.71< pH < 9.25 range. For the 2.41 and 30 %AMPS capillaries, V = 10

kV, and t_{elec} = 10 minutes. For the 60 and 90 %AMPS capillaries, V = 5 kV, and t_{elec} = 10 minutes. It can be seen that μ^{EOF} for the 4 capillaries increased only slightly over the entire pH range tested.

Table 11. μ^{EOF} for the AMPS-coated capillaries in the 2.71 < pH < 9.25 range.

%AMPS	μ^{EOF} / 10^{-5} cm^2 V^{-1} s^{-1}			
	pH 2.71	pH 4.72	pH 7.46	pH 9.25
2.41	2.63	2.81	3.25	3.50
30	18.2	18.5	19.1	19.5
60	29.0	29.3	29.6	29.9
90	34.9	35.1	35.3	35.4

4.3.4 Testing the stability of the AMPS-coated capillaries in low and high pH BGEs

Having found that μ^{EOF} in the AMPS-coated capillaries is practically independent of the pH, the long term stability of this pH-independent EOF was determined. The capillaries, BGEs, V and t_{elec} values used were the same as in Section 4.3.3. The stability testing period was 4 months long. Ten μ^{EOF} determinations were completed daily for two weeks and once a week thereafter for 4 months. After each μ^{EOF} determination the capillaries were stored with pH 2.71 and pH 9.25 BGEs inside them. Table 12 shows the average μ^{EOF} values determined for the capillaries at the end of the 4 month-long

stability tests. Figure 58 is a graphical representation of the data in Table 12, combined with the μ^{EOF} values of an untreated fused silica reference capillary.

Table 12. μ^{EOF} values determined for the AMPS-coated capillaries in the 2.71< pH< 9.25 range during 4 months of stability testing.

%AMPS		μ^{EOF} / 10^{-5} cm^2 V^{-1} s^{-1}			
		pH 2.71	**pH 4.72**	**pH 7.46**	**pH 9.25**
2.41	Initial	2.63	2.81	3.25	3.50
	4 months	2.89	3.21	3.67	3.82
30	Initial	18.2	18.5	19.1	19.5
	4 months	19.1	19.3	20.7	20.9
60	Initial	29.0	29.3	29.6	29.9
	4 months	29.6	29.8	30.7	31.2
90	Initial	34.9	35.1	35.3	35.4
	4 months	35.7	35.9	36.8	37.3

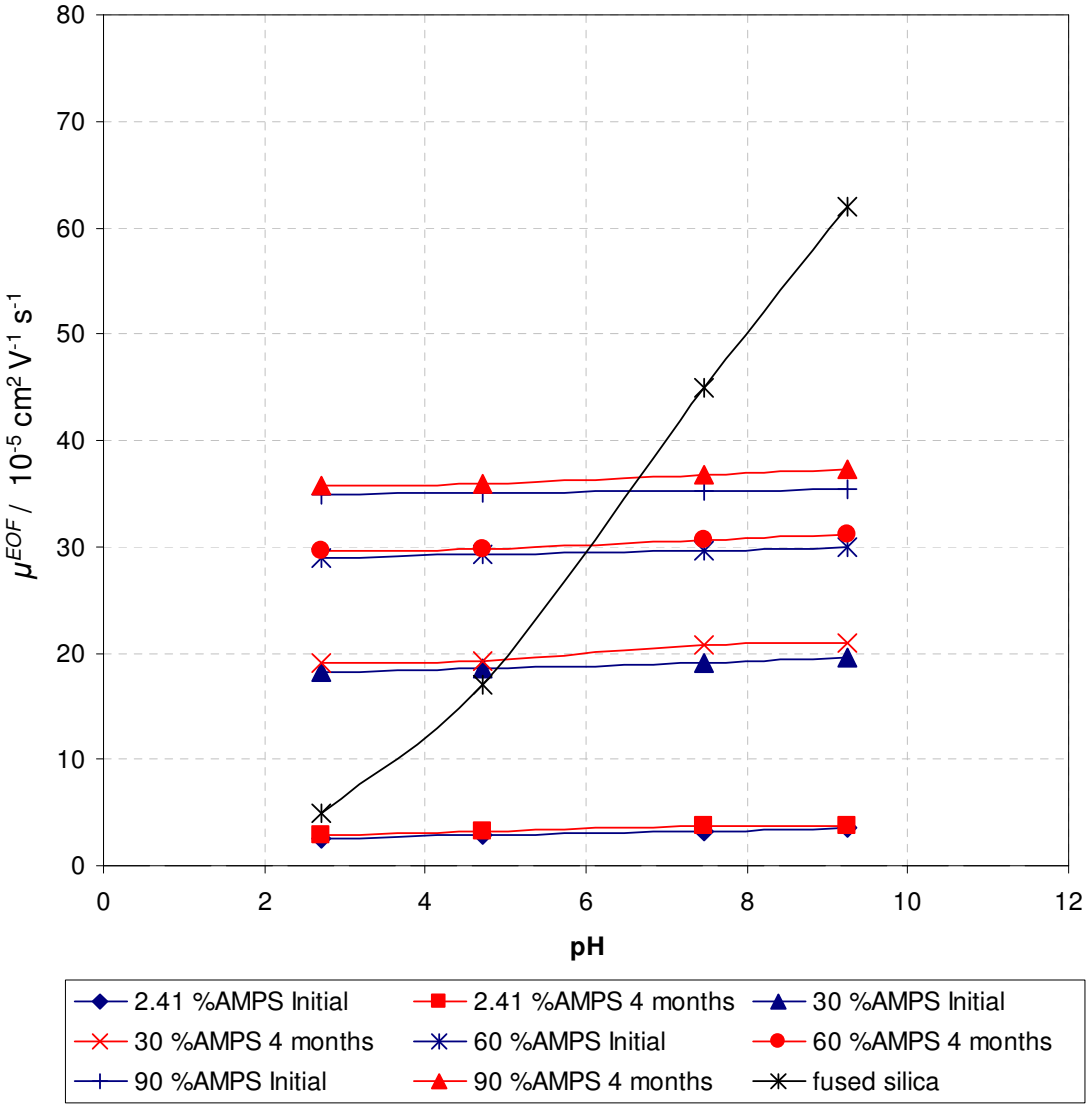

Figure 58. μ^{EOF} as a function of pH for the 4 AMPS-coated capillaries. Blue points are the initial μ^{EOF} values, the red points are the μ^{EOF} values after 4 months of storage and use in the low and high pH BGEs.

After 4 months of storage and use of the capillaries in the low and high pH BGEs, μ^{EOF} increased, on average, by less than 10 %. This could be caused by a minor degradation of the coating introducing carboxylate groups or exposing silanol groups on the surface of the capillary, or both. Nonetheless, the long term stability of these capillaries is much better than what is seen with non-crosslinked polymers [63].

4.3.5 μ^{EOF} as a function of the ionic strength of the BGE

A 400 mM HEPES titrated with ethanolamine to pH 6.9 BGE was prepared (IS = 99.8 mM). Portions of the 99.8 mM IS BGE were diluted to make 4 other BGEs with ionic strengths of 9.97, 24.9, 49.9, and 74.8 mM. The 5 BGEs made were used, along with a 2-band PreMCE method, for the determination of the μ^{EOF} values in a 46.7-cm L_t, 40-cm L_d, 50-µm ID 60 %AMPS-coated capillary and an untreated fused silica capillary (UFSC) used as reference capillary. The μ^{EOF} values were then fitted by the equation:

$$y = a - b\frac{\sqrt{x/1000}}{1 + c\sqrt{x/1000}} \qquad (18)$$

where ***y*** is the EOF mobility, ***a*** and ***b*** are constants that depend on the physical, electronic, and thermodynamic properties of the bulk solution, ***c*** is a constant that depends on the electronic and thermodynamic properties of the ion, as well as its hydrodynamic diameter, in the Guoy-Chapman layer, and finally ***x*** is the ionic strength of the BGE (mM), using the Origin Ver. 5.1 software package.

It can be seen in Figure 59 that the measured μ^{EOF} values fit Eq. 18 very well. Table 13 lists the fitting constants and the r^2 values. This good fit allows us to precisely control the magnitude of μ^{EOF} by simply altering the ionic strength of the BGE, and thus optimize peak resolution in a CE separation.

Table 13. Constants for the fit of the measured μ^{EOF} values by Eq. 18 for the untreated fused silica and AMPS-coated capillaries.

Constant	**untreated fused silica**	**60% APMS-coated**
a	0.00099 ± 0.0	0.00043 ± 0.0
b	0.00778 ± 0.0	0.00224 ± 0.0
c	7.7736 ± 0.6	5.4048 ± 3.1
r^2	0.9999	0.9959

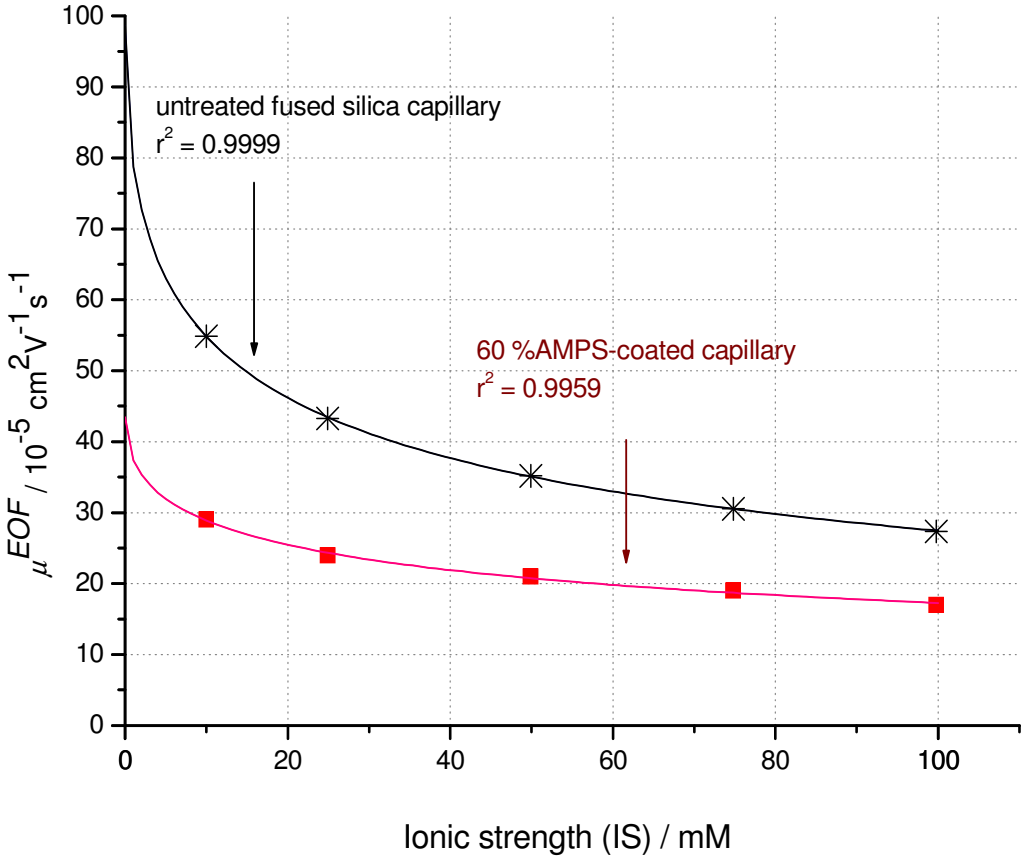

Figure 59. μ^{EOF} as a function of the ionic strength of the BGE for an untreated fused silica capillary and a 60 %AMPS-coated capillary. The points are the experimental values, the lines were calculated by the fit.

4.4 Manufacture of capillaries coated with a cationic polymer

Capillaries coated with a cationic polymer were made *via* free radical copolymerization of (3-acrylamidopropyl)trimethylammonium chloride (APTA), acrylamide (AA), *N,N′*-methylenebis(acrylamide) (MBA), and the methacrylate anchor group on the bifunctionalized surface of the fused-silica capillary. The next sections describe the

procedures in the design and manufacture of these capillaries and the results in their quality tests.

4.4.1 Design, materials and methods

The methodology used for the AMPS-coated capillaries (Sections 4.1.5 and 4.1.6) was also applied for the APTA-coated capillaries. 3.2 %T, 0.2% C solutions containing different $m_{APTA}/(m_{APTA} + m_{AA} + m_{MBA})$ ratios were used to obtain capillaries with different positive surface charge densities. Freshly-prepared concentrated stock solutions of the polymerizable reagents were mixed in appropriate volumes to yield the desired amounts needed to make each APTA-coated capillary. Table 14 lists the actual amounts of APTA, AA, MBA, and TEMED used for each stock coating solution. 10 μL of a 4 %APS solution was used to initiate the polymerization reaction in all 4-g aliquots taken from the stock solutions.

Table 14. Composition of the coating solutions used to prepare the immobilized cationic polymers. 10 µL of 4 %APS is also added to the 4-g aliquots taken from each stock to initiate the polymerization.

100-g stock solution (3.2 %T, 0.2 %C)					4-g aliquot
m_{MBA}	m_{AA}	m_{APTA}	%APTA	vol_{TEMED}	$vol_{4\ \%APS}$
g	*g*	*g*	%	*µL*	*µL*
0.0064	2.87	0.326	10.2	100	10
0.0064	2.70	0.502	15.7	100	10

In Table 14, %APTA is equal to 100 * $m_{APTA}/(m_{APTA} + m_{AA} + m_{MBA})$. There were 2 APTA stock solutions made yielding 2 capillaries with different μ^{EOF} values. From here onward, each capillary will be designated according to the %APTA used in the coating solution. Figure 60 shows a possible schematic structure of the anchored polymer layer for the 10.2 %APTA-coated capillary.

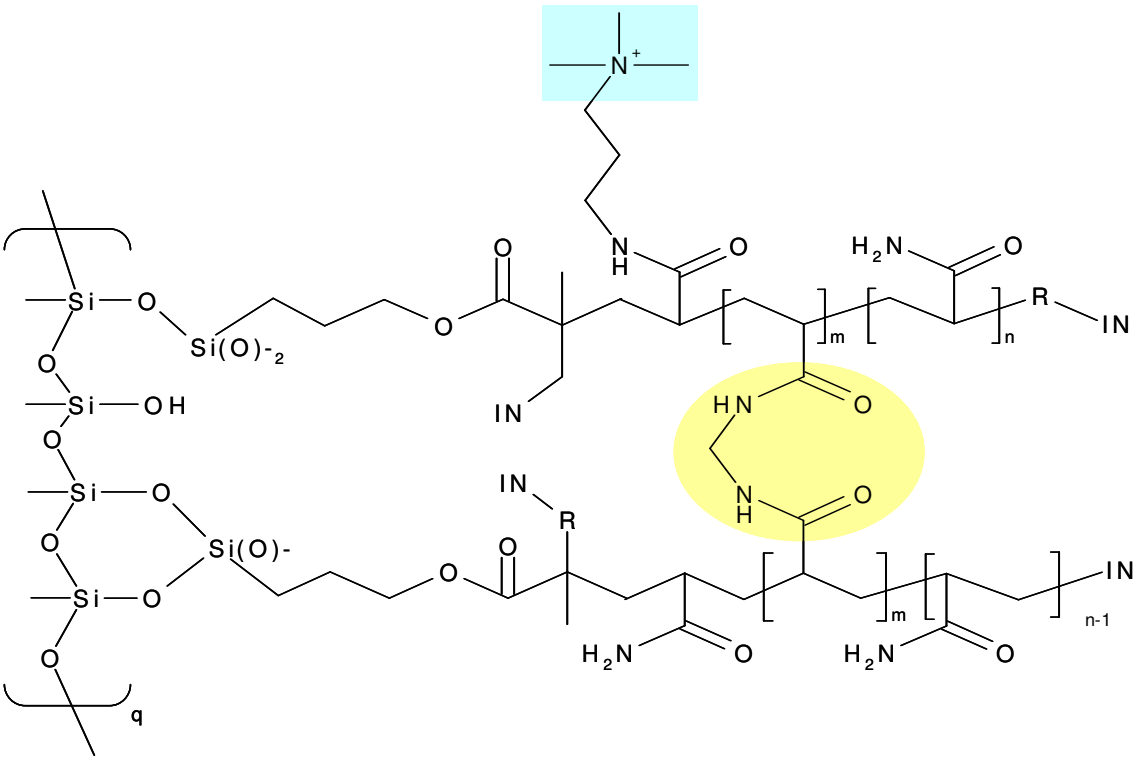

Figure 60. Possible schematic structure of the anchored polymer layer in an APTA-coated capillary. For a 10.2 %APTA-coated capillary (0.326g APTA in 3.2 g APTA+AA+MBA) with 3.2% T, 0.2 % C, there should be about 0.0196 mole of MBA (m) per 7.80 mole of AA (n) and 1 mole of APTA. IN-R: (1) initiator-monomer radical (terminator), where the monomer is APTA, AA, or MBA; or (2) initiator-polymer radical (terminator), where the polymer is $-[APTA]_r-[AA]_s-[MBA]_t-$ and r, s, and t depend on the composition of the coating solution.

Capillaries with stable polymeric layers were obtained only with coating solutions having %APTA < 15.7. Coatings obtained with higher %APTA values degraded after only a few CE runs.

4.4.2 μ^{EOF} as a function of %APTA in the coating solution

The 10.2 %APTA and 15.7 %APTA solutions yielded capillaries in which the μ^{EOF} values were -11.3 x 10^{-5} $cm^2V^{-1}s^{-1}$ and -16.7 x 10^{-5} $cm^2V^{-1}s^{-1}$, respectively, in the 10 mM ionic strength, 12.6 mM H_3PO_4 titrated with LiOH to pH 2.71 BGE, and -9.85 x 10^{-5} $cm^2V^{-1}s^{-1}$ and -14.6 x 10^{-5} $cm^2 V^{-1} s^{-1}$, respectively, in the 10 mM ionic strength, 20 mM H_3BO_3 titrated with LiOH to pH 9.25 BGE.

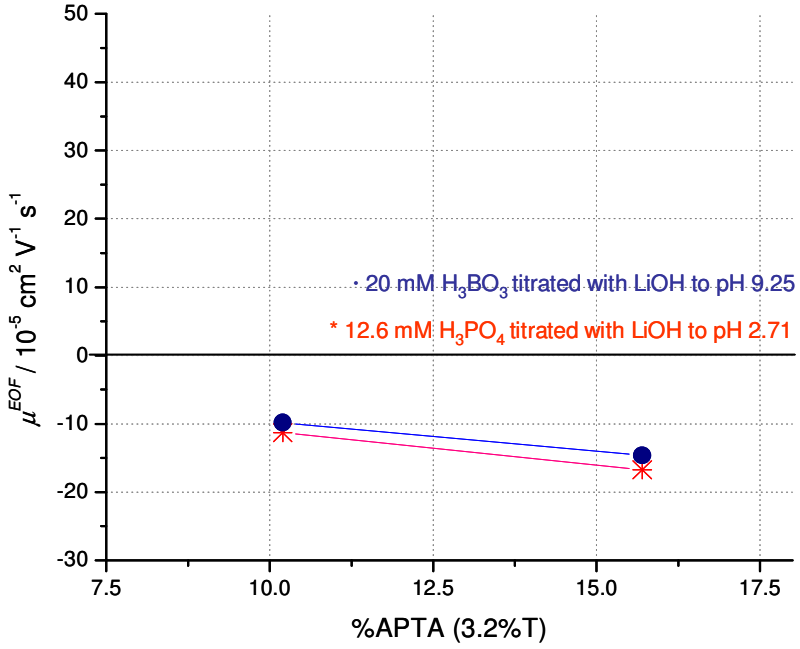

Figure 61. μ^{EOF} as a function of %APTA in the low and high pH BGEs. Both BGEs have ionic strengths of 10 mM.

In Figure 61, at pH 9.25, the anodic μ^{EOF} values are about 10 % lower than in the pH 2.71 BGE, indicating that a small portion of the surface silanol groups dissociate at high pH and decrease the positive surface charge density.

4.4.3 μ^{EOF} as a function of the pH of the BGE

The μ^{EOF} values of the APTA-coated capillaries were also tested in four 10 mM ionic strength BGEs with different pH values. 12.6 mM phosphoric acid and 20 mM formic acid (HCOOH) were titrated with LiOH to pH 2.71 and pH 3.71 respectively; and 20 mM 2-bis(2-hydroxyethyl)amino-2-(hydroxymethyl)-1,3-propanediol (BisTris) and 16 mM lysine were titrated with gluconic acid to pH 6.44 and pH 8.93 respectively.

Though the counter-ions are different in these four BGEs, according to the PeakMaster 5.1 program [13], their effective mobilities are similar. Table 15 shows the compositions of the BGEs made.

Table 15. List of BGEs used in the determination of μ^{EOF} for the APTA-coated capillaries. All BGEs have ionic strengths of 10 mM.

BGEs	Counter-ion	PeakMaster
		μ^{eff} / 10^{-5} cm^2 V^{-1} s^{-1}
12.6 mM H_3PO_4 titrated with LiOH to pH 2.71	$H_2PO_4^-$	-23.6
20 mM HCOOH titrated with LiOH to pH 3.71	$HCOO^-$	-23.1
20 mM BisTris titrated with gluconic acid to pH 6.44	gluconate	-23.8
16 mM lysine titrated with gluconic acid to pH 8.93	gluconate	-23.9

Table 16 lists the average μ^{EOF} values for the two APTA-coated capillaries in the four different BGEs in the 2.71 < pH < 8.93 range, at V = 10 kV, and t_{elec} = 10 min. It can be seen that μ^{EOF} in the 2 capillaries decreased by less than 15 % over the 2.71 < pH < 8.93 range.

Table 16. EOF generated for the APTA-coated capillaries from pH 2.71-8.93.

%APTA	μ^{EOF} / 10^{-5} cm^2 V^{-1} s^{-1}			
	pH 2.71	pH 3.71	pH 6.44	pH 8.93
10.2	-11.3	-10.9	-10.3	-9.85
15.7	-16.7	-15.9	-14.9	-14.6

4.4.4 Testing the stability of the APTA-coated capillaries in low and high pH BGEs

The long term stability of the APTA-coated capillaries was tested similarly to what was done for the AMPS-coated capillaries (Section 4.4.3). Ten μ^{EOF} determinations were carried out daily for two weeks, then once weekly for 4 months. After each measurement, the capillaries were stored with pH 2.71 and pH 8.93 BGEs inside them. Table 17 shows the average μ^{EOF} values determined for the capillaries during the 4 months of stability testing. Figure 62 is a graphical representation of the data in Table 17 and includes the μ^{EOF} values for an untreated fused silica reference capillary.

Table 17. μ^{EOF} values determined for the APTA-coated capillaries in the 2.71 < pH < 8.93 range over a period of 4 months.

% APTA		μ^{EOF} / 10^{-5} cm^2 V^{-1} s^{-1}			
		pH 2.71	**pH 3.71**	**pH 6.44**	**pH 8.93**
10.2	Initial	-11.3	-10.9	-10.3	-9.85
	4 months	-10.1	-9.65	-8.54	-8.24
15.7	Initial	-16.7	-15.9	-14.9	-14.6
	4 months	-15.4	-14.7	-13.6	-13.3

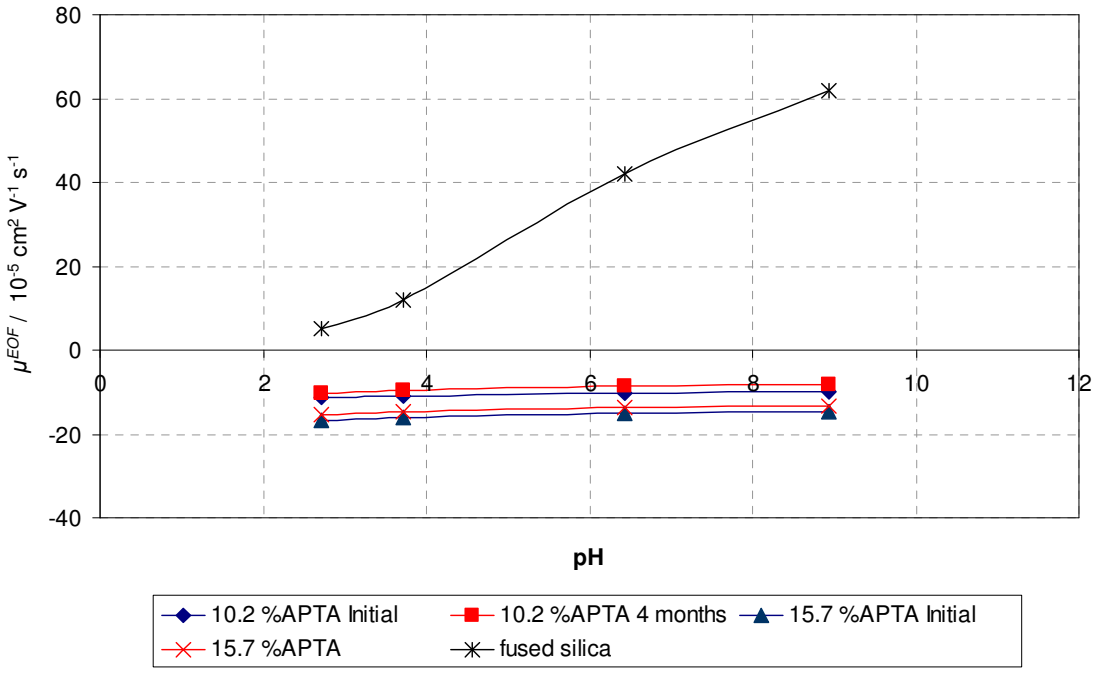

Figure 62. μ^{EOF} as a function of pH for the two APTA-coated capillaries. Blue points are the initial μ^{EOF} values, the red points are the μ^{EOF} values at the end of the 4-month long testing period.

4.4.5 μ^{EOF} as a function of the ionic strength of the BGE

165 mM H_3PO_4 titrated with NaOH to pH 2.2 BGE was prepared (IS= 100 mM). Portions of the 100 mM IS BGE were diluted to make 4 other BGEs with ionic strengths of 11.6, 25.9, 45.6, and 76.0 mM. The 5 BGEs were used for the determination of μ^{EOF} in a 46.7-cm L_t, 40-cm L_d, 50-µm ID 10.2 %APTA-coated capillary as a function of the ionic strength of the BGE . The measured μ^{EOF} values were fitted by Eq. 18 as in described in Section 4.3.5. Table 18 lists the fitting constants and r^2 values for both capillaries. The measured and calculated (from the fit) μ^{EOF} values agree well, as shown in Figure 63.

Table 18. Constants for the fit of the measured μ^{EOF} values by Eq. 18 for the untreated fused silica and APTA-coated capillaries.

Constant	untreated fused silica	10.2 %APTA-coated
a	0.00099 ± 0.0	0.00016 ± 0.0
b	0.00778 ± 0.0	0.00058 ± 0.0
c	7.7736 ± 0.6	1.2655 ± 1.0
r^2	0.9999	0.9974

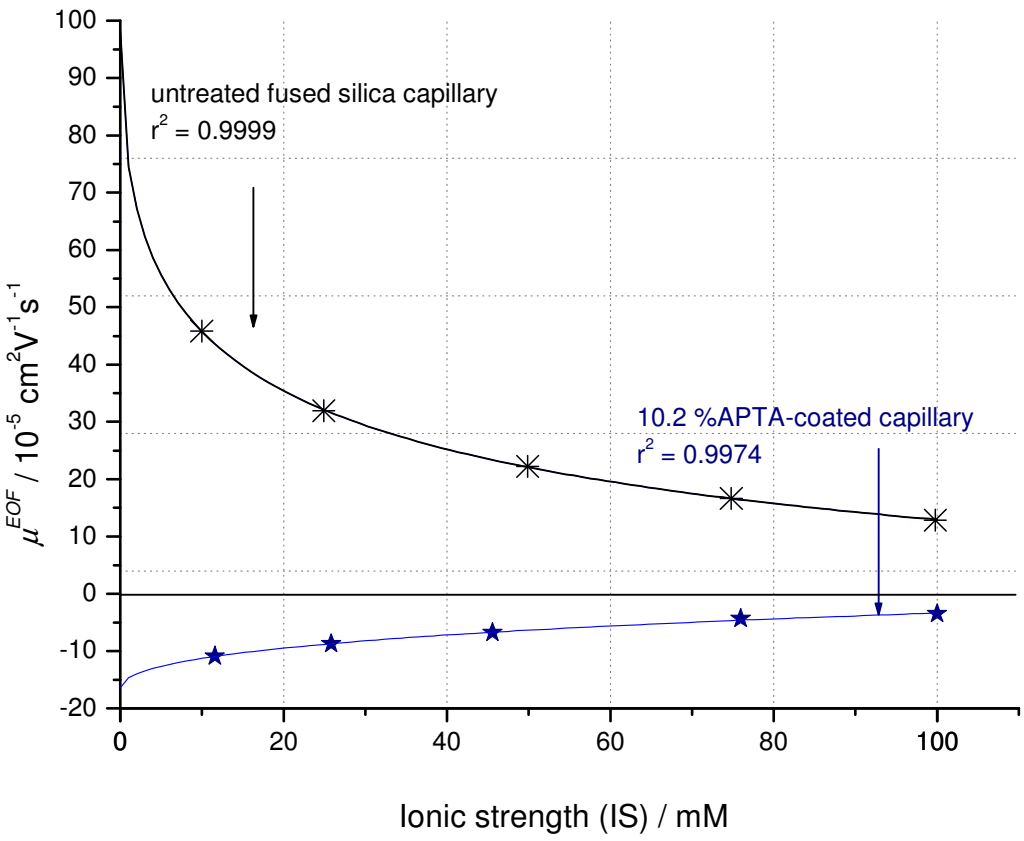

Figure 63. μ^{EOF} as a function of the ionic strength of the BGE for an untreated fused silica reference capillary and the 10.2 %APTA-coated capillary. The points are the experimentally determined μ^{EOF} values, the lines were calculated from the fit.

5 CAPILLARIES WITH CHARGED COATINGS ON THE INNER WALL: IMPROVING ANALYTE RESOLUTION AND MINIMIZING ANALYTE ADSORPTION

5.1 Improving analyte resolution

5.1.1 Background and objectives

The efficient analyses of enantiomeric drugs and proteins are critical to the biotech industry. In enantiomer separations, chiral resolving agents are added to the background electrolyte to create differential interactions between the enantiomers and the chiral resolving agent that lead to the formation of diastereomeric complexes *via* a dynamic equilibrium. If the enantiomer-chiral selector complexation constants or the ionic mobilities of the diastereomeric complexes are different, enantiomer separation in CE can be achieved.

Cyclodextrins have been used as such chiral selectors as reviewed by Rizzi and Amini, [163-166] Cyclodextrins (CD) are bucket-shaped molecules composed of 6-8 glucopyranose units linked *via* α-1,4 glycosidic bonds. CDs can be in native form or derivatized. Enantiomers can form complexes with CDs using three major interactions: (i) hydrophobic interactions with the core, (ii) hydrophilic interactions with the surface, and or (iii) electrostatic interactions with charged functionalities on derivatized cyclodextrins [167-173].

In 1997, Williams and Vigh took a dry look at the charged resolving agent migration (CHARM) model and found, as shown in Figure 64, that peak resolution is a function of 3 major variables: (1) separation selectivity (α), which is defined as the mobility of the fast analyte (μ_1^{eff}) over the mobility of the slow one (μ_2^{eff}), (2) z^{eff}, which is the effective charge of the analyte, and (3) the normalized EOF mobility (β), which is equal to the mobility of the EOF (μ^{EOF}) over the mobility of the slow analyte (μ_2^{eff}).

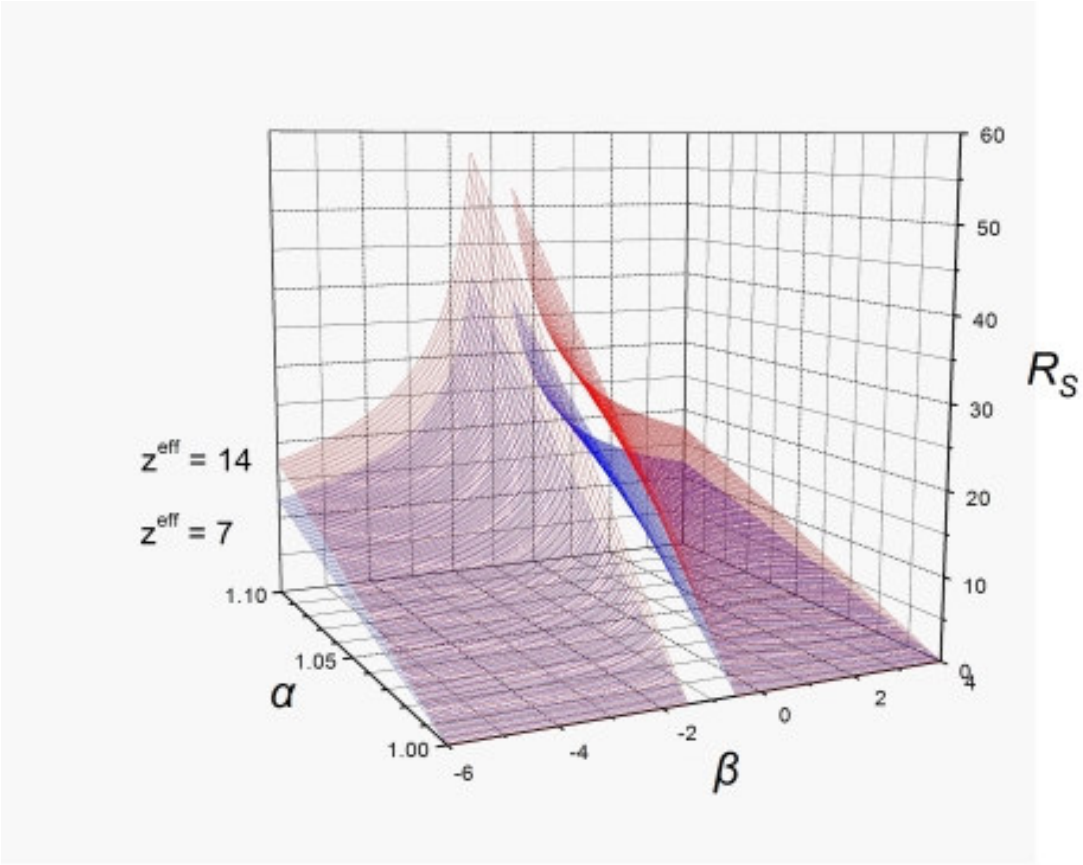

Figure 64. The dependence of peak resolution, R_s on α, z^{eff}, and β [164].

It can be seen from Fig. 64 that when α is 1, then R_s is zero; for every other α value, when z^{eff} increases, R_s increases; and when β approaches -1, R_s approaches infinity.

Capillaries that have adjustable EOF can be used to optimize enantiomer separations. By using a capillary with an EOF mobility that is appropriately matched with the mobility of the enantiomer band but has opposite sign, the β value for the separation, and thus, resolution, can be optimized. This capability will be demonstrated in the following sections.

In protein analyses, protein isoforms can have close p*I* values and thus have close mobilities. Capillary isoelectric focusing (cIEF) has been used to resolve protein isoforms. However, online coupling to downstream analysis like mass spectrometry proves difficult as the CAs suppress ionization of the proteins and result in poorer sensitivity for the targets. Moreover, in cIEF, as proteins focus into sharp zones, their net charge becomes zero. This decreases their solubility and increases their adsorption onto the capillary wall.

Capillary zone electrophoresis (cZE) provides another alternative in the analysis of proteins. In cZE, the pH of the BGE is typically changed to optimize effective mobilities of the proteins, and achieve separation. Protein analysis is often carried out at pH > 4, because many proteins become denatured upon prolonged exposure to acidic solutions [174]. Other ways to affect the mobility of proteins include ion-pairing with

heptanesulfonic acid which has been used to improve cZE separation of CNBr fragments of several types of collagen [175]; the use of liposomes based on 1-palmitoyl-2-oleyol-*sn*-glycero-3-phosphocholine as pseudostationary phases [176, 177]; or field gradient electrophoresis which has been demonstrated to separate *R*-phycoerythrin [178].

Culbertson [179] and Williams [180] also demonstrated the use of a hydrodynamic counterflow to optimize the resolution of analytes in cZE. Unfortunately, the laminar flow-induce band broadening brought about by the technique diminishes its utility. The plate-height contribution to band broadening by Taylor dispersion is greater than the contribution of EOF (a plug-like flow) to peak dispersion [181-185].

Thus, the use of coated capillaries with permanent charges and with precisely-controlled EOF mobilities provides another alternative in the cZE analysis of proteins. The choice of the capillary with the appropriate β value to optimize resolution is critical for an efficient analysis. The capability of these coated capillaries with pH-independent EOF in optimizing the resolution of protein isoforms will also be demonstrated in the following sections.

5.1.2 Separation of enantiomers

5.1.2.1 Instrument, materials, and methods

The P/ACE 2000 was used for all analyses. The wavelength of the UV-detector was set at 214 nm. 46.7-cm L_t, 40-cm L_d, 50-µm ID, and 186-µm OD 60 %AMPS-coated, 10.2 %APTA-coated, and untreated fused silica capillaries were used.

R,S-Ciprofibrate (CIP) and *R,S*-naproxen (NAP) were the enantiomers chosen to demonstrate the utility of the coated capillaries. CIP was analyzed with heptakis-(2,3-dimethyl-6-sulfo)-β-cyclodextrin (HDMS-β-CD) in the anionic coated capillary. NAP was analyzed with mono(6-deoxy-6-*N,N,N',N',N'*-pentamethylethylenediammonio)-cyclomaltoheptaose (PEMEDA-β-CD) in the cationic coated capillary. Both enantiomers were also analyzed in an untreated fused silica capillary (used as reference), and the results were compared. The enantiomer-CD pairs were chosen based on the results of previous work [172, 186]: in untreated fused silica capillaries these enantiomers could not be baseline resolved. Figure 65 shows the structures of the enantiomers and the cylcodextrins used.

A 60 %AMPS-coated capillary was used for the CIP analysis. For the NAP analysis, a 10.2 %APTA-coated capillary was used. *R,S*-ciprofribrate was analyzed with 10 mM HDMS-β-CD dissolved in a BGE made by titrating a 20 mM boric acid solution with lithium hydroxide to pH 9.25. *R,S*-Naproxen was analyzed with 3 mM PEMEDA-β-CD dissolved in a BGE made by titrating a 12.6 mM phosphoric acid solution to pH 2.71

with lithium hydroxide. For comparison, the runs were repeated in untreated fused silica capillaries as well.

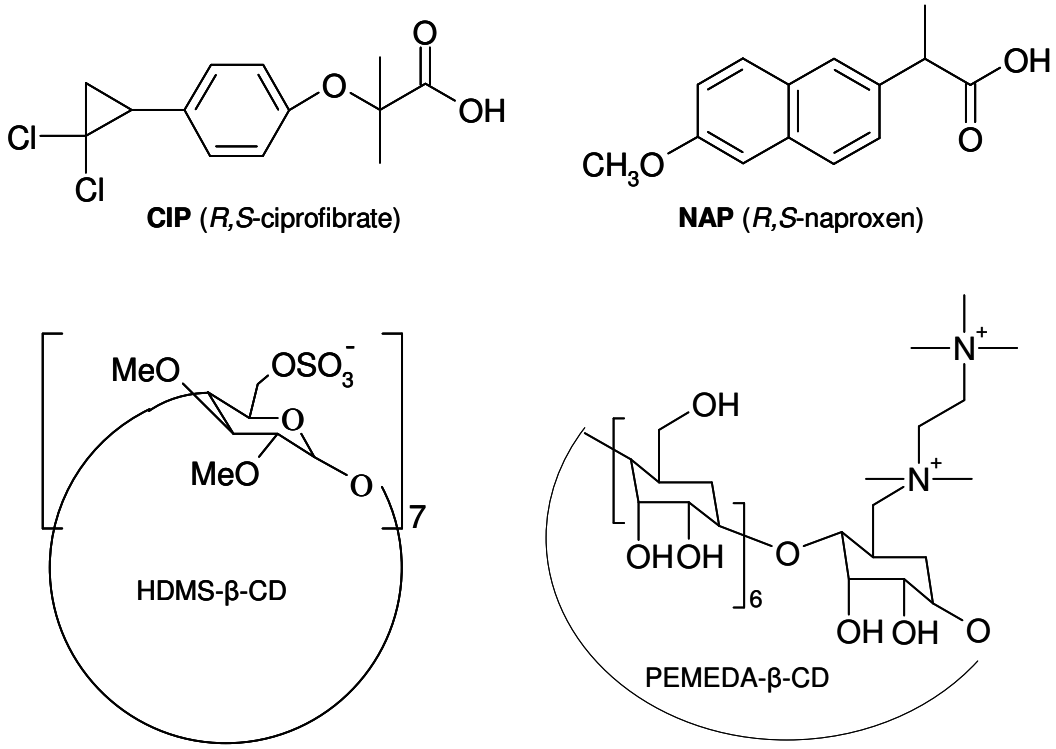

Figure 65. Structures of the enantiomers and the cyclodextrins used in the analyses.

The sample was injected for 1 second with 0.5 psi of pressure. A potential of 20000 V was applied with a negative polarity at the detector side of the capillary. The run was completed after both enantiomer peaks were recorded. Effective mobilities, μ_1^{eff} and μ_2^{eff} for the enantiomer bands (where μ_1^{eff} refers to the faster migrating band), selectivity α, μ^{EOF} , and β values were calculated.

5.1.2.2 Results and discussion

Figure 66 shows the analysis of *R,S*-ciprofibrate in the untreated fused silica capillary while Figure 67 shows the analysis in the anionic coated capillary. The 60 %AMPS-coated capillary used for the CIP analysis generated a constant cathodic μ^{EOF} of 25.6 x 10^{-5} $cm^2V^{-1}s^{-1}$. The untreated fused silica (UFS) capillary generated a μ^{EOF} of 64.5 x 10^{-5} $cm^2V^{-1}s^{-1}$. Table 19 lists the parameters used to determine the separation selectivity (α) and dimensionless electroosmotic flow mobility (β) value for the CIP analysis.

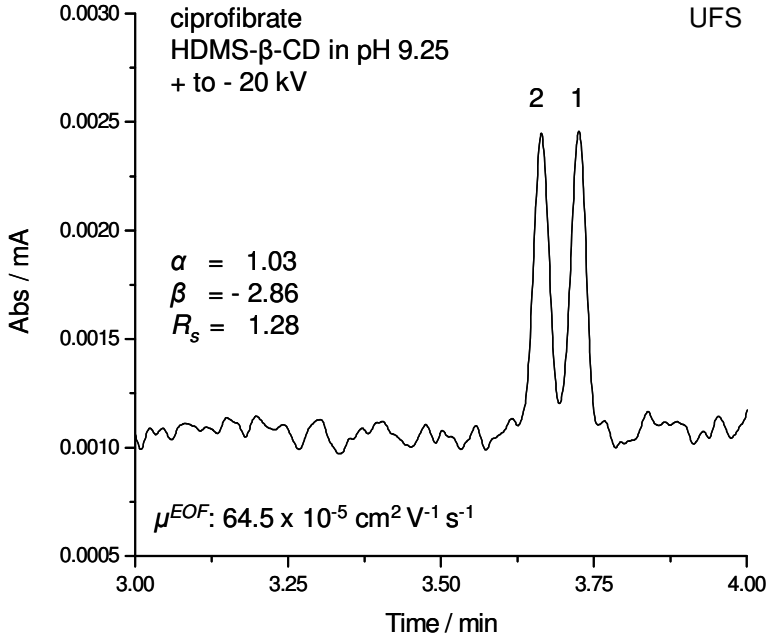

Figure 66. Analysis of *R,S*-ciprofibrate with HDMS-β-CD in an untreated fused silica capillary. L_t = 46.7 cm, L_d = 40 cm, V = 20 kV, polarity: + to –,BGE: 20 mM boric acid titrated to pH 9.25 with LiOH containing 10 mM HDMS-β-CD. UV detection set at 214 nm.

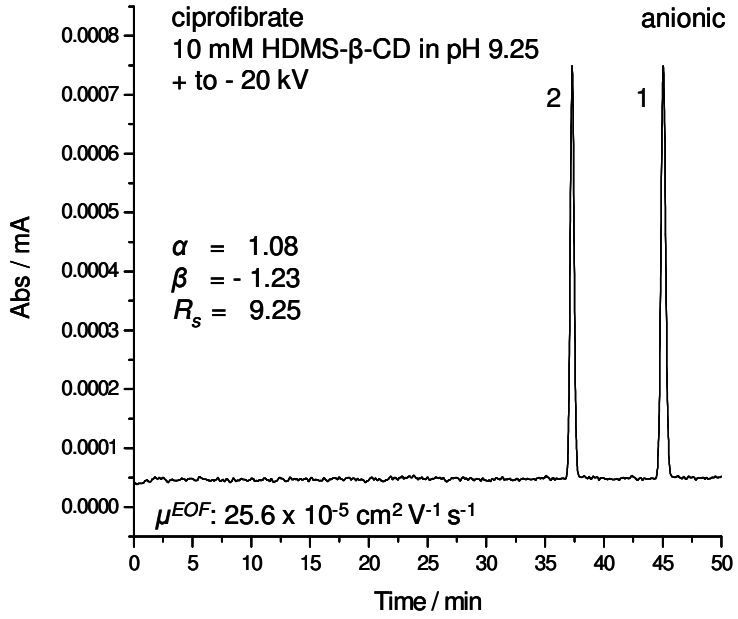

Figure 67. Analysis of *R,S*-ciprofibrate with HDMS-β-CD in a 60 %AMPS-coated capillary. L_t = 46.7 cm, L_d = 40 cm, V = 20 kV, polarity: + to –,BGE: 20 mM boric acid titrated to pH 9.25 with LiOH containing 10 mM HDMS-β-CD. UV detection at 214 nm.

Table 19. Data obtained from the analysis of *R,S*-ciprofibrate.

capillary	t_s^{obs}	t_r^{obs}	μ_s^{obs}	μ_r^{obs}	μ_s^{eff}	μ_r^{eff}	μ^{EOF}
	minutes		10^{-5} cm^2 V^{-1} s^{-1}				
untreated fused silica	3.663	3.724	41.97	41.22	-22.56	-23.31	64.53
60 %AMPS	37.30	45.06	4.771	3.311	-20.81	-22.21	25.58

t_1^{obs} and t_2^{obs} are the observed migration times for the enantiomer bands, μ_1^{obs} and μ_2^{obs} are their observed mobilities, μ_1^{eff} and μ_2^{eff} are their effective mobilities, and μ^{EOF} is the electroosmotic flow mobility generated by the particular capillary with the BGE used in the analysis, where:

$$\mu^{obs} = \frac{L_d L_t}{V * t^{obs}} \qquad (19)$$

and L_d is the length of the capillary to the detector, L_t is the total length of the capillary, V is the applied potential in volts and t^{obs} is the observed mobility of the band in seconds.

From Eq. 5, the effective mobility is calculated as:

$$\mu^{eff} = \mu^{obs} - \mu^{EOF} \qquad (20)$$

From the values in Table 19, the selectivity, α, and the normalized EOF mobility, β, can be calculated as:

$$\alpha = \frac{\mu_1^{eff}}{\mu_2^{eff}} \qquad (4) \text{ and } \beta = \frac{\mu^{EOF}}{\mu_2^{eff}} \qquad (6)$$

The peak resolution values, R_s, were calculated using the following equation:

$$R_s = \frac{2(t_2^{obs} - t_1^{obs})}{(w_1 + w_2)} \qquad (21)$$

where, w_1 and w_2 are the average peak widths at the base (in units of time) of the respective peaks.

Analysis with the untreated fused silica capillary gives an α = 1.02, β = -2.86, and R_s = 1.28. Analysis with the anionic coated capillary gives an α = 1.21, β = -1.23, and an R_s = 9.25.

Theoretically, for the same set of separation conditions (*e.g.* BGE concentration, potential applied, *etc.*), the effective mobilities of analytes should be the same in both capillaries, and thus should be the separation selectivities. However, since the analysis in the untreated fused silica capillary was done in 4 minutes, it can be argued that the system has not been fully equilibrated resulting in μ^{EOF} and μ^{eff} values that are slightly different from those determined in a longer run, such as the one in the anionic coated capillary.

For the NAP analysis, the 10.2 %APTA-coated capillary generated an anodic EOF of -10.0 x 10^{-5} $cm^2V^{-1}s^{-1}$. The same calculations used for the CIP analysis above were used for the NAP analysis. The untreated fused silica capillary gives an α = 1.03, β = 0.2, and an R_s = 1.00 [186]. The cationic coated capillary gives an α = 1.09, β = -0.69, and an R_s = 2.24. Clearly, the better β value (closer to -1) in the coated capillary dramatically improves the resolution of the enantiomers. Figure 68 shows the electropherogram for the analysis of NAP in a 10.2 %APTA-coated capillary.

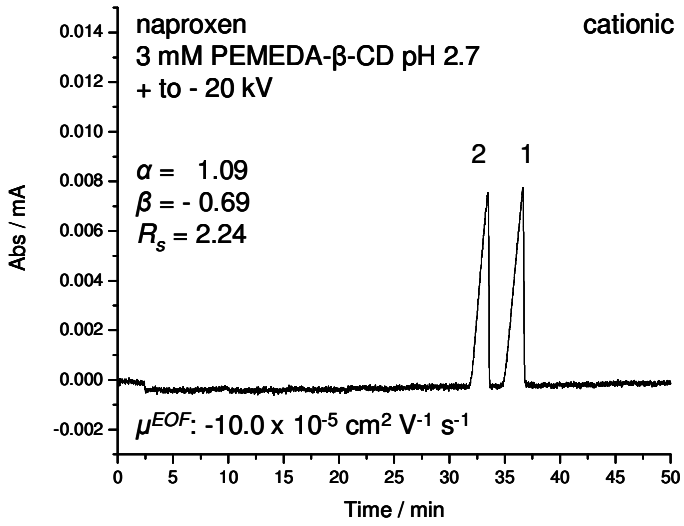

Figure 68. Analysis of *R,S*-naproxen with PEMEDA-β-CD in a 10.2 %APTA-coated capillary. L_t = 46.7 cm, L_d = 40 cm, V = 20 kV. BGE: 12.6 mM phosphoric acid titrated to pH 2.71 with LiOH containing 3 mM PEMEDA-β-CD. UV detection at 214 nm.

5.1.3 Separation of protein isoforms

5.1.3.1 Instrument, materials, and methods

The P/ACE 2000 was used for all analyses. UV-detection was at 214 nm. 46.7-cm L_t, 40-cm L_d, 50-µm ID, and 186-µm OD 80 %AMPS-coated and untreated fused silica capillaries were used.

Conventional field-amplified sample stacking (FASS) capillary electrophoresis was used with both the untreated fused silica and the coated capillaries to maximize sensitivity and minimize injection-related broadening of the peaks. In this method, the sample is prepared in a low-conductivity solution, which is different from the BGE (a high-

conductivity buffer). Initially, the capillary is filled with the high-conductivity BGE, then the sample solution is injected into the capillary. When voltage is applied, the electric field strength is greater across the lower conductivity sample zone. This causes the ions to migrate faster in the sample zone. Once the analytes reach the boundary between the sample zone and the BGE, the electric field strength suddenly decreases and migration velocity slows. This results in the concentration of the analytes at the boundary of the low conductivity sample zone and high conductivity BGE zone [187].

Horse myoglobin (MYO), 17 kDa with p*I* 7.0-7.4 (SIGMA, St. Louis, MO) was used as the test protein. The protein sample was prepared by adding to the 1 mg/mL protein solution enough sodium hydroxide to increase the pH to 10. This made all the protein isoforms negatively charged. The conductance of the sample protein solution was 50 μS. The BGE was a 50-mM ethanolamine solution titrated to pH 9 with methanesulfonic acid; its conductance was 3000 μS. Horse myoglobin was analyzed in both an 80 %AMPS-coated capillary and an untreated fused silica capillary (reference).

The sample was injected into the capillary (untreated fused silica and anionic coated capillary) for 1 s at 0.5 psi. A potential of 10000 V was applied with a negative polarity at the detector side of the capillaries. The run was terminated after all the protein isoform peaks were recorded.

5.1.3.2 Results and discussion

The 80 %AMPS-coated capillary generated a cathodic μ^{EOF} of 24.3 x 10^{-5} $cm^2V^{-1}s^{-1}$ with the pH 9, 50-mM ethanolamine BGE. The untreated fused silica capillary generated a cathodic μ^{EOF} of 69.2 x 10^{-5} $cm^2V^{-1}s^{-1}$. In the pH 9 BGE, the acidic groups of horse myoglobin are fully dissociated, giving the protein a net negative charge. The mobility of the cathodic EOF, μ^{EOF}, is higher in magnitude than the effective mobility of the anionic protein, thus the protein moves toward the cathode. Figures 69 and 70 show the analyses in the untreated fused silica and the coated capillaries, respectively. The resolution between the isoforms of myoglobin is better with the coated capillary because the β value is better.

A

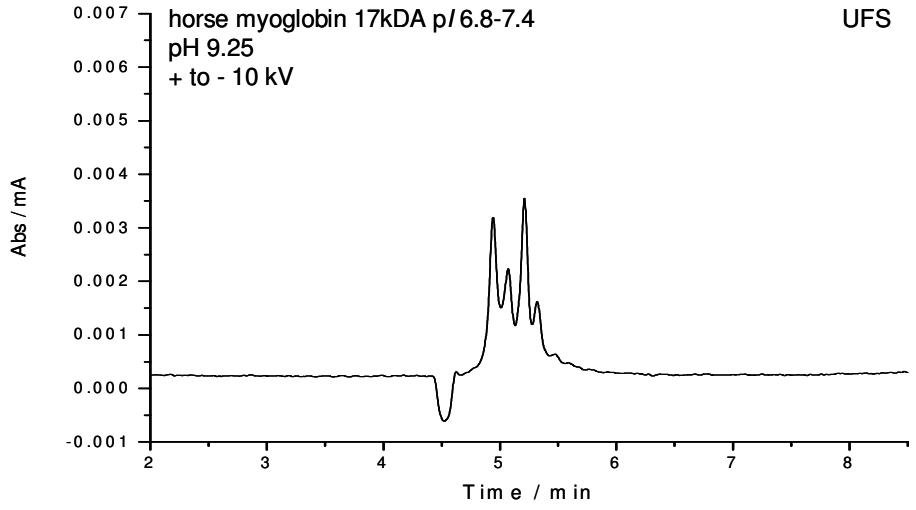

Figure 69. Analysis of MYO in an untreated fused silica capillary with a μ^{EOF} of 69.2 x 10^{-5} $cm^2V^{-1}s^{-1}$ in a pH 9, 50-mM ethanolamine BGE. In electropherogram A, the X axis is in time scale, and in electropherogram B, the X axis is in μ^{eff} scale.

B

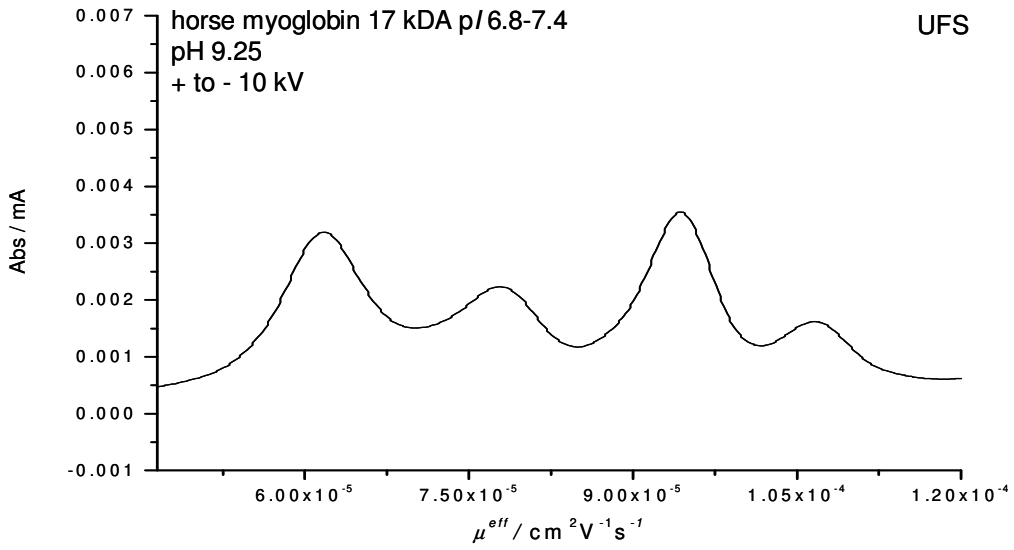

Figure 69. Continued.

A

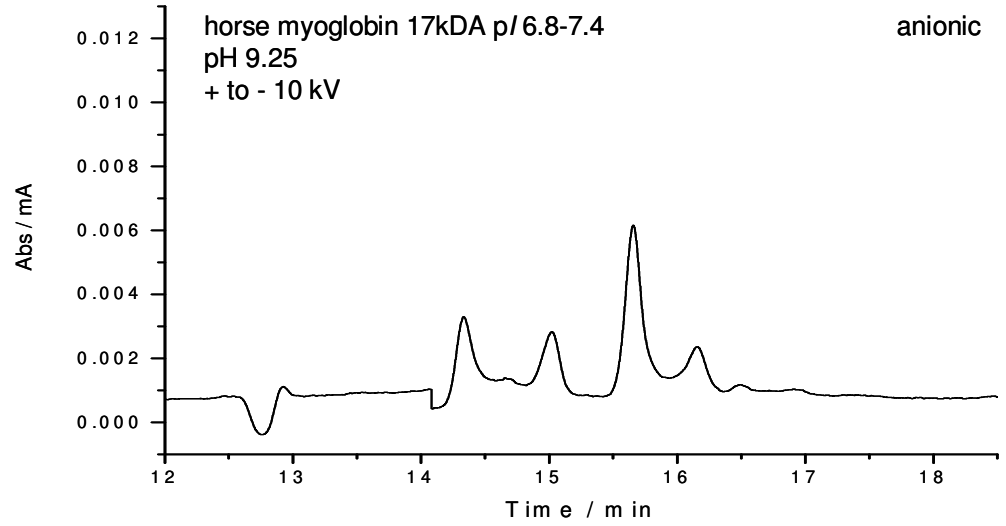

B

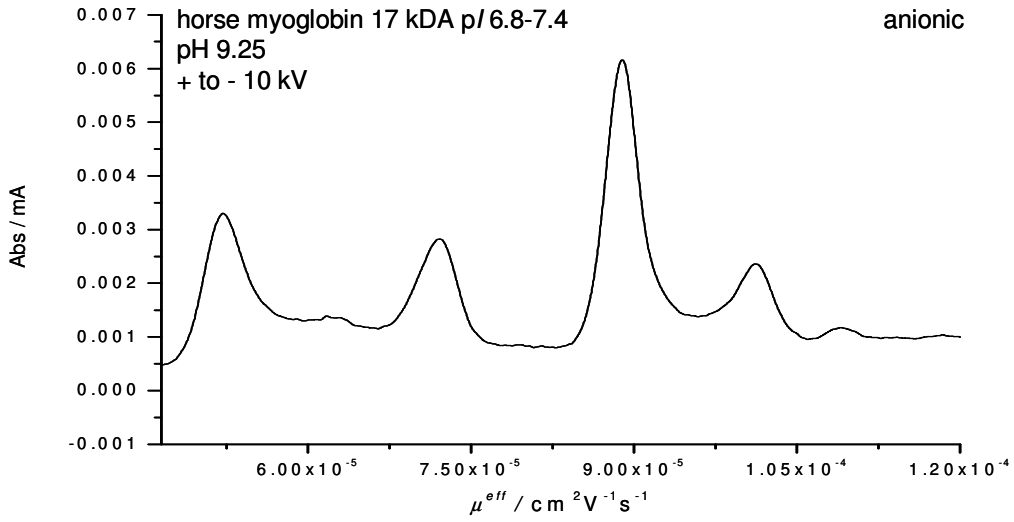

Figure 70. Analysis of MYO in an 80 %AMPS-coated capillary with a μ^{EOF} of 24.3 x 10^{-5} $cm^2V^{-1}s^{-1}$ in a pH 9, 50-mM ethanolamine BGE. In electropherogram A, the X axis is in time scale, and in electropherogram B, the X axis is in μ^{eff} scale.

The calculations done for the enantiomers above were also made for the proteins. With reference to the slowest migrating peak, β = -11.16 and β = -9.29 were calculated in the untreated fused silica and the 80 %AMPS-coated capillary, respectively.

5.2 Minimizing analyte adsorption

5.2.1 Background and objectives

Nonspecific analyte adsorption in an untreated fused silica capillary can be due to hydrophobic and electrostatic interactions. For hydrophobic interactions, binding occurs between the siloxane bridges of the untreated fused silica and the hydrophobic regions of the solute. For electrostatic interactions, there is attraction between the positive charges on the analyte and the negative charges on the surface of the untreated fused silica capillary. An analyte of charge z will have an electrostatic interaction energy, E_{es}, depending on its distance, X, from a surface that has an electrostatic potential, Φ_0, where κ^{-1} is the Debye length [188]:

$$E_{es} = zF\phi_0 \exp(-\kappa X) \qquad (22)$$

Application of a coating to the surface of fused silica can reduce the surface potential and increase the distance between the analyte and the silica surface. Thus, if a neutral hydrophilic coating, such as a polyacrylamide coating is used, analyte adsorption is minimized by reducing both the electrostatic and the hydrophobic interactions.

Experiments, however, have proven that there is still modest interaction between analytes and the polyacrylamide coating [189, 190] and may be associated with rapid

adsorption-desorption kinetics between the analyte and the coating. The random-walk theory (from chromatography), a first approximation model of an analyte's adsorption-desorption kinetics [191, 192] has been extended to electrophoresis [193]. The random-walk theory considers a solute moving down the capillary in discrete steps. The peak variance is expressed as:

$$\sigma_s^2 = 2\left(\frac{k'}{1+k'}\right)^2 \nu_{ep} t_d L \qquad (23)$$

where t_d = desorption time of analyte, k' = chromatographic retention factor, L= length of capillary, and v_{ep} = observed electrophoretic velocity of the analyte. If the adsorption and desorption kinetics are the same, no tailing is observed and peak resolution is better. Due to the chromatographic retention, v_{ep} is:

$$\nu_{ep} = \nu^{ek} / (1+k') \qquad (24)$$

where v^{ek} = true electrokinetic velocity of the analyte (without retention) [189].

The following sections will probe the adsorption properties of the capillaries that were prepared with charged hydrophilic coatings. Small permanent anions, cations, and proteins were analyzed in the coated and untreated fused silica capillaries and the results are compared.

5.2.2 Separation of small-molecules

5.2.2.1 Instrument, materials, and methods

The P/ACE 2000 was used for all separations. UV-detection was at 214 nm. A 46.7-cm L_t, 40-cm L_d, 50-µm ID, and 186-µm OD 90 %AMPS-coated, 15.7 %APTA-coated, and untreated fused silica capillaries were used.

Benzyltrimethylammonium ion ($BTMA^+$), benzyl viologen ion (BV^{2+}), p-toluenesulfonate ion (PTS^-), 8-hydroxy-pyrenetrisulfonate ion ($HPTS^{3-}$), 2-naphthalenesulfonate ion (NS^-), 1,5-naphthalenedisulfonate ion (NDS^{2-}), and 10-(3-sulfopropyl) acridinium betaine zwitterion ($SAB^{\pm}$), all small ions (MW< 500) that have quaternary ammonium or sulfonate groups were used as the probe analytes (Figure 71).

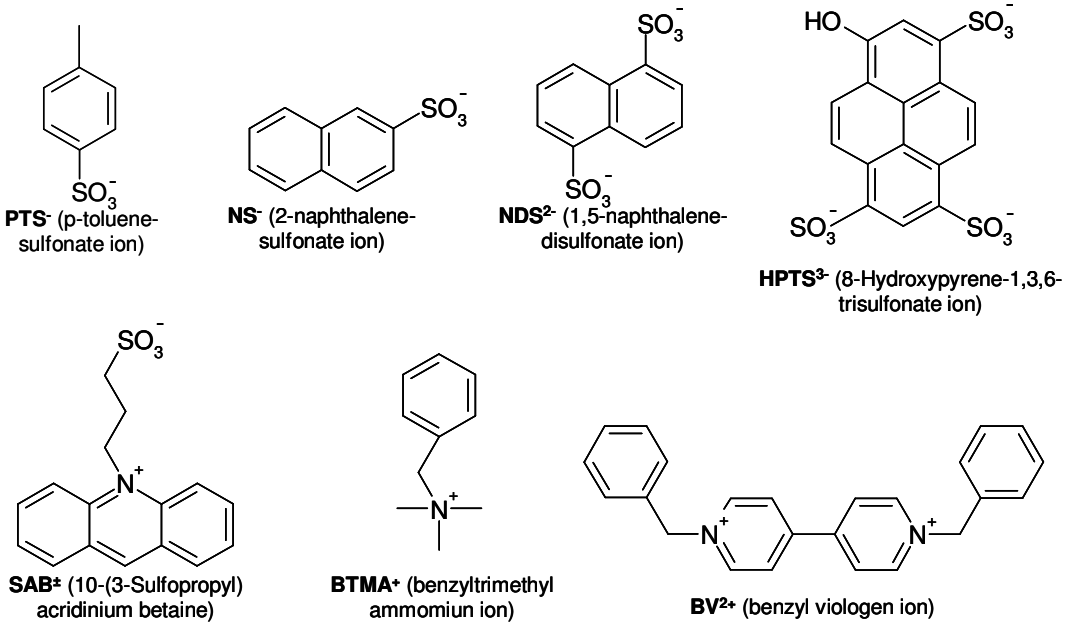

Figure 71. Small ions used to probe adsorption on the coated capillaries.

BV^{2+} was analyzed with a BGE made by titrating a 12.6 mM phosphoric acid solution (with 10 %DMSO w/w) to pH 2.71 with lithium hydroxide and a BGE made by titrating a 20 mM boric acid solution (with 5 %DMSO w/w) to pH 9.25 with lithium hydroxide. $HPTS^{3-}$ was analyzed with a BGE made by titrating a 35 mM chloroacetic acid solution (with 50 %DMSO w/w) to pH 2.4 with diaminohexane and a BGE made by titrating a 12 mM diaminohexane solution (with 50 %DMSO w/w) to pH 9 with methanesulfonic acid. The addition of DMSO provided the hydro-organic environment needed to fully dissolve BV^{2+} and $HPTS^{3-}$. All other test analytes were analyzed with an aqueous BGE made of a 12.6 mM phosphoric acid solution titrated to pH 2.71 with lithium hydroxide and 20 mM boric acid solution titrated to pH 9.25 with lithium hydroxide.

As indicated by the small difference in the mobility of the EOF at low and high pH, the surface charge of the capillary was not the same in the low and high pH BGEs, possibly because uncovered free silanol groups could have been left on the surface.

In comparing the untreated fused silica capillary with the 90 %AMPS-coated capillary, a BGE made by titrating a 20 mM acetic acid solution to pH 4.98 with lithium hydroxide was also used to match the mobility of the EOF in the AMPS-coated capillary and in the untreated fused silica capillary. This means that the surface charge densities in the two capillaries were also reasonably matched.

5.2.2.2 Results and discussion

The coated capillaries showed no adsorption for the small ions tested. The untreated fused silica capillary, however, showed adsorption of the zwitterion, $SAB^{\pm}$, at pH 9.25, and slight adsorption of BV^{2+} at pH 2.71 and a very strong one at pH 9.25. Table 20 summarizes the results. A negative sign (-) means that there was no detectable adsorption (no peak tailing), a plus sign (+) means slight adsorption (some peak tailing), double plus signs (++) mean significant adsorption (strong peak tailing), and triple plus signs (+++) mean very strong adsorption (very strong peak tailing).

Table 20. Analysis of small ions in an untreated fused silica (UFS), anionic-coated and cationic-coated capillaries at 3 different pH values to probe analyte adsorption. (-): no analyte adsorption, (+): slight adsorption, (++): strong adsorption, and (+++): very strong adsorption.

Ion	pH 2.71			pH 4.98		pH 9.25		
	UFS	anionic	cationic	UFS	anionic	UFS	anionic	cationic
$SAB^{\pm}$	n/a	-	-	-	-	++	-	-
$BTMA^{+}$	-	-	-	-	-	-	-	-
BV^{2+}	+	-	-	++	-	+++	-	-
PTS^{-}	-	-	-	-	-	-	-	-
NS^{-}	-	-	-	-	-	-	-	-
NDS^{2-}	-	-	-	-	-	-	-	-
$HPTS^{3-}$	-	-	-	-	-	-	-	-

Figure 72 to 75 are electropherograms that illustrate the peak shapes used to determine the extent of adsorption:

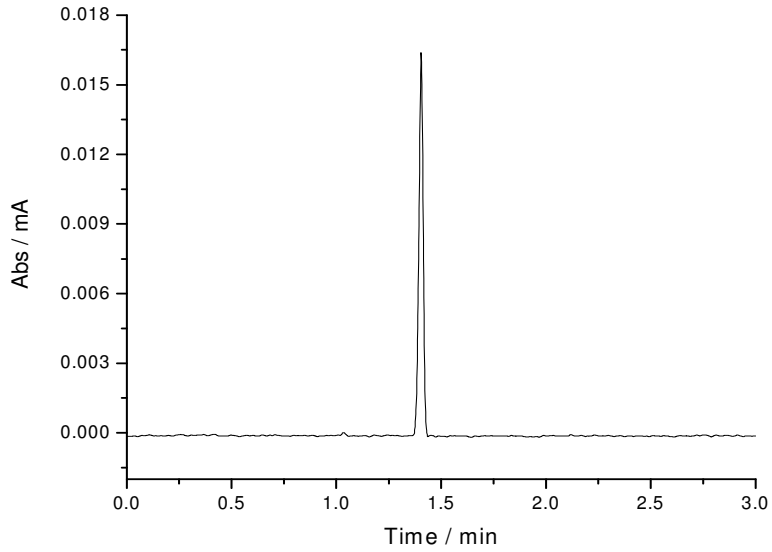

Figure 72. Typical electropherogram for an analyte with no detectable adsorption (no peak tailing) on the capillary surface. The analyte shown here is $HPTS^{3-}$, analyzed on a 15.7 %APTA-coated capillary with the pH 2.71 BGE.

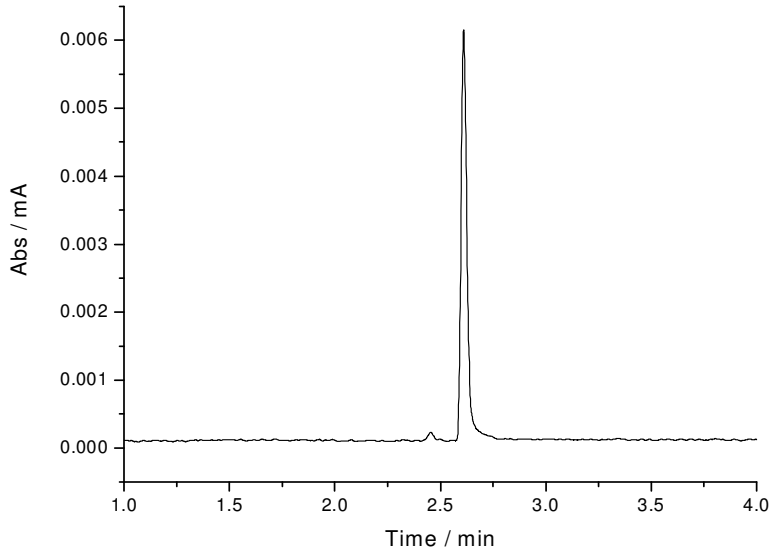

Figure 73. Typical electropherogram for an analyte with some adsorption (some peak tailing, +) on the capillary surface. The analyte shown here is BV^{2+}, analyzed on an untreated fused silica capillary with the pH 2.71 BGE .

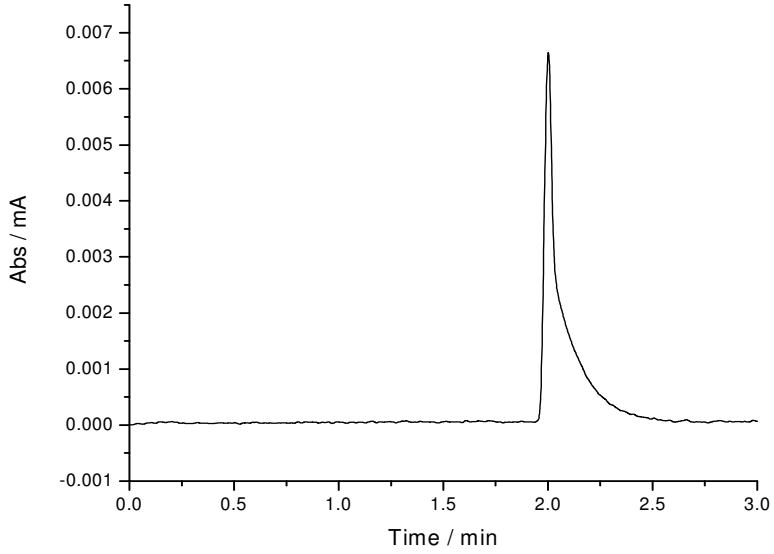

Figure 74. Typical electropherogram for an analyte with strong adsorption (strong peak tailing, ++) on the capillary surface. The analyte shown here is $SAB^{\pm}$, analyzed on an untreated fused silica capillary with the pH 9.25 BGE.

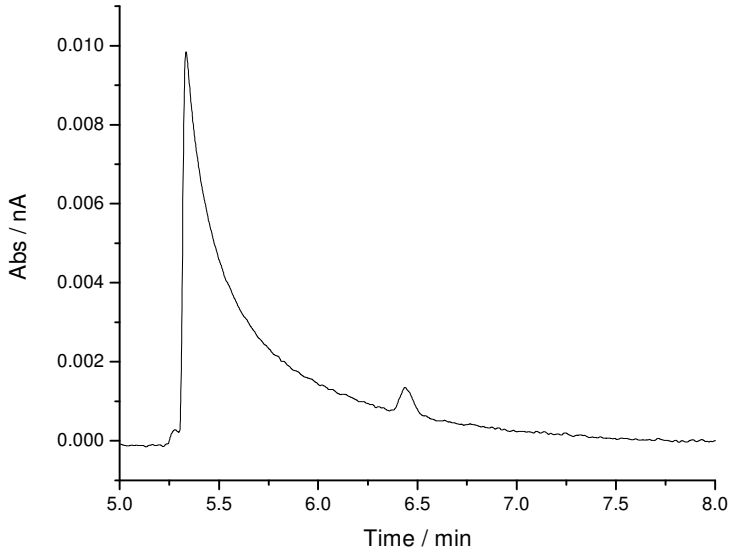

Figure 75. Typical electropherogram for an analyte with very strong adsorption (very strongly tailing peak, +++) on the capillary surface. The analyte shown here is BV^{2+}, analyzed on an untreated fused silica capillary with the pH 9.25 BGE.

5.2.3 Separation of proteins

5.2.3.1 Instrument, materials, and methods

The P/ACE 2000 was used for all separations. UV-detection was at 214 nm. 46.7-cm L_t, 40-cm L_d, 50-μm ID, and 186-μm OD 10.2 %APTA-coated, 80 %AMPS-coated and untreated fused silica capillaries were used.

Conventional field-amplified sample stacking (FASS) capillary electrophoresis was used with both the untreated fused silica and the coated capillaries to maximize sensitivity and minimize injection-related band width. Ovalbumin from chicken egg white (SIGMA, St. Louise, MO, USA) was used as the probe protein. An approximately 1 mg/mL protein solution was prepared and its pH was adjusted to 10 with sodium hydroxide to render the

proteins negatively charged. A 50 mM ethanolamine solution titrated to pH 9 with methanesulfonic acid was used as the BGE for all of the separations. A 1-second injection from the inlet side of the capillaries was made. With the untreated fused silica capillary, 10000 V was employed with negative polarity at the detector side of the capillary. With the 10.2 %APTA-coated capillary, 10000 V was employed with positive polarity at the detector side of the capillary. With the 80 %AMPS-coated capillary, 10000 V was employed with negative polarity at the detector side of the capillary.

5.2.3.2 Results and discussion

At pH 9, the acidic groups of ovalbumin are fully dissociated making the protein negatively charged. With the untreated fused silica capillary, negative polarity was used at the detector side, thus the EOF and the protein migrated in opposite directions. Figures 76 shows the electropherogram.

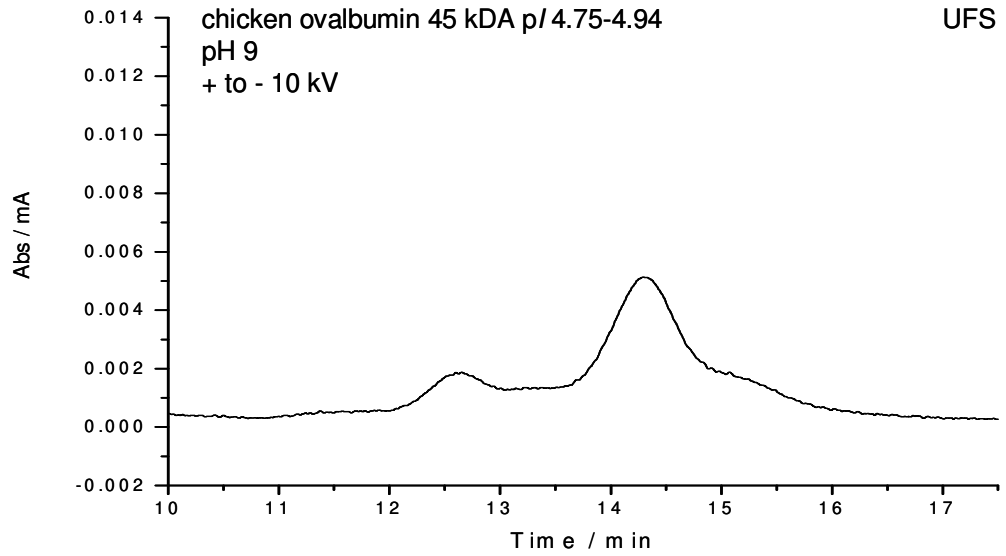

Figure 76. Electropherogram showing the separation of chicken ovalbumin with an untreated fused silica capillary.

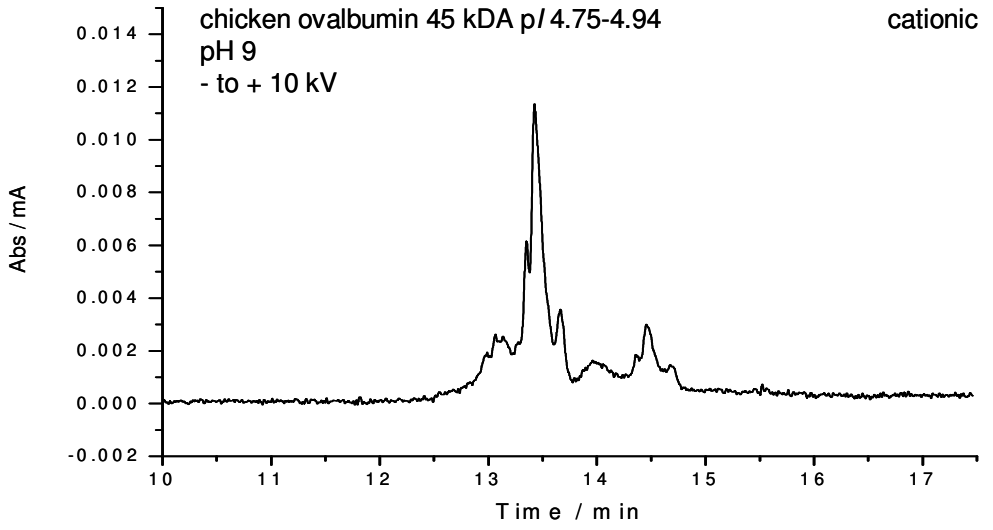

Figure 77. Electropherogram showing the separation of chicken ovalbumin with a 15.7 %APTA-coated capillary.

With the 10.2 %APTA-coated capillary, positive polarity was used at the detector side, thus the EOF and the protein migrated in the same directions. Figure 77 shows the electropherogram.

With the 80 %APS-coated capillary, negative polarity was used at the detector side, thus the EOF and the protein migrated in opposite directions. Figure 78 shows the electropherogram.

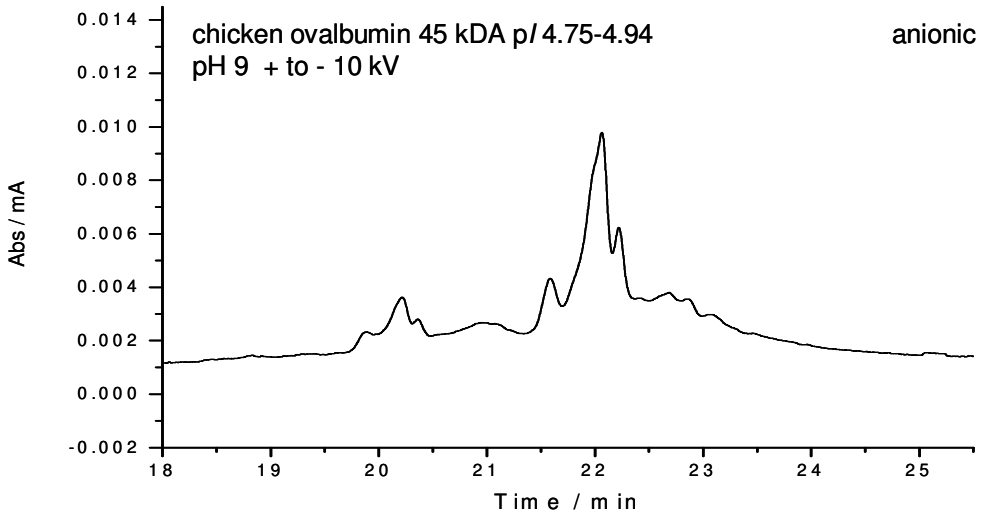

Figure 78. Electropherogram showing the separation of chicken ovalbumin with an 80 %AMPS-coated capillary.

The ovalbumin isoforms are better resolved with the cationic and anionic coated capillaries than with the untreated fused silica capillary. 10 shoulders can be observed when ovalbumin is analyzed with the cationic- and anionic-coated capillaries. Even

though the untreated fused silica capillary has negative charges on its surface at this pH and the protein has a net negative charge, there is still better resolution with the cationic coated capillary, despite its stronger electrostatic interactions with the negatively charged ovalbumin.

The effective mobility values (μ^{eff}) for the largest peak in the 3 electropherograms were as follows: untreated fused silica, μ^{eff} = -11.11 x 10^{-5} $cm^2V^{-1}s^{-1}$, cationic coated, μ^{eff} = -13.17 x 10^{-5} $cm^2V^{-1}s^{-1}$, anionic coated, μ^{eff} = -13.62 x 10^{-5} $cm^2V^{-1}s^{-1}$. This translates to β values of -2.88, 0.71, and -2.04 for the untreated fused silica, cationic coated and anionic coated capillaries, respectively. For the untreated fused silica capillary, the β value is 1.88 away from -1 (infinite resolution); for the cationic coated capillary, the β value is 1.71 away from -1, and finally; for the anionic coated capillary, the β value is 1.04 away from -1. Since the β values for the analyses in all capillaries are not significantly different from one another, the better resolution of the ovalbumin isoforms in the coated capillaries is due, primarily to lower adsorption-related band broadening, not so much to β value effects.

5.3 Concluding remarks

These series of experiments demonstrate the capabilities of the coated capillaries in improving the resolution while minimizing adsorption of enantiomers and protein isoforms.

6 CONCLUSIONS

6.1 Redesigned MEDUSA

For preparative protein separations, isoelectric trapping (IET) has proven to be an invaluable tool. The Twinflow [38] in pH-biased IET mode has been able to achieve high production rates and efficient separations. The major drawback of the Twinflow design, however, is that it can only be used for binary IET separations in a single run and thus can only purify maximum 2 components at a time. For the simultaneous separation of more than 2 target components, a multicompartmental electrolyzer is needed. The commercially available MCEs, however, have low production rates. Therefore, a new MCE that follows the design principles of the Twinflow was needed to achieve simultaneous IET separation of multiple components.

The MEDUSA [55], a multicompartmental electrolyzer originally designed to carry out simultaneous size-based and charge-sign based fractionation of proteins has been redesigned to carry out IET separations. Three main areas were improved: (i) the sealing system, (ii) the configuration of the liquid flow path and (iii) the cooling system.

The new sealing system is composed of silicone gaskets and poly(vinyl acetate) supports that are specifically assembled *vis-à-vis* each other to guarantee alignment of the access holes of the compartments with the access ports of the separation unit (thus minimizing undesirable flow resistance), maintain sealing between compartments and, since the

sealing elements don't possess elevated ridges (like the old MEDUSA grids), preserve the integrity of the membranes. Each separation compartment is about 1.5 mm deep, which results in an anode-to-cathode distance of about 25 mm for 12 separation compartments and 2 electrode compartments.

The configuration of the liquid flow path has been changed. The 81-cm stainless steel heat exchanger of the old MEDUSA originally situated at the outlet side of the separation unit has been discarded to eliminate uneven flow resistance in the separation compartments that would lead to untoward trans-membrane hydrodynamic flow and loss of the IET separation. The sample solutions now immediately cascade from the separation unit (through a minimum length of 1-cm ID tubing) into their respective collection reservoirs. The lengths of the inter-connecting silicone tubing have also been minimized to reduce dead volume and hydrophobic surface area.

The cooling system has been redesigned using external reservoirs with cooling jackets. The size of the reservoirs can be varied depending on the volume of the sample to be processed. The jackets are supplied with temperature-regulated coolant from an external chiller. The cooling system can maintain the solution temperature at 5-6°C, even when 60 W of power is applied. This cooling capability at high power loads dramatically improves production rates. The fractionation rate achieved in the redesigned MEDUSA for a 4-sample compartment separation of Ovoglobulin isoforms was about 200 mg/hour. This production rate compares very well with the rates reported for a binary

IET separation of chicken egg white proteins using the Twinflow [38] and is better than reported production rates by the Isoprime MCE [54].

The prefractionation capabilities of the instrument have been demonstrated by 4-compartment and 6-compartment IET separations of protein isoforms and small ampholytes.

6.2 Capillaries with charged coatings for capillary electrophoretic analysis of the fractions produced by IET

Anionic and cationic coated capillaries have been made that improve analyte resolution and minimize analyte adsorption. The coating was made *via* free-radical polymerization of acrylamide (AA), *N,N'*-methylenebis(acrylamide) (MBA), and 2-acrylamido-2-methyl-1-propanesulfonate (AMPS) for the anionic coated capillaries and (3-acrylamidopropyl)trimethylammonium (APTA) for the cationic-coated capillaries. TEMED was used as the catalyst, ammonium persulfate as the initiator.

With the P/ACE 2000, these capillaries could be manufactured ruggedly, rapidly and reproducibly. The coating solutions all contained 3.2 %T and 0.2 %C. Different ratios of AMPS or APTA relative to AA were used to manufacture coated capillaries with different EOF mobilities. The anionic coated capillaries had pH-independent cathodic EOF with mobilities in the 2.63 x 10^{-5} $cm^2V^{-1}s^{-1}$ to 35.4 x 10^{-5} $cm^2V^{-1}s^{-1}$ range. The cationic coated capillaries had pH-independent anodic EOF with mobilities in the -9.85 x

10^{-5} $cm^2V^{-1}s^{-1}$ to -16.7 x 10^{-5} $cm^2V^{-1}s^{-1}$ range. In these coated capillaries, the magnitude of μ^{EOF} depended on the ionic strength of the BGE [159, 160]. The coatings were stable for at least 4 months while constantly exposed to pH 2.71 to pH 9.25 BGEs.

The coated capillaries have been used to optimize analyte resolution by matching the mobility of the EOF to that of the analyte. Analyte adsorption was minimized through electrostatic repulsion of charged analytes and mitigation of hydrophobic interactions by the hydrophilic polyacrylamide network of the coating. These capillaries have been used to improve the analyses of small molecules and protein isoforms.

REFERENCES

[1] Huang, Y. F., Huang, C. C., Hu, C. C., Chang, H. T., *Electrophoresis* 2006, *27*, 3503-3522.

[2] Guiochon, G., *Journal of Chromatography A* 2002, *965*, 129-161.

[3] Gerberding, S. J., Byers, C. H., *Journal of Chromatography A* 1998, *808*, 141-151.

[4] Narayanan, S. R., *Journal of Chromatography A* 1994, *658*, 237-258.

[5] Yamamoto, S., Ishihara, T., *Journal of Chromatography A* 1999, *852*, 31-36.

[6] Kang, X., Frey, D. D., *Journal of Chromatography A* 2003, *991*, 117-128.

[7] Hjerten, S., Li, J.-P., *Journal of Chromatography A* 1989, *475*, 167-175.

[8] Sluyterman, L. A. A., Kooistra, C., *Journal of Chromatography A* 1990, *519*, 217-220.

[9] Sluyterman, L. A. A. E., Elgersma, O., *Journal of Chromatography A* 1978, *150*, 17-30.

[10] Xuezhen Kang, D. D. F., *Biotechnology and Bioengineering* 2004, pp. 376-387.

[11] Bjellqvist, B., Ek, K., Righetti, P. G., Gianazza, E., *Journal of Biochemical and Biophysical Methods* 1982, *6*, 317-339.

[12] Dossi, G., Celentano, F., Gianazza, E., Righetti, P. G., *Journal of Biochemical and Biophysical Methods* 1983, *7*, 123-142.

[13] Bours, J., in: Catsimpoolas, N., (Ed.), *Isoelectric Focusing*, Academic Press, New York 1976, 209-227.

[14] Hjerten, S., *Chromatographic Reviews* 1967, *9*, 122-219.

[15] Lundahl, Hjerten, S., *Annals of the New York Academy of Sciences* 1973, *209*, 94-111.

[16] Jonsson, M., Rilbe, H., *Electrophoresis* 1980, *1*, 3-14.

[17] Ivory, C. F., *Electrophoresis* 2004, *25*, 360-374.

[18] Bier, M., *Electrophoresis* 1998, *19*, 1057-1063.

[19] Tracy, N., Ivory, C. F., *Electrophoresis* 2004, *25*, 1748-1757.

[20] Burggraf, D., Weber, G., Lottspeich, F., *Electrophoresis* 1995, *16*, 1010-1015.

[21] Glukhovskiy, P., Vigh, G., *Electrophoresis* 2000, *21*, 2010-2015.

[22] Krivankova, L., Bocek, P., *Electrophoresis* 1998, *19*, 1064-1074.

[23] Nath, S., Schutte, H., Hustedt, H., Deckwer, W. D., Weber, G., *Biotechnology and Bioengineering* 1996, *51*, 15-22.

[24] Mosher, R. A., Thormann, W., Bier, M., *Journal of Chromatography* 1986, *351*, 31-38.

[25] Mosher, R. A., Thormann, W., Bier, M., *Journal of Chromatography* 1988, *436*, 191-204.

[26] Martin, A. J. P., Hampson, F., *Journal of Chromatography* 1978, *159*, 101-110.

[27] Williams, R. R., Waterman, R. E., *Proceedings of the Society for Experimental Biology and Medicine* 1929, *27*, 56-59.

[28] Righetti, P. G., Gelfi, C., Gianazza, E., *Acs Symposium Series* 1987, *335*, 33-53.

[29] Righetti, P. G. (Ed.), *Immobilized pH Gradients: Theory and Methodology*, Elsevier Biomedical Press, Amsterdam 1990.

[30] Faupel, M., Barzaghi, B., Gelfi, C., Righetti, P.G, *J. Biochem. Biophys. Methods* 1987, *15*, 147-161.

[31] Wenger, P., de Zuanni, M., Javet, P., Gelfi, C., Righetti, P. G., *J. Biochem. Biophys. Methods* 1987, *14*, 29-43.

[32] *Doctor pH Manual,* , Amersham Pharmacia Biotech, 1993, San Francisco, CA.

[33] Lalwani, S., Shave, E., Fleisher, H. C., Nzeadibe, K., *Electrophoresis* 2004, *25*, 2128-2138.

[34] Lalwani, S., Shave, E., Vigh, G., *Electrophoresis* 2004, *25*, 3323-3330.

[35] Fleisher, H. C., Vigh, G., *Electrophoresis* 2005, *26*, 2511-2519.

[36] Ogle, D., Ho, A., Gibson, T., Rylatt, D., *Journal of Chromatography A* 2002, *979*, 155-161.

[37] Lim, P., *Chemistry*, Texas A&M University, College Station, Texas, USA 2006.

[38] Shave, E., Vigh, G., *Electrophoresis* 2004, *25*, 381-387.

[39] Lalwani, S., Tutu, E., Vigh, G., *Electrophoresis* 2005, *26*, 2047-2055.

[40] Lalwani, S., Vigh, G., *Electrophoresis* 2005, *26*, 3-9.

[41] Lalwani, S., Tutu, E., Vigh, G., *Electrophoresis* 2005, *26*, 2503-2510.

[42] Shave, E., Vigh, G., *Journal of Chromatography A* 2003, *989*, 73-78.

[43] Shave, E., Vigh, G., *Journal of Chromatography A* 2004, *1036*, 3-6.

[44] North, R., Hwang, A., Lalwani, S., Shave, E., Vigh, G., *Journal of Chromatography A* 2006, *1130*, 232-237.

[45] Shave, E., Vigh, G., *Electrophoresis, in press* 2007.

[46] Barzaghi, B., Righetti, P. G., Faupel, M., *Journal of Biochemical and Biophysical Methods* 1987, *15*, 177-187.

[47] Giorgio Righetti, P., Barzaghi, B., Faupel, M., *Journal of Biochemical and Biophysical Methods* 1987, *15*, 163-176.

[48] Zuo, X., Speicher, D. W., *Analytical Biochemistry* 2000, *284*, 266-278.

[49] Zuo, X., Speicher, D. W., *Proteomics* 2002, *2*, 58-68.

[50] Zuo, X., Speicher, D.W., *ZOOM IEF Fractionator* 2000, 1-10.

[51] *IsoelectriQ*^{2} *Manual*, Proteome Systems Ltd., 2003, Woburn, MA.

[52] Sloane, A. J., Duff, J. L., Wilson, N. L., Gandhi, P. S., *Molecular & Cellular Proteomics* 2002, *1*, 490-499.

[53] IsoPrime Manual, Amersham Pharmacia Biotech, San Francisco, CA, USA.

[54] Righetti, P. G., Bossi, A., Wenisch, E., Orsini, G., *Journal of Chromatography B* 1997, *699*, 105-115.

[55] Ogle, D., Sheehan, M., Rumbel, B., Gibson, T., Rylatt, D. B., *Journal of Chromatography A* 2003, *989*, 65-72.

[56] Kodama, S., Yamamoto, A., Terashima, H., Honda, Y., Taga, A., Honda, S., *Electrophoresis* 2005, *26*, 4070–4078.

[57] Horvath, J., Dolnik, V., *Electrophoresis* 2001, *22*, 644-655.

[58] Stevens, T. S., Cortes, H. J., *Analytical Chemistry* 1983, *55*, 1365-1370.

[59] Giddings, J. C., *Separation Science* 1969, *4*, 181-183.

[60] Jorgenson, J. W., Lukacs, K. D., *Analytical Chemistry* 1981, *53*, 1298-1302.

[61] Rawjee, Y. Y., Vigh, G., *Analytical Chemistry* 1994, *66*, 619-627.

[62] Grossman, P. D., Colburn, J.C. , *Capillary Electrophoresis*, Academic Press, New York, 1992.

[63] Sun, P., Landman, A., Barker, G. E., Hartwick, R. A., *Journal of Chromatography A* 1994, *685*, 303-312.

[64] Fujiwara, S., Honda, S., *Analytical Chemistry* 1987, *59*, 487-490.

[65] Fujiwara, S., Honda, S., *Analytical Chemistry* 1986, *58*, 1811-1814.

[66] Herren, B. J., Snyder, R. S., *Journal of Colloid and Interface Science* 1987, *115*, 46-55.

[67] Mazzeo, J. R., Krull, I. S., *Analytical Chemistry* 1991, *63*, 2852-2857.

[68] Hjerten, S., *Journal of Chromatography A* 1985, *347*, 191-198.

[69] Cordova, E., Gao, J. M., Whitesides, G. M., *Analytical Chemistry* 1997, *69*, 1370-1379.

[70] Chiari, M., Cretich, M., Damin, F., Ceriotti, L., Consonni, R., *Electrophoresis* 2000, *21*, 909-916.

[71] Bendahl, L., Gammelgaard, B., *Electrophoresis* 2001, *22*, 2565-2573.

[72] MacDonald, A. M., Lucy, C. A., *Journal of Chromatography A* 2006, *1130*, 265-271.

[73] Yassine, M. M., Lucy, C. A., *Anal. Chem.* 2005, *77*, 620-625.

[74] Righetti, P. G., Gelfi, C., Verzola, B., Castelletti, L., *Electrophoresis* 2001, *22*, 603-611.

[75] Huang, M., Vorkink, W. P., Lee, M. L. , *Journal of Microcolumn Separations* 1992, *4*, 135-143.

[76] Bruin, G. J. M., Poppe, H., *Journal of Chromatography A* 1989, *471*, 429-436.

[77] Towns, J. K., Regnier, F. E., *Journal of Chromatography A* 1990, *516*, 69-78.

[78] Cobb, K. A., Dolnik, V., Novotny, M., *Analytical Chemistry* 1990, *62*, 2478-2483.

[79] Doherty, E. A. S., Meagher, R. J., Albarghouthi, M. N., Barron, A. E., *Electrophoresis* 2003, *24*, 34-54.

[80] Lanz, C., Marti, U., Thormann, W., *Journal of Chromatography A* 2003, *1013*, 131-147.

[81] Gelfi, C., Vigano, A., Ripamonti, M., Righetti, P. G., *Analytical Chemistry* 2001, *73*, 3862-3868.

[82] Corradini, D., Cannarsa, G., Fabbri, E., Corradini, C., *Journal of Chromatography A* 1995, *709*, 127-134.

[83] Corradini, D., Cannarsa, G., *Electrophoresis* 1995, *16*, 630-635.

[84] Verzola, B., Gelfi, C., Righetti, P. G., *Journal of Chromatography A* 2000, *868*, 85-99.

[85] Oda, R. P., Madden, B. J., Spelsberg, T. C., Landers, J. P., *Journal of Chromatography A* 1994, *680*, 85-92.

[86] Cifuentes, A., Rodriguez, M. A., GarciaMontelongo, F. J., *Journal of Chromatography A* 1996, *742*, 257-266.

[87] Emmer, A., Roeraade, J., *Electrophoresis* 2001, *22*, 660-665.

[88] Emmer, A., Jansson, M., Roeraade, J., *Journal of Chromatography A* 1991, *547*, 544-550.

[89] Baryla, N. E., Melanson, J. E., McDermott, M. T., Lucy, C. A., *Analytical Chemistry* 2001, *73*, 4558-4565.

[90] Yeung, K. K. C., Lucy, C. A., *Analytical Chemistry* 1997, *69*, 3435-3441.

[91] Towns, J. K., Regnier, F. E., *Analytical Chemistry* 1991, *63*, 1126-1132.

[92] Castelletti, L., Verzola, B., Gelfi, C., Stoyanov, A., Righetti, P. G., *Journal of Chromatography A* 2000, *894*, 281-289.

[93] Chiari, M., Cretich, M., Stastna, M., Radko, S. P., Chrambach, A., *Electrophoresis* 2001, *22*, 656-659.

[94] Preisler, J., Yeung, E. S., *Analytical Chemistry* 1996, *68*, 2885-2889.

[95] Gilges, M., Kleemiss, M. H., Schomburg, G., *Analytical Chemistry* 1994, *66*, 2038-2046.

[96] Iki, N., Yeung, E. S., *Journal of Chromatography A* 1996, *731*, 273-282.

[97] Ng, C. L., Lee, H. K., Li, S. F. Y., *Journal of Chromatography A* 1994, *659*, 427-434.

[98] Albarghouthi, M. N., Buchholz, B. A., Huiberts, P. J., Stein, T. M., Barron, A. E., *Electrophoresis* 2002, *23*, 1429-1440.

[99] Chiu, R. W., Jimenez, J. C., Monnig, C. A., *Analytica Chimica Acta* 1995, *307*, 193-201.

[100] Erim, F. B., Cifuentes, A., Poppe, H., Kraak, J. C., *Journal of Chromatography A* 1995, *708*, 356-361.

[101] Katayama, H., Ishihama, Y., Asakawa, N., *Analytical Chemistry* 1998, *70*, 5272-5277.

[102] Chiari, M., Cretich, M., Horvath, J., *Electrophoresis* 2000, *21*, 1521-1526.

[103] Chiari, M., DellOrto, N., Gelain, A., *Analytical Chemistry* 1996, *68*, 2731-2736.

[104] Katayama, H., Ishihama, Y., Asakawa, N., *Analytical Chemistry* 1998, *70*, 2254-2260.

[105] Fujimoto, C., Fujise, Y., Matsuzawa, E., *Analytical Chemistry* 1996, *68*, 2753-2757.

[106] Burns, N. L., Vanalstine, J. M., Harris, J. M., *Langmuir* 1995, *11*, 2768-2776.

[107] Hjerten, S., Kubo, K., *Electrophoresis* 1993, *14*, 390-395.

[108] Mechref, Y., Elrassi, Z., *Electrophoresis* 1995, *16*, 617-624.

[109] Shen, Y. F., Smith, R. D., *Journal of Microcolumn Separations* 2000, *12*, 135-141.

[110] Smith, J. T., Elrassi, Z., *Electrophoresis* 1993, *14*, 396-406.

[111] Towns, J. K., Bao, J. M., Regnier, F. E., *Journal of Chromatography A* 1992, *599*, 227-237.

[112] Bao, J. J., *Journal of Liquid Chromatography & Related Technologies* 2000, *23*, 61-78.

[113] Liu, Y., Fu, R. O., Gu, J. L., *Journal of Chromatography A* 1995, *694*, 498-506.

[114] Liu, Y., Fu, R. N., Gu, J. L., *Journal of Chromatography A* 1996, *723*, 157-167.

[115] Nashabeh, W., El Rassi, Z., *Journal of Chromatography A* 1991, *559*, 367-383.

[116] Emoto, K., Harris, J. M., VanAlstine, J. M., *Analytical Chemistry* 1996, *68*, 3751-3757.

[117] Xu, R. J., VidalMadjar, C., Sebille, B., DiezMasa, J. C., *Journal of Chromatography A* 1996, *730*, 289-295.

[118] Mccormick, R. M., *Analytical Chemistry* 1988, *60*, 2322-2328.

[119] Cifuentes, A., de Frutos, M., Santos, J. M., Diez-Masa, J. C., *Journal of Chromatography A* 1993, *655*, 63-72.

[120] Schmalzing, D., Karger, B. L., *Journal of Chromatography A* 1993, *652*, 149-159.

[121] Chiari, M., Micheletti, C., Nesi, M., Fazio, M., Righetti, P. G., *Electrophoresis* 1994, *15*, 177-186.

[122] Gelfi, C., SimoAlfonso, E., Sebastiano, R., Citterio, A., Righetti, P. G., *Electrophoresis* 1996, *17*, 738-743.

[123] Lindberg, P., Righetti, P. G., Gelfi, C., Roeraade, J., *Electrophoresis* 1997, *18*, 2909-2914.

[124] Gelfi, C., Curcio, M., Righetti, P. G., Sebastiano, R., *Electrophoresis* 1998, *19*, 1677-1682.

[125] Gilges, M., Husmann, H., Kleemiss, M. H., Motsch, S. R., Schomburg, G., *Hrc-Journal of High Resolution Chromatography* 1992, *15*, 452-457.

[126] Tikhonova, L. S., Makarov, K. A., *Electrokhimiya* 1982, *18*, 1110-1114.

[127] Kishore, K., Bhanu, V. A., *J. Polym. Sci. Polym. Chem. Ed.* 1986, *24*, 379-381.

[128] Zhao, L., Yang, J.-l., Ma, L.-g., Huang, Y., *Materials Letters* 2002, *56*, 990-994.

[129] Cifuentes, A., Canalejas, P., Diez-Masa, J. C., *Journal of Chromatography A* 1999, *830*, 423–438.

[130] Suen, T. J., Jen, Y., Lockwood, J. V., *Journal of Polymer Science* 1958, *31*, 481-497.

[131] Riggs, J. P., Rodrigue.F, *Journal of Polymer Science Part a-1-Polymer Chemistry* 1967, *5*, 3151-3153.

[132] Riggs, J. P., Rodrigue.F, *Journal of Polymer Science Part a-1-Polymer Chemistry* 1967, *5*, 3167-3170.

[133] Kay, T. A., Rodriguez, F., *Journal of Applied Polymer Science* 1983, *28*, 633-646.

[134] Suen, T. J., Senior, A., Swanson, D. L., Jen, Y., *Journal of Polymer Science* 1960, *45*, 289-303.

[135] Feng, X. D., Guo, X. Q., Qiu, K. Y., *Makromolekulare Chemie-Macromolecular Chemistry and Physics* 1988, *189*, 77-83.

[136] Greaves, G. N., Smith, W., Giulotto, E., Pantos, E., *Journal of Non-Crystalline Solids* 1997, *222*, 13-24.

[137] Lin, G., Shaorong, Liu., *Anal. Chem.* 2004, *76*, 7179-7186.

[138] Huang, M., Vorkink, W. P., Lee, M. L. , *J. Microcolumn Sep.* 1992, *4*, 233-238.

[139] Liu, Q., Hartwick, R., *Journal of Liquid Chromatography & Related Technologies* 1997, *20*, 707-718.

[140] Liu, Q. C., Lin, F. M., Hartwick, R. A., *Journal of Chromatographic Science* 1997, *35*, 126-130.

[141] Srinivasan, K., Pohl, G., Avdalovic, N., *Analytical Chemistry* 1997, *69*, 2798-2805.

[142] Desert, C., Guerin-Dubiard, C., Nau, F., Jan, G., *Journal of Agricultural and Food Chemistry* 2001, *49*, 4553-4561.

[143] Poduslo, J. F., *Analytical Biochemistry* 1981, *114*, 131-139.

[144] Huang, T. L., Richards, M., *Journal of Chromatography A* 1997, *757*, 247-253.

[145] Beeley, J. G., *Biochemical Journal* 1971, *123*, 399-401.

[146] Beeley, J. G., *Biochimica Et Biophysica Acta* 1971, *230*, 595-600.

[147] Li-Chan, E., Nakai, S., *Crit. Rev. Poultry Biol.* 1989, *2*, 21-58.

[148] Davis, J. G., Zahnley, J. C., Donovan, J. W., *Biochemistry* 1969, *8*, 2044-2050.

[149] Nisbet, A. D., Saundry, R. H., Moir, A. J. G., Fothergill, L. A., Fothergill, J. E., *European Journal of Biochemistry* 1981, *115*, 335-345.

[150] Stevens, L., *Comparative Biochemistry and Physiology B-Biochemistry & Molecular Biology* 1991, *100*, 1-9.

[151] Craver, H. F., Vigh, G., *Poly(vinyl alcohol)-based Buffering Membranes for Isoelectric Trapping Separations*, Ph.D. Dissertation, Texas A&M University, College Station 2007.

[152] Korpela, J., *Medical Biology* 1984, *62*, 5-26.

[153] George, M. H., Ghosh, A., *Journal of Polymer Science: Polymer Chemistry Edition,* 1978, *16*, 981-995.

[154] Williams, B. A., Vigh, C., *Analytical Chemistry* 1996, *68*, 1174-1180.

[155] Friedl, W., Reijenga, J. C., Kenndler, E., *Journal of Chromatography A* 1995, *709*, 163-170.

[156] Reijenga, J. C., Kenndler, E., *Journal of Chromatography A* 1994, *659*, 417-426.

[157] Reijenga, J. C., Kenndler, E., *Journal of Chromatography A* 1994, *659*, 403-415.

[158] Nashabeh, W., El Rassi, Z., *Journal of Chromatography A* 1990, *514*, 57-64.

[159] Jaros, M., Gas, B., *Electrophoresis* 2002, *23*, 2667-2677.

[160] Onsager, L. F., Raymond M, *Journal of Physical Chemistry* 1932, *36*, 2689-2778.

[161] Gas, B., Jaros, M., Hruska, V., Zuskova, I., Stedry, M., *LC GC Europe* 2005, 18-21.

[162] Michal Jaros, B. G., *Electrophoresis* 2002, *23*, 2667-2677.

[163] Rawjee, Y. Y. V., Gyula, *Analytical Chemistry* 1994, *66*, 619-627.

[164] Williams, B. A., Vigh, G., *Journal of Chromatography A* 1997, *777*, 295-309.

[165] Ahmad, A., *Electrophoresis* 2001, *22*, 3107-3130.

[166] Andreas, R., *Electrophoresis* 2001, *22*, 3079-3106.

[167] M. Brent Busby, G. V., *Electrophoresis* 2005, *26*, 3849-3860.

[168] Li, S., Vigh, G., *Journal of Chromatography A* 2004, *1051*, 95-101.

[169] Sanchez-Vindas, S., Vigh, G., *Journal of Chromatography A* 2005, *1068*, 151-158.

[170] Zhu, W., Vigh, G., *Journal of Chromatography A* 2003, *987*, 459-466.

[171] Dawn Kirby Maynard, G. V., *Electrophoresis* 2001, *22*, 3152-3162.

[172] Cai, H., Vigh, G., *Journal of Pharmaceutical and Biomedical Analysis* 1998, *18*, 615-621.

[173] Vincent, J. B., Vigh, G., *Journal of Chromatography A* 1998, *816*, 233-241.

[174] Hjerten, S., Mohabbati, S., Westerlund, D., *Journal of Chromatography A* 2004, *1053*, 181-199.

[175] Miksik, I., Charvatova, J., Eckhardt, A., Cserhati, T., *Journal of Chromatography B-Analytical Technologies in the Biomedical and Life Sciences* 2004, *800*, 161-167.

[176] Corradini, D., Mancinia, G., Bello, C., *Journal of Chromatography A* 2004, *1051*, 103-110.

[177] Corradini, D., Mancini, G., Bello, C., *Chromatographia* 2004, *60*, S125-S132.

[178] Warnick, K. F., Francom, S. J., Humble, P. H., Kelly, R. T., *Electrophoresis* 2005, *26*, 405-414.

[179] Culbertson, C. T., Jorgenson, J. W., *Analytical Chemistry* 1994, *66*, 955-962.

[180] Williams, B. A., Vigh, G., *Enantiomer* 1996, *1*, 183-191.

[181] Martin, M., Guiochon, G., Walbroehl, Y., Jorgenson, J. W., *Analytical Chemistry* 1985, *57*, 559-561.

[182] Martin, M., Guiochon, G., *Analytical Chemistry* 1984, *56*, 614-620.

[183] Gas, B., Stedry, M., Kenndler, E., *Journal of Chromatography A* 1995, *709*, 63-68.

[184] Gas, B., Kenndler, E., *Electrophoresis* 1997, *18*, 2123-2133.

[185] Minarik, M., Groiss, F., Gas, B., Blaas, D., Kenndler, E., *Journal of Chromatography A* 1996, *738*, 123-128.

[186] Nzeadibe, K., Vigh, G., *Synthesis of New, Single-isomer Quaternary Ammonium Derivatives of β-Cyclodextrin for Electrophoretic Enantiomer Separations*, Ph.D. Dissertation, Texas A&M University, College Station 2004.

[187] Lin, C. H., Kaneta, T., *Electrophoresis* 2004, *25*, 4058-4073.

[188] Huang, X. Y., Doneski, L. J., Wirth, M. J., *Analytical Chemistry* 1998, *70*, 4023-4029.

[189] Cai, H., Vigh, C., *Analytical Chemistry* 1998, *70*, 4640-4643.

[190] Graf, M., García, R. G. Wätzig, H., *Electrophoresis* 2005, *26*, 2409–2417.

[191] Dolan, J. W., Snyder, L.R. (Ed.), *Troubleshooting LC Systems*, Humana Press New Jersey 1989.

[192] Weber, S. G., *Analytical Chemistry* 1984, *56*, 2104-2109.

[193] Weinberger, R. (Ed.), *Practical Capillary Electrophoresis* Academic Press Limited, New York 1993.

VITA

Name:	Joseph Brian Montejo Sinajon
Address:	The Dow Chemical Company, Freeport, Texas 77541
E-mail Address:	brian_sinajon@yahoo.com
Education:	B.S. Chemistry, University of San Carlos, Cebu City, Cebu, Philippines, 1998. Ph.D. Chemistry, Texas A&M University, College Station, Texas, USA, 2007.